Abstract

Study on structure-property relationship of isoindigo and thienoisoindigo: synthesis, characterization and application for organic field-effect transistors

Youngjoo Park

WCU Hybrid Materials Program

Department of Materials Science and Engineering

The Graduate School

Seoul National University

Over the past decades, numerous lactam functionalized organic compounds have been synthesized for their application in optoelectronic devices to show promising advantages; stabilized LUMOs, broad absorption range, planar structure of lactam moiety, and so on. Among others, isoindigo (IID) and thienoisoindigo (TIID) derivatives showed remarkable performance as donor materials in organic solar cell devices and organic field-effect transistors. However, the structure-property relationship between IID and TIID-based molecules has rarely been explored in spite of their structural similarity. Characteristic twisted geometry comprising carbonyl oxygen and phenyl hydrogen in IID significantly hampers effective π-π interaction between IID molecules. Recently, with a view to overcome such an undesirable limit in

extending π-conjugation, thienoisoindigo moiety (TIID) has newly been developed. Replacing phenyl ring with thiophene ring is believed to reduce the steric hindrance and thus enhance the planarity along the backbone.

In this work, new series of IID and TIID-based small molecules and D-A type polymers have been synthesized to explore the structure-property correlation in them with special focus on their applications in OFET.

To compare the fundamental properties of IID and TIID,core and brominated core of them were synthesized and characterized using UV/VIS, CV, IR and DFT calculation. It was clearly found that TIID was more planar in structure to have broader absorption range and lower bandgap energy. Furthermore, relatively larger electron donating property of thiophene ring in TIID resulted in its high-lying HOMO compared to that in IID. FT-IR spectra has also supported S···O secondary bonding interaction for planarization of TIID backbone. Aiming at developing a new class of n-type OFET molecules, strong electron withdrawing dicyanovinyl units were introduced into the IID and TIID core structures. Structure-property relationship was investigated in terms of their optical and electrochemical properties measured by UV-VIS, CV, and DFT calculation. Top-contact bottom-gate type OFET devices were fabricated using vacuum deposition method. It was found that the IID based devices, EHIIDPDCV and EHIIDTDCV, showed decent n-type performance; maxima electron mobility were 1.70×10^{-3} $cm^2V^{-1}s^{-1}$ and 1.83×10^{-2} $cm^2V^{-1}s^{-1}$, respectively.

On the other hand, novel class of D-A type polymers were designed and synthesized using IID and TIID as an effective acceptor(A) unit. From UV/VIS and CV data, D-A polymers were shown to have low bandgap energy and appropriate frontier MO levels for OFET application. DFT calculation suggested that TIID-based D-A polymer would have much more planar structure through polymer backbone compared to that in IID-based polymer. Solution-processed OFET devices were fabricated using 0.3wt% chloroform solution for each polymer. Both polymers were shown to have ambipolar charge

transport ability. While IID-based D-A copolymer showed maxima mobilities of $\mu_e = 3.09 \times 10^{-4} cm^{-1}V^{-1}s^{-1}$ and $\mu_h = 3.04 \times 10^{-2} cm^{-1}V^{-1}s^{-1}$, TIID-based D-A copolymer showed more balanced ambipolar performances with maximum mobility of $\mu_e = 4.44 \times 10^{-3} cm^{-1}V^{-1}s^{-1}$ and $\mu_h = 1.14 \times 10^{-2} cm^{-1}V^{-1}s^{-1}$.

Keywords: Isoindigo, Thienoisoindigo, Small molecule, D-A polymer, Structure-Property Relationship, Organic Field-Effect Transistor.

Student Number: 2013-22475

Contents

Chapter 1 Introduction 1
1.1 Organic field-effect transistors (OFET)s 1
1.1.1 Operation principle of OFETs 1
1.1.2 Material aspect of OFETs 7
1.2 Organic dyes containing lactam moiety 13
1.2.1 Why lactam functionalized materials are of interest 13
1.2.2 Isoindigo 14
1.2.3 Thienoisoindigo 18
1.3 Resarch Objectives 20
1.4 Bibliography 22

Chapter 2. Study on Structure-Property Relationship of Isoindigo and Thienoisoindigo cores with Tuning Frontier Molecular Orbital 27
2.1 Introduction 27
2.2 Experimental 31
2.2.1 Synthesis 31
2.2.2 Instruments and measurements 44
2.2.3 Fabrication and evaluation of organic thin-film transistors 46
2.3 Results and Discussion 47
2.3.1 Theoretical molecular orbital calculation used density functional theory (DFT) 47
2.3.2 Optical and electrochemical properties of IID and TIID-based Small molecules 53
2.3.3 IR analysis of IID and TIID core 67

2.3.4 Thermal stability of molecules....69
2.3.5 OFETs performance....71
2.4 Conclusion....77
2.5 Bibliography....78

Chapter 3. Structure-Property Relationship of Isoindigo and Thienoisoindigo as Acceptor Units in D-A Polymers....79
3.1 Introduction....79
3.2 Experimental....83
3.2.1 Synthesis....83
3.2.2 Instruments and measurements....93
3.2.3 Fabrication and evaluation of organic thin-film transistors 95
3.3 Results and Discussion....96
3.3.1 Theoretical molecular orbital calculation used density functional theory (DFT)....96
3.3.2 Optical and electrochemical properties of polymers....100
3.3.3 Thermal properties of polymers....107
3.3.4 GI-XRD analysis....109
3.3.5 OFETs performance....112
3.3.6 Morphology studies of polymer OFET devices....118
3.4 Conclusion....123
3.5 Bibliography....125

Abstract in Korean....126
List of Presentation....129

List of Tables

Table 2.1 Theoretical molecular orbital of EHIIDPDCV, EHIIDTDCV, EHTIIDPDCV, and EHTIIDTDCV 52
Table 2.2 Optical properties of IID- and TIID-based small molecules in solution and solid state 57
Table 2.3 Electrochemical properties and energy levels of IID and TIID cores in solution and film states. 63
Table 2.4 Electrochemical properties and energy levels of IID- and TIID-based small molecules in solution and solid state. 64
Table 2.5 Position of carbonyl stretch peak of cores and references 68
Table 2.6 Electrical performance of OFET devices based on EHIIDPDCV vacuum deposited thin films with Au electrodes.....73
Table 2.7 Electrical performance of OFET devices based on EHIIDTDCV vacuum deposited thin films with Au electrodes.....73

Table 3.1 Theoretical molecular orbital of two polymers, P(EHIID2T-HDIDIDF) and P(EHTIID2T-HDIDIDF) 99
Table 3.2 Optical properties of two polymers in solution and film state..102
Table 3.3 Electrochemical properties and energy levels of each polymers on solution and solid state. 104
Table 3.4 Thermal properties of polymers.....107
Table 3.5 Electrical performance of OFET devices based on polymer P(EHIID2T-HDIDIDF) solution-processed thin films with Au electrodes ...114
Table 3.6 Electrical performance of OFET devices based on polymer P(EHTIID2T-HDIDIDF) solution-processed thin films with Au electrodes. 115

List of Schemes

Scheme 2.1 First target molecules for basic studies on structure-property relationships by using optoelectronic properties 29
Scheme 2.2 (a) Overall design strategy of 4 small molecules typed A-D-A-D-A. (b) Particular structures of 4 small molecules 30
Scheme 2.3 Synthetic route for 4 cores (EHIID, EHIID2Br, EHTIID, and EHTIID2Br) 31
Scheme 2.4 Synthetic route of isoindigo (IID) derivatives. (EH-IID-P-DCV, EH-IID-T-DCV) 32
Scheme 2.5 Synthetic route of thienoisoindigo (TIID) derivatives (EH-TIID-P-DCV, EH-TIID-T-DCV) 33

Scheme 3.1 Schematic figure of design rules of two polymers. Upper : P(EHIID2T-HDIDIDF), Bottom : P(EHTIID2T-HDIDIDF.....82
Scheme 3.2 Synthetic route of monomers based on IID and TIID core for accepting unit 83
Scheme 3.3 Suzuki polymerization schemes of two polymers P(EHIID2T-HDIDIDF) and P(EHTIID2T-HDIDIDF) 84

List of Figures

Figure 1.1 Structure of OFET devices (a) top-contact (b) bottom-contact configurations.....1

Figure 1.2 Ideal energy level diagram of an OFET at (a) gate bias=0, (b-e) Demonstration of the principle of OFET operation for the case of electron (b) accumulation and (d) transport and hole (c) accumulation and (e) transport.....4

Figure 1.3 Typical electrical characteristics of OFET devices. (a) Example of I_D-V_D curves (output curve) for various values of V_G. (b) Example I_D-V_G curves (transfer curve) plotted on semi-logarithmic axes for various values of V_D. 6

Figure 1.4 Reported p-type semiconducting organic materials.....8

Figure 1.5 Reported n-type semiconducting organic materials.....9

Figure 1.6 Proper frontier molecular energy levels of organic materials for OFET applications.....11

Figure 1.7 Chemical structures of lactam-functionalized building block for organic semiconductors.....16

Figure 1.8 Structure of indigo and isoindigo dyes 17

Figure 1.9 Structure of isoindigo and thienoisoindigo 17

Figure 2.1 The calculated geometry on ground state. Optimized geometries after calculation using basis set B3LYP/6-31G*. (Upper: top view, Lower: front view) (a) EHIID, (b) EHIID2Br, (c) EHTIID, and (d) EHTIID2Br (All alkyl chains were simplified from ethylhexyl to methyl for simple calculation).....48

Figure 2.2 The calculated geometry on ground state. Optimized geometries after calculation using basis set B3LYP/6-31G*. (Upper: top view, Lower: front view) (a) EHIIDPDCV, (b) EHIIDTDCV, (c) EHTIIDPDCV, and (d) EHTIIDTDCV (All alkyl chains were simplified from ethylhexyl to methyl for simple calculation) 50

Figure 2.3 Calculated FMO energy levels and electron density maps of (a) EHIID, (b) EHIID2Br, (c) EHTIID, (d) EHTIID2Br, (e) EHIIDPDCV, (f)

EHIIDTDCV, (g) EHTIIDPDCV, and (h) EHTIIDTDCV. Calculation method was DFT and basis set was B3LYP/6-31G*.....51
Figure 2.4 UV/VIS absorption spectra (a) EHIID, (b) EHIID2Br, (c) EHTIID, and (d) EHTIID2Br at solution and film state.....54
Figure 2.5 UV/VIS absorption spectra (a) for each derivatives in solution and solid state. Absorption spectra of all derivatives (b) in solution state and (c) in film state. 55
Figure 2.6 Molar absorption coefficient for each materials. All data was calculated by solution absorbance spectra.....56
Figure 2.7 Cyclic voltammetrams of IID and TIID cores (blanked) at solution (left) and film (right) state. (a) EHIID, (b) EHIID2Br, (c) EHTIID, and (d) EHTIID2Br. At solution state, supporting electrolyte was TBATFB in acetonitrile (DCM). Ferrocene (filled) with TBATFB in DCM solution as the reference. All were drop-casting for doping on ITO glass and supporting electrolyte was TBAHFB in acetonitrile (ACN). Ferrocene (filled) with TBAHFB in ACN solution as the reference.....60
Figure 2.8 Ultraviolet photoelectron microscopy data for HOMO as an aspect of electrical property, respectively (a) EHIIDPDCV, (b) EHIIDTDCV, (c) EHTIIDPDCV, and (d) EHTIIDTDCV.....61
Figure 2.9 Cyclic voltammetrams of IID- and TIID-based small molecules (filled) named (a) EHIIDPDCV, (b) EHIIDTDCV, (c) EHTIIDPDCV, and (d) EHTIIDTDCV. All small molecules were drop-casting for doping on ITO glass and supporting electrolyte was TBAHFB in acetonitrile (ACN). Ferrocene (blank) with TBAHFB in ACN solution as the reference. 62
Figure 2.10 FT-IR spectrum of core molecules named EHIID2Br and EHTIID2Br. EHTPD (synthetic route 6) is reference for comparing change of peak position. 68
Figure 2.11 TGA analysis of molecules for checking thermal stability. Increase of temperature is 10℃/min and range of temperature is 600℃ 70
Figure 2.12 Transfer I-V curve for EHIIDPDCV at each temperature. (a) room

temperature, (b) 70℃, (c) 100℃ and (d) 120℃.....74

Figure 2.13 Transfer I-V curve for EHIIDTDCV at each temperature. (a) Room temperature, (b) 70℃, (c) 90℃ (d) 110℃, (e) 115℃, and (f) 130℃..75

Figure 2.14 Transfer and output curve of vacuum deposited device of EHIIDTDCV at optimized condition at 130℃. 76

Figure 2.15 AFM images of vacuum deposited devices at (a) 90℃, (b) 115℃, (c) 130℃, and (d) 150℃ of EHIIDTDCV.....76

Figure 3.1 Optimized structure of P(EHIID2T-HDIDIDF). Upper : top view, Bottom : side view.....98

Figure 3.2 Optimized structure of P(EHTIID2T-HDIDIDF). Upper : top view, Bottom : side view.....98

Figure 3.3 UV/VIS absorption spectra of polymers in solution and film state. Solution and film state UV/VIS absorption spectra of (a)P(EHIID2T-HDIDIDF) and (c)P(EHTIID2T-HDIDIDF). Film state absorption spectra via annealing substrates with increasing temperatures (b) P(EHIID2T-HDIDIDF) and (d)P(EHTIID2T-HDIDIDF).....101

Figure 3.4 (a) UV/VIS spectra and (b) CV graph of each polymers in film state. Polymers were spin-coated on glass for UV/VIS absorption spectra. Polymers were drop-casting for doping on ITO glass and supporting electrolyte was TBAHFB in acetonitrile (ACN) for CV detection. Ferrocene (blank) with TBAHFB in ACN solution as the reference.....103

Figure 3.5 DSC results of (a) P(EHIID2T-HDIDIDF) and (b) P(EHTIID2T-HDIDIDF), and TGA traces of (c) P(EHIID2T-HDIDIDF) and (d) P(EHTIID2T-HDIDIDF).....108

Figure 3.6 XRD diffraction data of (a) P(EHIID2T-HDIDIDF) with 3000rpm and (b) P(EHTIID2T-HDIDIDF) with 2000rpm, using 0.3wt% chloroform solution at each optimized conditions and pristine films in GI-mode.....111

Figure 3.7 Transfer curves of (a) p-channel operation and (b) n-channel operation. Output curves of (c) p-channel operation and (d) n-channel operation. These characteristics of P(EHIID2T-HDIDIDF) were detected at best conditions 116
Figure 3.8 Transfer curves of (a) p-channel operation and (b) n-channel operation. Output curves of (c) p-channel operation and (d) n-channel operation. These characteristics of P(EHTIID2T-HDIDIDF) were detected at best conditions 117
Figure 3.9 Tapping mode AFM topology of P(EHIID2T-HDIDIDF) devices fabricated using 0.3wt% chloroform solution with spin rate (a) 1000rpm, (b) 2000rpm and (c) 3000rpm.....119
Figure 3.10 Tapping mode AFM topology of P(EHIID2T-HDIDIDF) devices fabricated using 0.3wt% chloroform solution with spin rate 3000rpm at (a) RT, (b) 100℃, (c) 150℃and (d) 200℃.....120
Figure 3.11 Tapping mode AFM topology of P(EHTIID2T-HDIDIDF) devices fabricated using 0.3wt% chloroform solution with spin rate (a) 1000rpm, (b) 2000rpm and (c) 3000rpm.....121
Figure 3.12 Tapping mode AFM topology of P(EHTIID2T-HDIDIDF) devices fabricated using 0.3wt% chloroform solution with spin rate 2000rpm at (a) RT, (b) 100℃, (c) 150℃and (d) 200℃.....122

Chapter 1. Introduction

1.1 Organic Field-Effect Transistors (OFETs)

1.1.1 Operational principle of OFETs

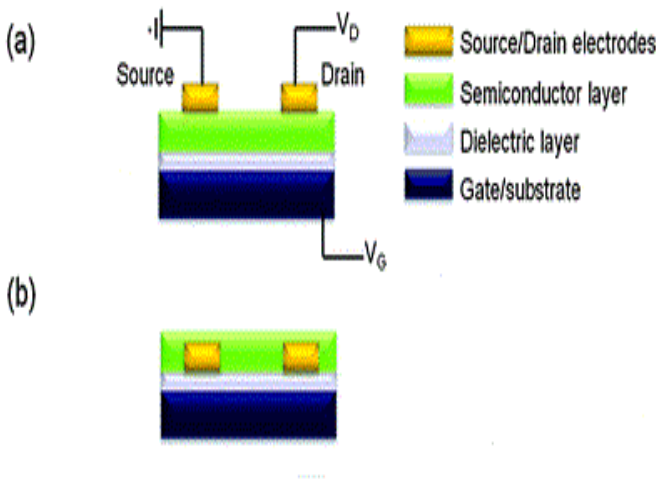

Figure 1. 1 Structure of OFET devices (a) top-contact (b) bottom-contact configurations[5)]

Field-effect transistors (FETs) are main logic units in electronic circuits, where they are usually used as either a switch or an amplifier. [1)] The principle of the FET was proposed in 1930. After 30 years later, fabrication of silicon-based FET was developed as metal-oxide-semiconductor FET (MOSFET) by Kahng and Atalla in 1960.[2)] Although first descriptions of MOSFET dated back to 1970, [3)] organic FETs (OFETs) have only been recognized as potential units of optoelectronic devices since the first report by Koezuka and co-workers on a structure based on polythiophene was published.[4)]

OFETs are sets of conductors, which are source, drain, and gate electrodes; dielectric layer; and organic active layer. Fabrication of OFETs has been mainly based on two structures: top-contact and bottom-contact electrode configurations (Figure 1.1). Operation process of OFETs is as follows. When there is no voltage applied to the gate electrode, only small current flows between source and drain electrode, and this is called 'off-state' of transistor. When negative bias was applied to the gate electrode, positive charge carriers (normally called hole) injected from source electrodes are accumulated at the interface between dielectric layer and organic active layer. Then, p-type channel is developing between source and drain electrode. This is referred to 'on-state' of transistor. Likewise, when positive bias is applied to the gate, negative charge carriers (normally called electron) are accumulated at the interface of organic active layer/dielectric layer and making n-channel between source and drain electrodes.[5)]

In terms of energy level, at 'off-state' of transistor, the positions of the highest occupied molecular orbitals (HOMOs) and the lowest occupied molecular orbitals (LUMOs) of organic active layer are relative shifted to the Fermi levels(E_F) of the source and drain contacts. In this case, gate voltage is zero

(Figure 1.2 (a)). If negative gate bias was applied into gate electrode, energy levels (HOMO and LUMO) of organic semiconductors shift up to the Fermi levels (E_F) of the metal electrode. When HOMO becomes resonant with E_F, hole carriers could flow from organic semiconductors to electrode. It results in current flow between source and drain. These materials are called p-type semiconductors. If positive gate bias was applied into gate, HOMO and LUMO of organic semiconductors shift down to the Fermi levels (E_F) of the metal. When LUMO becomes resonant with E_F, electron carriers are accumulated and flow from organic semiconductor to electrode. Consequently, current flows between source and drain electrodes. These materials are called n-type semiconductors (Figure 1.2).[6)]

In general, both gate voltage (V_G) and source/drain voltage (V_{SD}) can modulate the current flow (I_{SD}). The current, which flows from the source to the drain electrode (J_{SD}) under the given V_G, increases almost linearly with the increasing V_{SD}. The current gradually becomes saturated as shown in Figure 1.3. The current (I_{SD}) is given by eq. 1,

$$I_{SD} = \frac{C_i W \mu_{FET}}{L}\left[(V_G - V_T)V_{SD} - \frac{{V_{SD}}^2}{2}\right]. \qquad (1)$$

Where, μ_{FET} is the field-effect mobility of the charge carrier, L is the channel length, W is the channel width, C_i is the capacitance per unit area of the dielectric, and V_T is the threshold voltage. The current I_{SD} in the linear and saturation regions is given by eqs. 2 and 3, respectively.

$$I_{SD,linear} = \frac{C_i W_i \mu_{FET}}{L}(V_G - V_T)V_{SD} \qquad (2)$$

$$I_{SD,sat} = \frac{C_i W \mu_{FET}}{2L}(V_G - V_T)^2 \qquad (3)$$

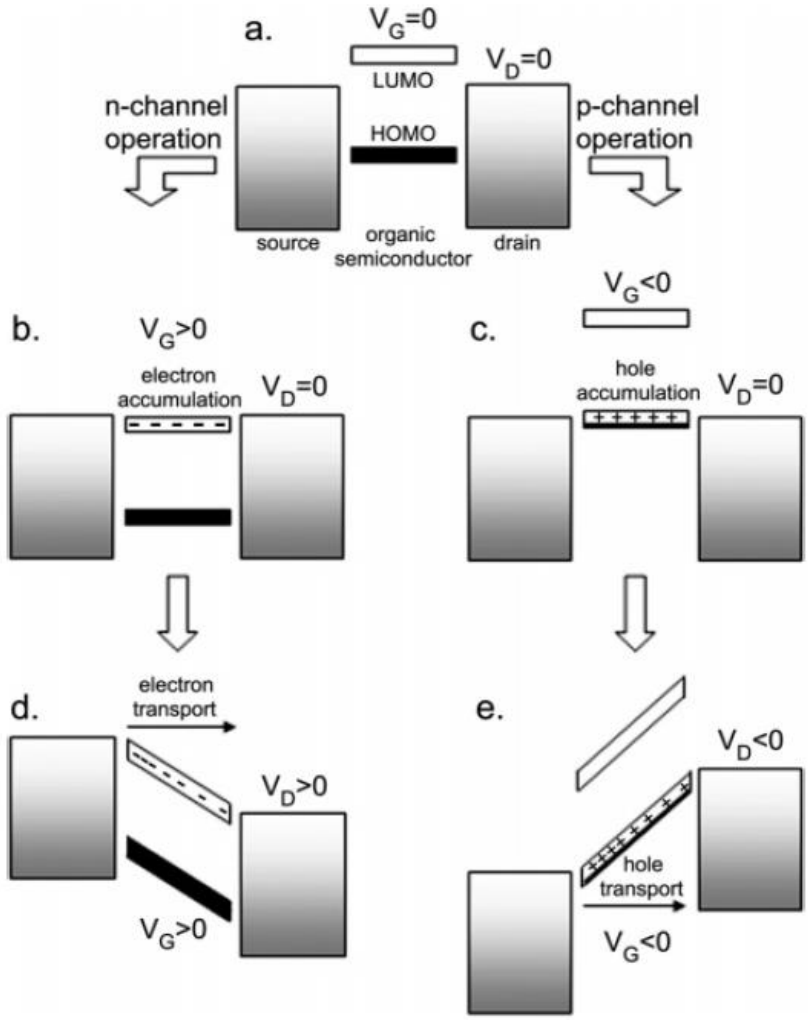

Figure 1. 2 Ideal energy level diagram of an OFET at (a) gate bias=0, (b-e) Demonstration of the principle of OFET operation for the case of electron (b) accumulation and (d) transport and hole (c) accumulation and (e) transport.[6)]

The most important parameters indicating device performance of OFETS are the charge carrier mobility (μ_{FET}), current on/off ratio ($I_{on/off}$), and the threshold voltage (V_T). The mobility, μ_{FET}, could be calculated from slope of plots of $I_{SD}^{1/2}$-V_G curve, $I_{on/off}$ is the ratio of drain current in on-state and off-state at particular gate voltage, and V_T could be extracted from the linear fit to zero yields in transfer curve. Not only organic semiconductor but the gate dielectric materials greatly affect the device performance.[7)]

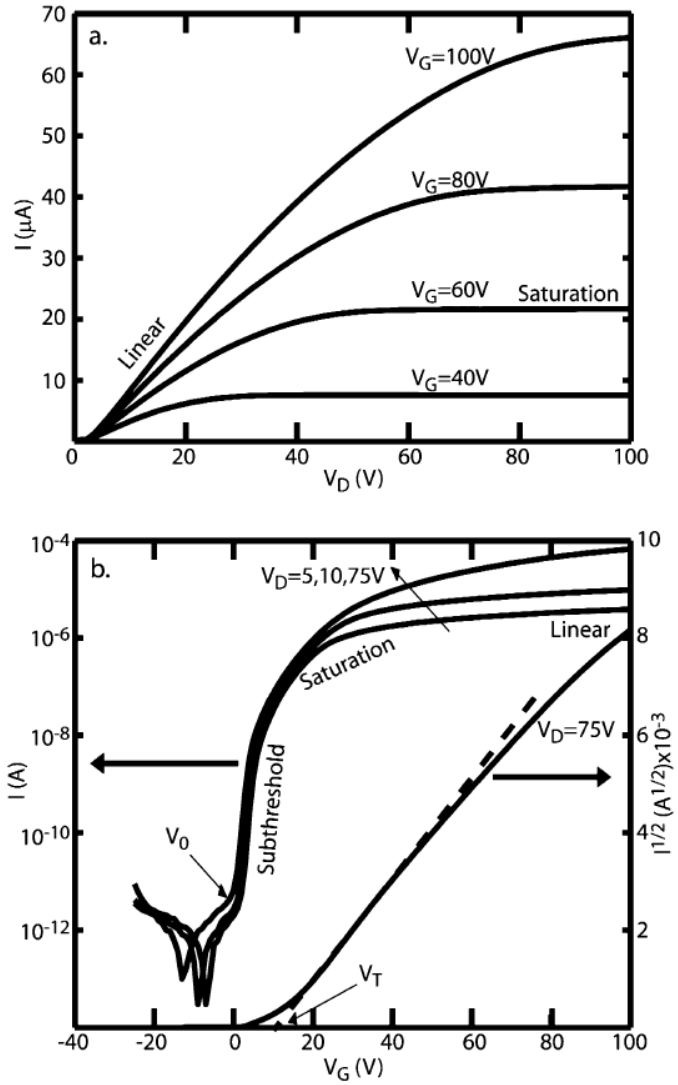

Figure 1. 3 Typical electrical characteristics of OFET devices. (a) Example of I_D-V_D curves (output curve) for various values of V_G. (b) Example I_D-V_G curves (transfer curve) plotted on semi-logarithmic axes for various values of V_D. [7)]

1.1.2 Material aspect of OFETs

As aspect of materials in fields of OFETs, in 1986, in case of polymer, polythiophene film was used as an active layer, showing mobility of 10^{-5} cm^2 $V^{-1}s^{-1}$, which was first ever report of OFETs. After several years, π-conjugated small molecules, such as oligothiophenes, were reported with mobility of 10^{-2} $cm^2V^{-1}s^{-1}$ [9]. In these days, enormous progress of materials has been made in the field of OFETs[8a-n), 13a-o)], with hole mobility up to 43 $cm^2V^{-1}s^{-1}$ (average value of 25 $cm^2V^{-1}s^{-1}$) and electron mobility of 11 $cm^2V^{-1}s^{-1}$ (average value of 5.2 cm^2 $V^{-1}s^{-1}$). Those are quite comparable results with amorphous silicon (mobility of amorphous silicon is around 1 $cm^2V^{-1}s^{-1}$ and that of polycrystalline silicon is 10~100 $cm^2V^{-1}s^{-1}$).

For high-performance OFETs, several design rules are needed. Transitioning from a single molecule to a micrometer-scale thin film device, supramolecular self-assembly plays an important role. As a result, supramolecular approaches have been widely employed for achieving desired film morphologies with reduced grain boundaries[10], as well as well-aligned orientations[11a-b)] to facilitate charge transport. Organic chemists are highly skilled in tuning electronic properties at the molecular level such as molecular frontier orbitals and alignment of molecules. [12] Organic chemists have to consider three main concepts. First, semiconductors should have appropriate frontier molecular orbitals (FMOs) for Ohmic contact. For n-type semiconductors, LUMOs should match with E_F of Au or Ag electrode. In contrast, for p-type, HOMOs empirical window is in the range on -4.8 ~ -5.5eV.[14] Further, FMOs are important for stability of device on ambient condition. Second is backbone coplanarity for good intermolecular π-orbital overlap. Building blocks with minimal steric hindrance lead enhancing mobility of OFETs by appreciable backbone planarity.

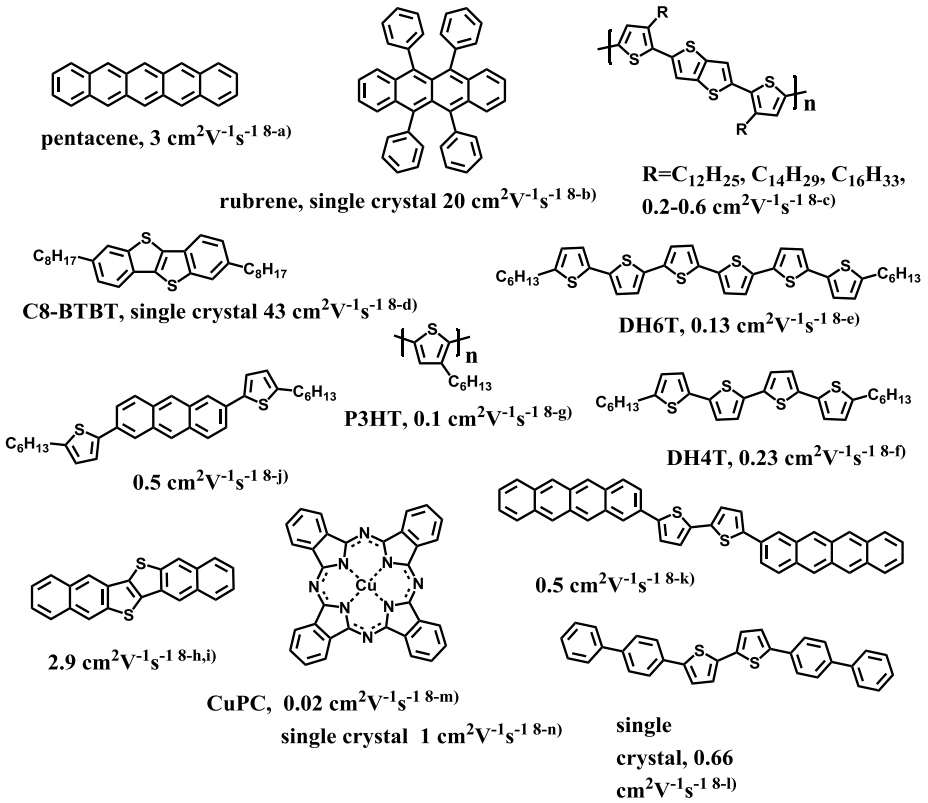

Figure 1. 4 Reported p-type semiconducting organic materials [8a-n)]

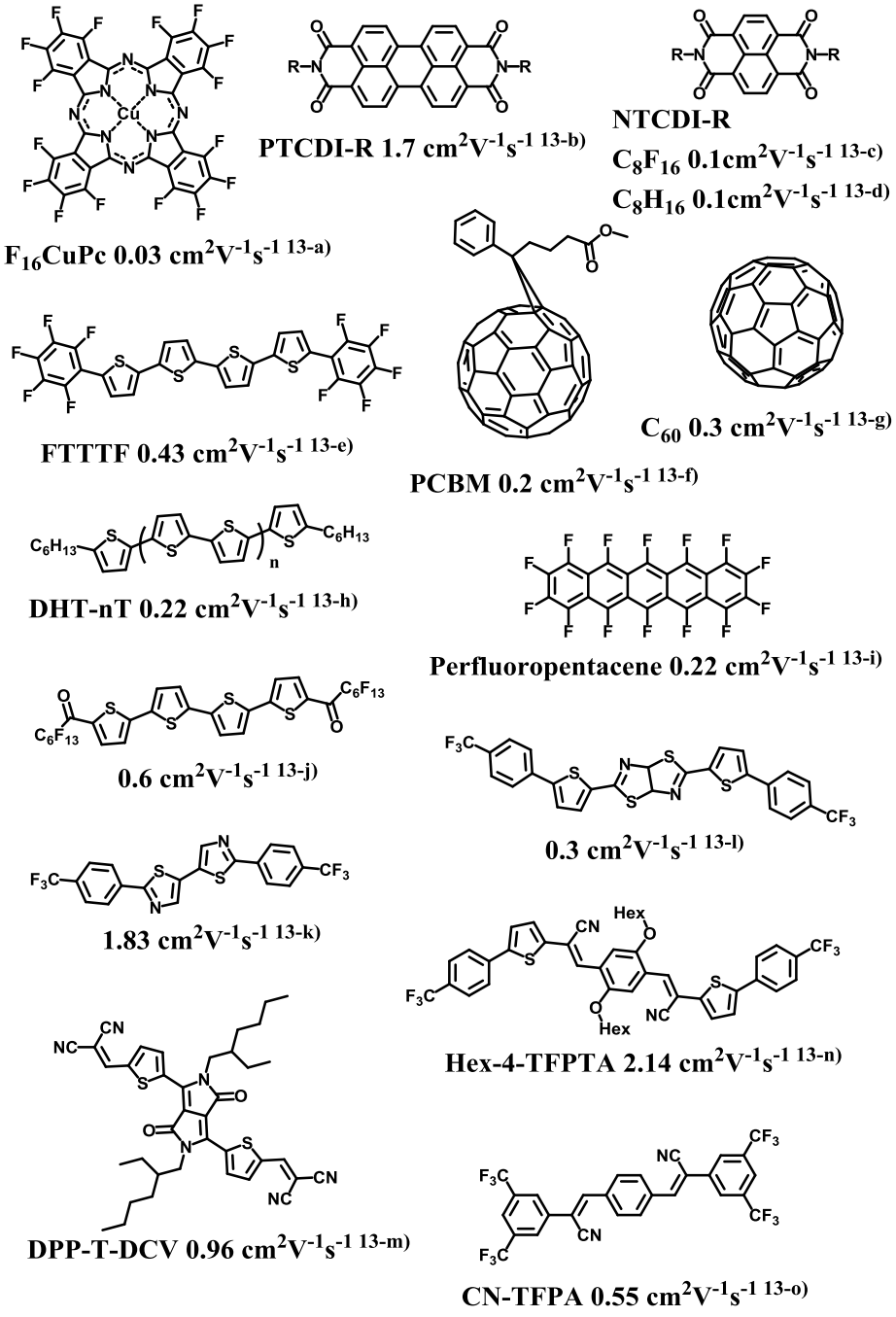

Figure 1. 5 Reported n-type semiconducting organic materials [13a-o)]

This happens by facilitating charge injection, fostering interchain transportation and maximizing intermolecular hopping that are limiting factor of organic semiconductor mobility. For expecting these, theoretical computational method, DFT, is useful. Finally, film morphologies and microstructural studies are important as synthetic efforts. In addition, solubility and processability of materials are considerate.

Even single-crystal OFETs (SC-OFETs) have disadvantages because of difficulty of technological fabrication; many efforts have been focused toward large-area fabrication through method of aligning single-crystals in large-area substrate. [15] Most widely known materials for p- and n-type organic semiconductors are shown in Figure 1.4 and Figure 1.5, respectively. Although those molecules are shown high mobility, fabrication of integrated circuit through unipolar approach has some limits: lots of process steps, complex process, huge manufacturing cost, and so on. However, ambipolar charge transporting materials are solution of these limits. Typically used single-component ambipolar organic semiconductor are reported for alternative.[16]

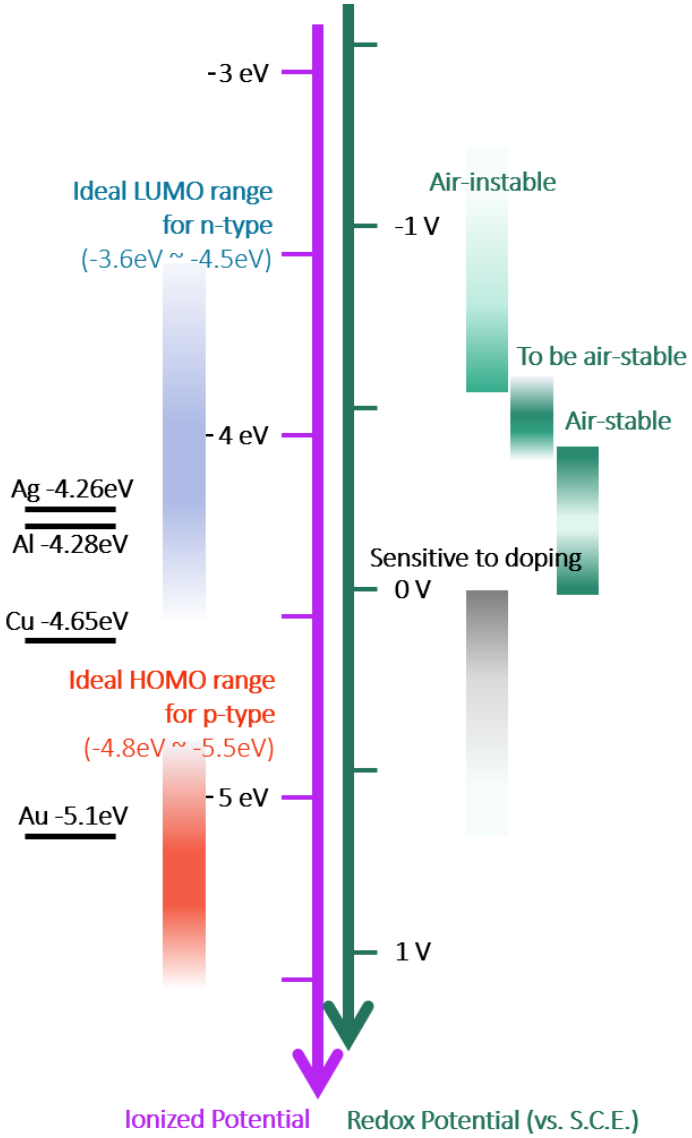

Figure 1. 6 Proper frontier molecular energy levels of organic materials for OFET applications.

Like above materials, organic materials for OFET application should have fulfilled their FMOs with work functions of electrode metal. For generate p-type transistor, as shown in Figure 1.6, HOMOs of organic materials are in range of -4.8eV to -5.5eV for matching work function of gold metal. In case of n-type transistor, LUMOs of organic materials are in range of -3.6eV to -4.5eV for effective electron injection.[14)]

Organic materials for OFET application are satisfied several conditions like that. Besides their FMO energy levels, high degree of coplanarity, intermolecular π-orbital overlap in plane of backbone, film morphology, and solubility are also considered necessarily.

1.2 Organic dyes containing lactam moiety

1.2.1 Why lactam-functionalized materials are of interest

Chemical modification of lactam groups does not effectively alter optoelectronic properties of semiconductors because of the orbital nodes. Theses orbital nodes are at the nitrogen atom on lactam in frontier molecular orbitals (FMOs). Therefore, many researchers' effort results in lactam-functionalized organic semiconductors utilizing core-substituted acenes. Once lactam moiety is including to core, it is enable to tune band-gap energy (E_g) and lower LUMOs. It leads facile charge injection between electrode and organic active layers and improves device stability in ambient condition.[17] Until now, lactam-functionalized molecules are one of the most successful n-type organic semiconductors.[13-b,c,d,m] Some reviews summarized the synthetic methods, optoelectronic properties, structure-property relationships, and performance of lactam containing molecules.[18]

The advantages of lactam-containing molecules are follows: 1) stabilize LUMOs of molecules due to strong electron withdrawing property. 2) well-expanded π-conjugation without disturbing co-planar structure of backbone. 3) introduce N-alkyl chain or N-aryl functionalities. It could be controlled solubility, film morphology, and steric hindrance between adjacent molecules. 4) For upper reasons, intermolecular hopping of charge carriers are efficient and it facile materials accessibility.[12]

1.2.2 Isoindigo

As outlined above, lactam-containing organic dyes are promising for high performance organic semiconductors. Figure 1.7 shows variety of reported lactam-containing dyes with mentioned strategy at previous section named perlyene diimide, naphthalene diimide, pyromellitic diimide, thieno[3,4-c]pyrrole-4,6-dione, thienoisoindoledione, isoindigo (IID), thienoisoindigo (TIID), pechmann dyes, bithiophene imide, phthalimide, diketopyrrolopyrrole, and so on.

Among those molecules, IID is much preferred backbone for organic semiconductors. IID, structural isomer of the natural pigment indigo extracted from plants named isatis tinctoria (woad) [19-a, b, c], is naturally occurring indigoid dye. Isoindigo was evaluated in 1882 and its synthesis scheme was reported at 1988.[19-d] Although synthesis scheme of IID was reported early and a few of IID-based copolymers were patented in 2008, it was not in limelight as a building block for optoelectronic devices yet. When Reyonlds *et al*.[20] reported IID-based small molecules for organic photovoltaics, isoindigo was soon recognized as an ideal building block for optoelectronics. IID building block had strong electron-deficient character and broad absorption range. The first photovoltaic property was reported to different journal dependently in 2011.[21] The properties were not so much high at photovoltaics, soon after, another isoindigo-based polymer gave a PCE of 6.3% with $PC_{71}BM$.[22] IID has both strong electron-withdrawing character and shifting down LUMO levels of resulting polymers. The first OFET property was reported also in 2011.[23] High performance field-effect transistors (FETs) based on IID polymers were also realized with hole mobility as high as 3.62 $cm^{-2}V^{-1}s^{-1}$.[24] Since isoindigo was come to the spotlight in 2010, more than 100 papers appeared in the literature

covering various aspects of the blooming IID-material system. Some reviews were summarized isoindigo-based polymer and small molecules for opto-electronic devices with focus on structure-property relationships.[25)]

To sum up, IID has proven successful as an electron-accepting building block for the preparation of electroactive materials for organic electronics. Synthesis of IID is high yielding and easy to scale-up. It supports to enable the rapid development of a large number of molecular and polymeric isoindigo-based materials. Many materials have been shown remarkable optical, physical and electronic properties. The progress of isoindigo-based materials has been outstanding during 4 years, focusing in particular applications: OPVs and OFETs.

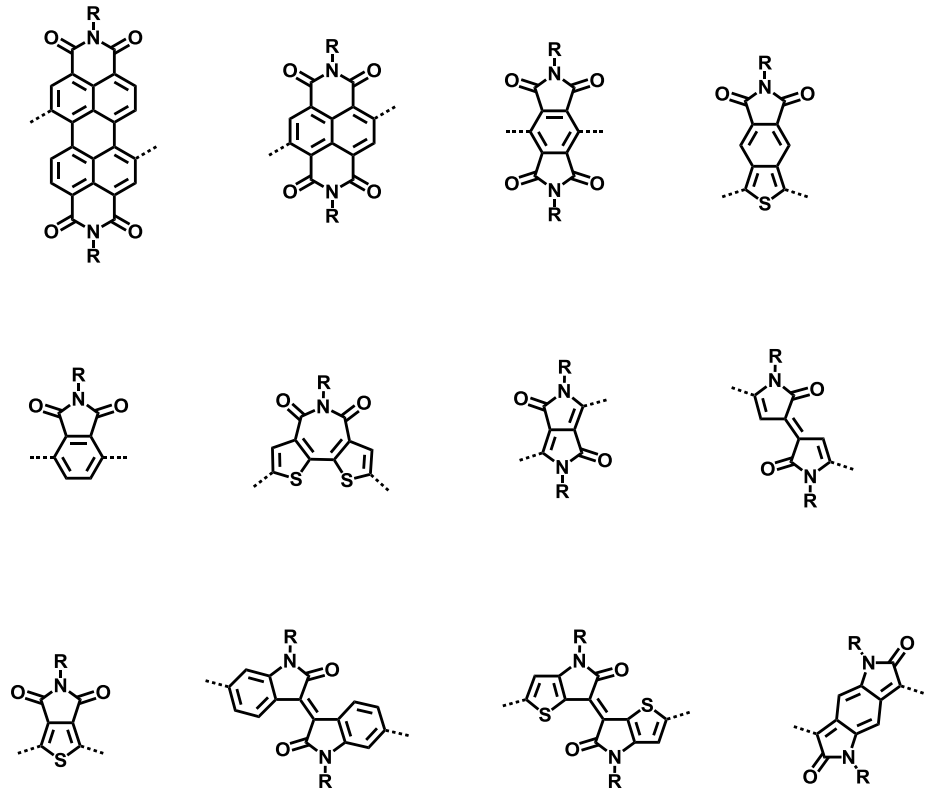

Figure 1. 7 Chemical structures of lactam-functionalized building block for organic semiconductors

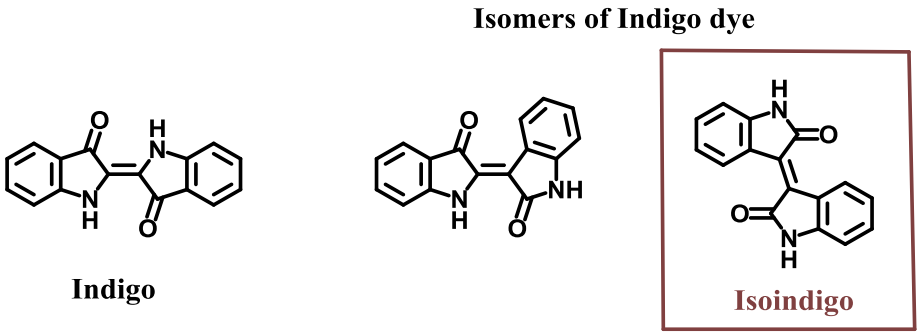

Figure 1. 8 Structure of indigo and isoindigo dyes

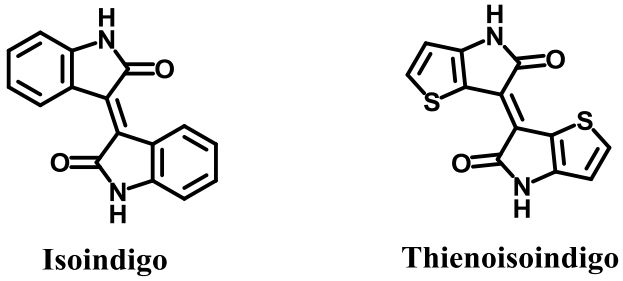

Figure 1. 9 Structure of isoindigo and thienoisoindigo

1.2.3 Thienoisoindigo

Recently, much more development of optoelectronics has been continuous. One of that, IID derivatives showed remarkable improvement as donor materials in organic solar cell and were take-off stage materials for OFETs. In other words, the promising device performance of IID polymers has encouraged their structural modifications for performance improvement especially in fields of OFETS. Even though IID building blocks promise absorption spectra, electrochemical, photovoltaic and FET properties, [22-25] some limits were existence. For this reason, McCulloch group reported new backbone called thienoisoindigo (TIID).[26] Figure 1.9 shows its structure. TIID geometry should lead to reduced steric hindrance in comparison to isoindigo. Slightly twisted geometry between carbonyl oxygen and phenyl hydrogen of IID hinders effective π- π interactions among the building blocks. Replacing phenyl ring with thiophene might exclude the possibility of steric hindrance and enhance the planarity along the backbone due to S···O interaction.

The unique structural features of TIID are capable of 1) inducing higher planarity to the molecular plane via S···O [27] favorable coulombic interactions, 2) enhancing the charge delocalization via quinoidal structure of the backbone, and 3) high lying HOMOs due to donating property of thiophene. Those characters lead to better molecular ordering, π-conjugation expansion, and charge transport efficiency.[28] First reported thienoisoindigo-based D-A polymer had good performance that was balanced ambipolar nature with 0.1 $cm^{-2}V^{-1}s^{-1}$ of hole mobility and 0.14 $cm^{-2}V^{-1}s^{-1}$ of electron mobility.[26] Recently, unprecedented mobility of 14.4 $cm^{-2}V^{-1}s^{-1}$ using naphthalene and TIID polymer with high-dielectric constant (k) gate dielectric was reported.[28]

To sum up, TIID has more broad absorption range in comparison to IID (it is

called panchromatic absorption). Because of thiophene unit, coplanarity is improved and better-expanded π-conjugation occurs. In addition, donating property of it leads high-lying HOMOs and it can be expected ambipolarity, which is unexpected result on isoindigo-based materials. If some synthetic problems were solved, TIID is future building block replaced IID or diketopyrrolopyrrole (DPP).

1.3 Research objectives

The research about the relationships among structure, optoelectric properties, and device application has drawn great attention in a field of material science and engineering. In particular, I was interested in the interplay of structure-property relationships, which is a significant issue for material design at a first level. Since supramolecular structures can determine self-assembly property, it is crucial to understand their correlations, which are decisive factors in applications.

Isoindigo (IID) and thienoisoindigo (TIID) are promising electron accepting units for D-A type polymer. Lactam moieties decide above mentioned their unique properties and encourage to design of various derivatives. For solubilizing, substitution of alkyl chains on nitrogen atom in lactam was useful and common method. In addition, aromatic groups were substitution for conjugation expansion of entire system. Further, as case of polymer system, there were already lots of IID or TIID-based materials with high performance on optoelectronic devices. However, in case of small molecules, there were few of materials reported and many chances for research were exist with some concepts. Moreover, comparison of isoindigo and thienoisoindigo had not been reported yet although two cores are similar and different.

Herein, I focused the two electron-accepting building block shown at Figure 1.8, which were, IID and TIID, for comparison of structure-property relationships. Among the related papers, there had been no paper for direct comparison between IID and TIID as aspect of structure. Therefore, I concentrated on direct comparison of features between IID and TIID backbone. Based on molecular designed, I studied different series of IID and TIID

molecules and investigated their optoelectronic properties. In particular, I focused the structure-property relationships based on S···O interaction in TIID core.

In chapter 2, I juxtaposed two cores, IID and TIID, and OFET targeted four small molecules for exploring structure-property relationships using IID and TIID backbone. Basic optoelectronic properties were recorded by UV/VIS spectroscopy and electrochemical properties were determined by using cyclic voltammetry (CV) and ultraviolet photoelectron spectroscopy (UPS). Their structures were predicted by density functional theory (DFT) and visualized by drop-casting single crystal formation. For supporting existence of S···O secondary interaction, FT-IR analysis was followed. Consequently, I demonstrated properties of molecules when they were used by organic active layer in OFET device.

In chapter 3, I designed new D-A type polymer for comparison of two backbones. Of course, I used IID and TIID as acceptor-units. I chose donor-unit called fluorinated indoloindole (IDIDF) as a strong donor-unit not yet reported. Polymer structures and frontier molecular orbital energy levels could be predicted by density functional theory (DFT) calculation. Basic characteristics were extracted from UV/VIS, GPC, CV, and DSC. Through those characteristics, two polymers were very low bandgap D-A polymers so that they were identified sufficiently targeting ambipolar OFET application. Finally, I demonstrated ambipolar field-effect properties using solution-processed OFET devices.

1.4 Bibliography

1) M. Mas-Torrent, C. Rovira, *Chem. Soc. Rev*., **2008**, 37, 827

2) G. Horowitz, *Adv. Mater*. **1998**, 10, 365

3) (a) D. F. Barbe, C. R. Westgate, *J. Phys. Chem. Solids* **1970**, 31, 2679. (b) M. L. Petrova, L. D. Rozenshtein, Fiz. Tverd. Tela *(Sov. Phys.-Solid State)* **1970**, 12, 961. (c) F. Ebisawa, T. Kurokawa, S. Nara, *J. Appl. Phys*. **1983**, 54, 3255.

4) H. Koezuka, A. Tsumura, T. Ando, *Synth. Met*. **1987**, 18, 699; A. Tsumura, H. Koezuka, Y. Ando, *Synth. Met*. **1988**, 25, 11.

5) Y. Shirota, H. Kageyama, *Chem. Rev.,* **2007,** 107, 953

6) C.R. Newman, C.D. Frisbie, D.A. da Silva Filho, J-L. Bredas, P.C. Ewbank, K.R. Mann, *Chem. Mater.,* **2004**, 16, 4436

7) Veres, J., Ogier, S., Lloyd,G., de Leeuw, D.,Chem Mater, **2004**, 16, 4543

8) (a) Klauk H, Halik M, Zschieschang U, Schmid G, Radlik W and Weber W *J. Appl. Phys*. **2002**, 92, 5259. (b) Sundar V C, Zaumseil J, Podzorov V, Menard E, Willett R L, Someya T, GershensonM E and Rogers J A, Science, **2004**, 03, 1644. (c) McCulloch I et al., *Nat. Mater.,* **2006**, 5, 328. (d) Yuan, Y., G. Giri, A. L. Ayzner, A. P. Zoombelt, S. C. B. Mannsfeld, J. Chen, D. Nordlund, M. F. Toney, J. Huang, Z. Bao, *Nature Commun.* **2014**, 5, 3005. (e) Dimitrakopou los C D, Furman B K, Graham T, Hegde S and Purushothaman S *Synth. Met.* **1998**, 92, 47. (f) Katz H E, Lovinger A J and Laquindanum J G., *Chem. Mater*.,**1988**, 10, 457. (g) Sirringhaus H, Tessler N and Friend R H, *Science*, **1998**, 280, 1741 (h) Yamamoto T and Takimiya

K, *J. Am. Chem. Soc.*, **2007**, 129, 2224. (i) Takimiya K, Kunugi Y and Otsubo T, *Chem. Lett*., **2007**, 36, 578. (j) Meng H, Sun F, Goldfinger M B, Jaycox G D, Li Z, Marshall W J and Blackman G S, *J. Am. Chem. Soc*., **2005**, 127, 2406. (k) Merlo J A, Newman C R, Gerlach C P, Kelley T W, Muyres D V, Fritz S E, Toney M F and Frisbie C D, *J. Am. Chem. Soc.*, **2005**, 127, 3997. (l) Ichikawa M, Yanagi H, Shimizu Y, Hotta S, Suganuma N, Koyama T and Taniguchi Y, *Adv. Mater.,* **2002**, 14, 1272. (m) Bao Z, Lovinger A J and Dodabalapur A, *Appl. Phys. Lett*., **1996**, 69, 3066. (n) Zeis R, Siegrist T and Kloc Ch, *Appl. Phys. Lett*., **2005**, 86, 022103.

9) Horowitz G, Garnier F, Yassar A, Hajlaoui R and Kouki F, *Adv. Mater.* **1996**, 8, 52.

10) Diao, Y.; Tee, B. C. K.; Giri, G.; Xu, J.; Kim, D. H.; Becerril, H. A.; Stoltenberg, R. M.; Lee, T. H.; Xue, G.; Mannsfeld, S. C. B.; Bao, Z. *Nat. Mater.* ***2013,*** 12, 665.

11) (a) Park, J. H.; Jung, E. H.; Jung, J. W.; Jo, W. H. *Adv. Mater*. **2013**, 25, 2583. (b) Zhang, X.; Richter, L. J.; DeLongchamp, D. M.; Kline, R. J.;Hammond, M. R.; McCulloch, I.; Heeney, M.; Ashraf, R. S.; Smith, J. N.;Anthopoulos, T. D.; Schroeder, B.; Geerts, Y. H.; Fischer, D. A.; Toney, M. F. *J. Am. Chem. Soc.* **2011**, 133, 15073.

12) X. Guo, A. Facchetti, T. J. Marks, *Chem. Rev.*, 2014, 114, 8943

13) (a) Bao Z, Lovinger A J and Brown J, *J. Am. Chem. Soc*., **1998**, 120, 207. (b) Chesterfield R J, McKeen J C, Newman C R, Ewbank P C, da Silva Filho D A, Bredas J L, Miller L L, Mann K R and Frisbie C D, *J. Phys. Chem. B*, **2004**, 108, 19281. (c) Katz H E, Johnson J, Lovinger A J and Li W, *J. Am. Chem. Soc.*, **2000**, 122, 7787. (d) Katz H E, Lovinger A J,

Johnson J, Kloc C, Siegrist T, Li W, Lin Y and Dodabalapur A, *Nature*, **2000,** 404, 478. (e) Facchetti A, Yoon M H, Stern C L, Katz H E and Marks T J, *Angew. Chem. Int. Edn*, **2003,** 42, 3900. (f) Th. B. Singh, N. Marjanovic, P. Stadler, M. Auinger, G. J. Matt, S. Gu¨nes, N. S. Sariciftci, R. Schwo¨ diauer and S. Bauer, *J. Appl. Phys.*, **2005,** 97, 083714. (g) Haddon R C, Perel A S, Morris R C, Palstra T T M, Hebard A F and Fleming R M, *Appl. Phys. Lett.*, **1995**, 67, 121. (h) Laquindanum J G, Katz H E, Dodabalapur A and Lovinger A J, *J. Am. Chem. Soc.*, **1996**, 118, 11331. (i) Sakamoto Y, Suzuki T, Kobayashi M, Gao Y, Fukai Y, Inoue Y, Sato F and Tokito S, *J. Am. Chem. Soc.*, **2004,** 126, 8138. (j) Yoon M H, DiBenedetto S A, Facchetti A and Marks T J, *J. Am. Chem. Soc.*, **2005**, 127, 1348. (k) Ando S, Murakami R, Nishida J, Tada H, Inoue Y, Tokito S and Yamashita Y, *J. Am. Chem. Soc.*, **2005**, 127, 14996. (l) Ando S, Nishida J, Tada H, Inoue Y, Tokito S and Yamashita Y, *J. Am. Chem. Soc*.**,2005**, 127, 5336. (m) W.S. Yoon, S.K. Park, I. Cho, J. Oh, J. H. Kim, S.Y. Park, *Adv. Funct. Mater.*, **2013**, 23, 3519. (n) S.W. Yun, J.H. Kim, S.H. Shin, H.C. Yang, B.K. An, L. Yang, S.Y. Park, *Adv. Mater.*, **2012**, 24, 911 (o) S.K. Park, S.H. Kim, S.J. Yon, O.K. Kwon, B.K. An, S.Y. Park, *Chem. Mater.*, **2012**, 24, 3263.

14) McCulloch, I.; Heeney, M.; Chabinyc, M. L.; DeLongchamp, D.; Kline, R. J.; Cölle, M.; Duffy, W.; Fischer, D.; Gundlach, D.; Hamadani, B.; Hamilton, R.; Richter, L.; Salleo, A.; Shkunov, M.; Sparrowe, D.; Tierney, S.; Zhang, W. *Adv. Mater.* **2009**, 21, 1091.

15) I.G. Lezama and A.F. Morpurgo, *MRS Bulletin*, **2013**, 38, 51

16) T. Mori, *J.Phys.:Condens.Matter.*, **2008**, 20, 184010

17) Jones, B. A.; Facchetti, A.; Wasielewski, M. R.; Marks, T. J. *J. Am. Chem. Soc*. **2007**, 129, 15259.

18) (a) Zhan, X.; Facchetti, A.; Barlow, S.; Marks, T. J.; Ratner, M. A.; Wasielewski, M. R.; Marder, S. R. *Adv. Mater.* **2011**, 23, 268. (b) Jung, B. J.; Tremblay, N. J.; Yeh, M.-L.; Katz, H. E. *Chem. Mater.*, **2010**, 23, 568

19) (a) M. Puchalsk, K. Polec-Pawlak, I. Zadrozna, H. Hryszko, M. Jarosz, *J. Mass. Spectrom*. **2004**, 39, 1441. (b) Thierry Maugarda, Estelle Enauda, Patrick Choisyb, M. D. Legoya, *Phytochemistry.* **2001**, 58, 897. (c) T. Mohn, I. Plitzko, M. Hamburger, *Phytochemistry*. **2009**, 70, 924. (d) A. Baeyer, V. Drewsen, *Ber. Deut. Chem. Ges.* **1882**, 15, 2856

20) J. Mei, K. R. Graham, R. Stalder, J. R. Reynolds, *Org. Lett.* **2010**, 12, 660 .

21) G. Zhang, Y. Fu, Z. Xie, Q. Zhang. *Macromolecules*, **2011**, 44, 1414. (b) B. Liu, Y. Zou, B. Peng, B. Zhao, K. Huang, Y. He, C. Pan, *Polym. Chem.* **2011**, 2, 1156. (c) E. Wang, Z. Ma, Z. Zhang, P. Henriksson, O. Inganäs, F. Zhang, M. R. Andersson, *Chem. Commun.* **2011**, 47, 4908.

22) W. Elsawy, C.-L. Lee, S. Cho, S.-H. Oh, S.-H. Moon, A. Elbarbary, J.-S. Lee, *Phys. Chem. Chem. Phys.* **2013**, 15, 15193.

23) T. Lei, Y. Cao, Y. Fan, C.J. Kiu, S.C. Yuan, J. Pei, *J. Am. Chem. Soc.*, **2011**, 133, 6099.

24) (a) T. Lei, J.-H. Dou, Z.-J. Ma, C.-H. Yao, C.-J. Liu, J.-Y. Wang, J. Pei, *J. Am. Chem. Soc.* **2012**, 134, 20025. (b) J. Mei, D. H. Kim, A. L. Ayzner, M. F. Toney, Z. Bao, *J. Am. Chem. Soc.* **2011**, 133, 20130. (c) T. Lei, J.-H. Dou, J. Pei, *Adv. Mater.* **2012,** 24, 6457.

25) E. Wang, W. Mammo, M.R. Andersson, *Adv. Mater.* **2014**, 26, 1801

26) R.S. Ashraf, A.J. Kronemeijer, D.I. James, H. Sirringhaus, I. McCulloch, *Chem. Comm.* **2012**, 48, 3939.

27) J.G. Angyan, R.A. Poirier, A. Kucsman, I.G. Csizmadia, *J. Am. Chem. Soc.*, **1987**, 109, 2237 ; F. Temple Burling, and Barry M. Goldstein, *J. Am Chem. Soc.*, **1992**, 114, 2313

28) G. Kim, S. Kang, G.K. Dutta, Y.K. Han, T.J. Shin, Y.Y. Noh, C. Yang, *J. Am. Chem. Soc.*, **2014**, 136, 9477.

29) H. Chen, Y. Guo, G. Yu, Y. Zhao, J. Zhhang, D. Gao, H. Liu, Y. Liu, *Adv. Mater.* **2012**, 24, 4618

Chapter 2. Study on Structure-Property relationship of Isoindigo and Thienoisoindigo with Tuning Frontier Molecular Orbital

2.1 Introduction

The advantage of D-A type polymers is that the photoelectronic properties including absorption spectra and energy levels can be easily tuned by combining different electron-rich and electron-deficient units as well as by substituting different side groups.[1)] Even though polymer devices exhibit high performances, the variation in performances based on synthetic bath of polymer makes difficult to commercialize. Polymer synthesis has some problems *i.e.*, changing in solubility, molecular weight (and molecular weight distribution), and purity. Impurity in polymer is the main factor that determines the performance by decreasing charge carrier mobility in device. Whereas polymer has such problem, small molecules or oligomer solved the problems especially impurity. Advantages of small molecule or oligomer were no synthetic batch dependence, high purity, fixation of molecular weight, and relatively high charge carrier mobility. [2)]

In case of isoindigo (IID) -based small molecule (or oligomer), there was rarely reported paper about n-type OFET[3-a,b)] even though p-type OFET[3-c)] also. They were designed small molecules, which had low band-gap. In addition, Thienoisoindigo (TIID)-based small molecule was reported once for OPV before.[3-d)] Other reported TIID-based molecules were all polymer for optoelectronic devices. All these reports were focused on high performance. Even though isoindigo and thienoisoindigo were quite similar, no report about

differences of two cores based on structure-property relationships has been until now.

Herein, in this work, I studied structure-property relationships of isoindigo and thienoisoindigo. Study on structure-property relationships was suitable in small molecule systems because well-ordered supramolecular structure of small molecules support easy comparison. First, I studied basic optoelectronic properties of 4 core molecules named EHIID, EHIID2Br, EHTIID and EHTIID2Br at scheme 2.1. After that, I designed 4 small molecules shown at scheme 2.2 for targeting OFET device applications. I designed those molecules with fascinated concepts. 1) Structures were well-organized push-pull structure through novel A-D-A-D-A type for easy intramolecular charge transfer (ICT) and low band-gap. 2) Incorporation of dicyanovinyl (DCV) group, which is very strong electron-accepting units for lowering LUMO without distorting coplanarity of backbone.[4)] 3) For easy comparing to aromatic backbones, IID and TIID, I designed structure all-the-same details except core unit.

All target materials were successfully synthesized and characterized to confirm their basic optoelectronic properties. I identified the difference of IID series and TIID series by UV/VIS spectroscopy and DFT calculation.

For basic studies on core units, I recognized that thienoisoindigo core affected effective expansion of π-conjugation by planarization of core which caused by S···O secondary interaction as shown in UV/VIS spectra and DFT calculations.

As I mentioned above, for targeting low-lying LUMO levels, I incorporated DCV units to OFET targeted molecules and I successfully tuned the LUMO level, which was low-lying to about -4.0eV. In case of TIID series, HOMOs were high lying about 0.4eV higher than IID series because of donating

property of thiophene in thienoisoindigo core. Through this phenomenon, I expected that IID series were shown n-type transistor and TIID series were shown ambipolar transistors.

Fabrication type of OFETs was ‘bottom-gate top-contact’ and organic layers were vacuum deposited on SiO_2 substrates. Consequently, IID series named EHIIDPDCV and EHIIDTDCV were shown n-type charge transport properties and EHIIDTDCV was better than EHIIDPDCV. I also expected TIID series named EHTIIDPDCV and EHTIIDTDCV were shown ambipolar transistors as I mentioned above. Unfortunately, EHTIIDTDCV and EHTIIDPDCV was failed to deposit organic layers because of poor thermostability and poor processability at vacuum deposited conditions.

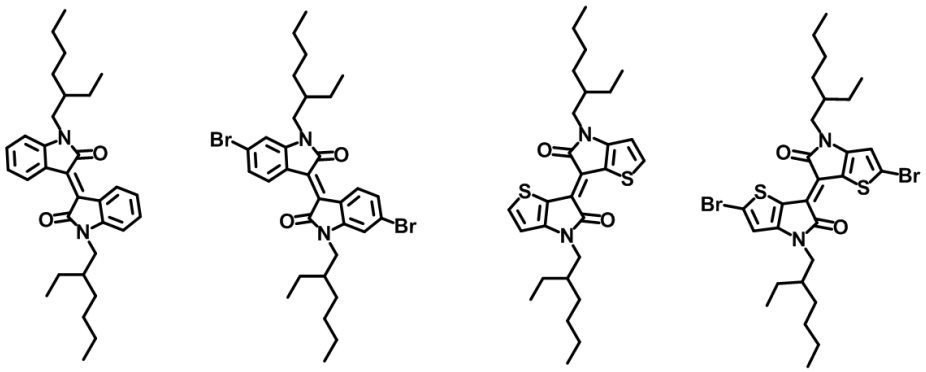

Scheme 2. 1 First target molecules for basic studies on structure-property relationships by using optoelectronic properties

(a)

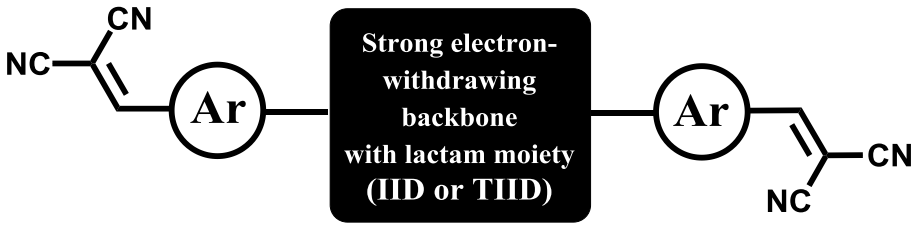

Ar = Benzene, Thiophene

(b)

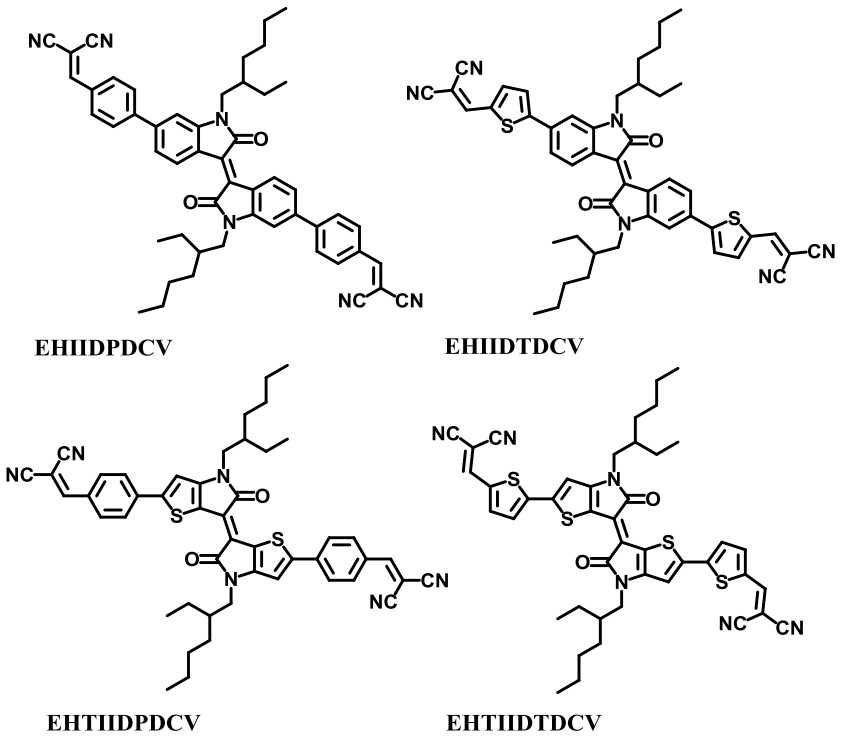

Scheme 2. 2 (a) Overall design strategy of 4 small molecules typed A-D-A-D-A. (b) Particular structures of 4 small molecules.

2.2 Experimental

2.2.1 Synthesis

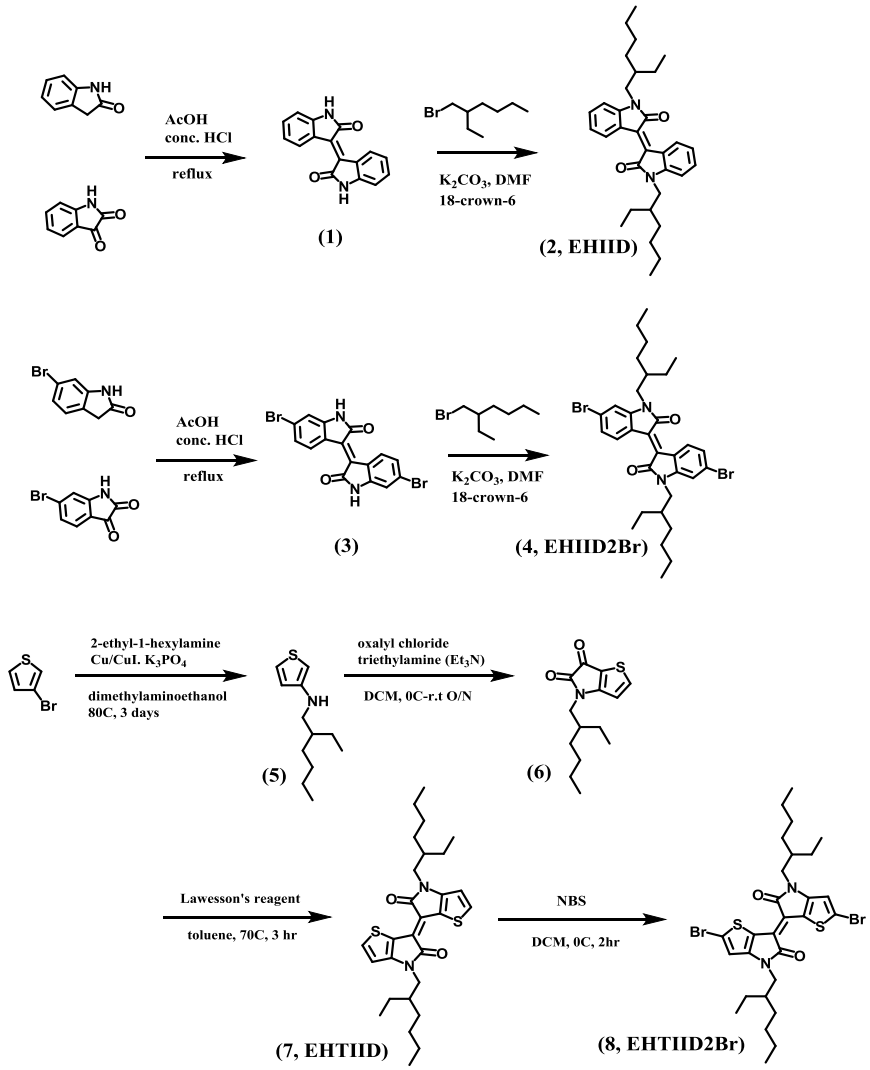

Scheme 2. 3 Synthetic route for 4 cores (EHIID, EHIID2Br, EHTIID, and EHTIID2Br)

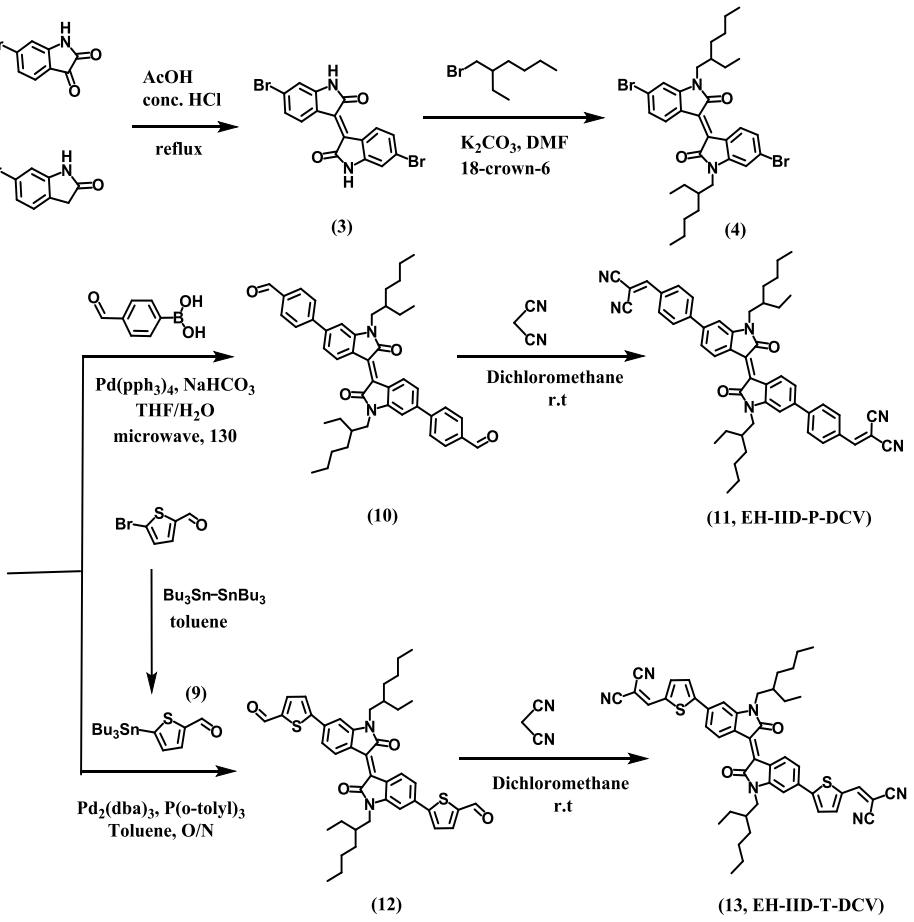

Scheme 2. 4 Synthetic route of isoindigo (IID) derivatives. (EH-IID-P-DCV, EH-IID-T-DCV)

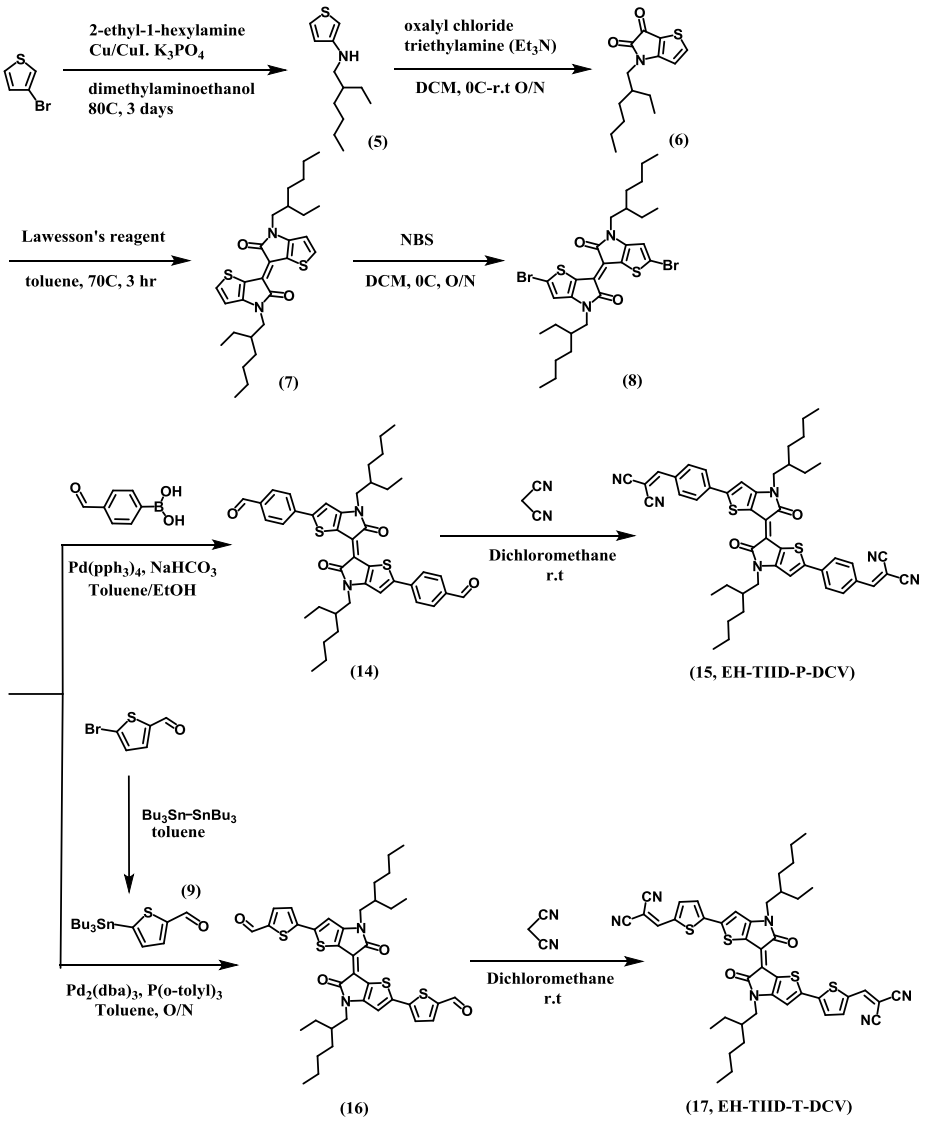

Scheme 2. 5 Synthetic route of thienoisoindigo (TIID) derivatives (EH-TIID-P-DCV, EH-TIID-T-DCV)

Target molecules were synthesized according to the procedure shown in Scheme 2.3, 2.4 and 2.5. Unless stated otherwise, all reagents were purchased at Sigma Aldrich, TCI, Acros Organics, and Alfa Aesar.

(E)-[3,3'-biindolinylidene]-2,2'-dione (1)

To a suspension of isatin (0.552g, 3.75mmol) and oxindole (0.5g. 3.75mmol) in acetic acid (30mL), concentrated HCl (0.2mL) was injected to a 100mL round bottom flask. The mixture was refluxed at 120℃ for 24hr. After cooling to room temperature, the mixture was filtrated. The powder was washed with H_2O, ethanol, and ethyl acetate many times. The resulting maroon colored powder was taken and dried overnight under vacuum. (0.7g, 2.67mmol, Yield 71.1%) ^{1}H NMR (300 MHz, DMSO) δ 10.89 (s), 9.06 (d, J = 7.7 Hz, 2H), 7.34 (td, J = 7.6, 1.0 Hz, 2H), 6.96 (dd, J = 11.4, 4.2 Hz, 2H), 6.84 (d, J = 7.6 Hz, 2H).

(E)-1,1'-bis(2-ethylhexyl)-[3,3'-biindolinylidene]-2,2'-dione (2, EHIID)

Compound (1) (0.7g, 2.67mmol) and potassium carbonate (1.844g, 13.35mmol) were dissolved in dimethyl formaldehyde (DMF) (40mL) to a 100mL round bottom flask and stirring for 1hr under Argon at 100℃. 2-ethyl-1-hexyl bromide (1.04mL, 5.87mmol) and 18-crown-6 ether (0.2g) was added. The mixture was refluxed overnight. After cooling to room temperature, mixture was poured into water. The organic phase was extracted with diethyl ether, washed with brine, and dried over $MgSO_4$. The organic solvent was evaporated and the deep red solids were purified by silica chromatography. The

resulting dark red colored powder was taken and dried overnight under vacuum. (0.81g, Yield 62.4%) ^{1}H NMR (300 MHz, $CDCl_3$) δ 9.16 (d, J = 8.0 Hz, 2H), 7.34 (t, J = 7.7 Hz, 2H), 7.04 (t, J = 7.8 Hz, 2H), 6.77 (d, J = 7.8 Hz, 2H), 3.80 – 3.55 (m, 4H), 1.96 – 1.75 (m, 2H), 1.48 – 1.16 (m, 16H), 1.04 – 0.79 (m, 12H).

(E)-6, 6'-dibromo-[3, 3'-biindolinylidene]-2, 2'-dione (3, EHIID2Br)

To a suspension of 6-bromoisatin (1.066g, 4.72mmol) and 6-bromooxindole (1.0g. 4.72mmol) in acetic acid (30mL), concentrated HCl (0.2mL) was injected to a 100mL round bottom flask. The mixture was refluxed at 120℃ for 24hr. After cooling to room temperature, the mixture was filtrated. The powder was washed with H_2O, ethanol, and ethyl acetate many times. The resulting maroon colored powder was taken and dried overnight under vacuum. (1.87g, 4.45mmol, Yield 94.4%) ^{1}H NMR (300 MHz, DMSO) δ 8.98 (d, *J* = 8.7 Hz, 2H), 7.17 (dd, *J* = 8.6, 1.9 Hz, 2H), 6.99 (sd, *J* = 1.9 Hz, 2H).

(E)-6, 6'-dibromo-1, 1'-bis (2-ethylhexyl)-[3, 3'-biindolinylidene]-2, 2'-dione (4, EH-IID-2Br)

Compound (3) (1.38g, 3.29mmol) and potassium carbonate (2.274g, 16.45mmol) were dissolved in dimethyl formaldehyde (DMF) (50mL) to a 100mL round bottom flask and stirring for 1hr under Argon at 100℃. 2-ethyl-1-hexyl bromide (1.29mL, 7.24mmol) and 18-crown-6 ether (0.2g) was added. The mixture was refluxed overnight. After cooling to room temperature, mixture was poured into water. The organic phase was extracted with diethyl ether, washed with brine, and dried over $MgSO_4$. The organic solvent was

evaporated and the deep red solids were purified by silica chromatography. The resulting dark red colored powder was taken and dried overnight under vacuum. (1.01g, Yield 47.9%) ^{1}H NMR (300 MHz, $CDCl_3$) δ 9.06 (d, *J* = 8.6 Hz, 2H), 7.17 (dd, *J* = 8.6, 1.8 Hz, 2H), 6.91 (sd, *J* = 1.8 Hz, 2H), 3.76 – 3.52 (m, 4H), 1.84 (s, 2H), 1.35 (dt, *J* = 13.2, 8.6 Hz, 16H), 1.05 – 0.78 (m, 12H).

N-(2-ethylhexyl)thiophen-3-amine (5)

Cupper powder (0.29g, 4.60mmol), Cupper Iodide (0.87g, 4.60mmol) and Potassium phosphate tribasic (39.06g, 184.01mmol) and dimethylaminoethanol 100mL was added to flame-dried 250mL round bottom flask. 3-bromothiophene (15.0g, 92.00mmol) was injected to mixture and vigorous stirred during 0.5hr. 2-ethyl-1-hexylamine (17.84g, 138.01mmol) was injected and refluxed 2days. After cooling to room temperature, the mixture was filtered with ethyl acetate. The filtrate was evaporated and crude oil was purified with column chromatography (eluent as ethyl acetate and hexane). The obtained yellowish brown oil was dried through vacuum oven. (Air-sensitive) (16g, Yield 82.28%) ^{1}H NMR (300 MHz, CDCl3) δ 7.14 (dd, J = 5.1, 3.0 Hz, 2H), 6.61 (dd, J = 5.1, 1.5 Hz, 2H), 5.92 (dd, J = 3.0, 1.5 Hz, 2H), 3.57 (s, 1H), 2.98 (d, J = 6.0 Hz, 2H), 1.67 – 1.48 (m, J = 11.9, 6.0 Hz, 2H), 1.48 – 1.33 (m, 6H), 1.00 – 0.75 (m, 10H).

4-(2-ethylhexyl)-4H-thieno[3,2-b]pyrrole-5,6-dione (6)

Compound (5) (3.0g, 14.19mmol) and dichloromethane 20mL was added to a flame-dried 100mL round bottom flask under Ar atmosphere and cooled down

using ice-bath. The dichloromethane (10mL) solution of oxalyl chloride (2.70g, 21.29mmol) was drop-wise added. The mixture was stirring for 0.5hr at 0℃. The dichloromethane (10mL) solution of trimethylamine (7.18g, 70.96mmol) was drop-wise added carefully. Then ice-bath was removed and the reaction mixture was stirred at room temperature during overnight. The mixture was worked-up with H_2O and extracted with dichloromethane. The organic phase was washed with brine over 3 times. The solvent was evaporated and crude solid was purified with column chromatography. The dark-orange oil was obtained and dried overnight though vacuum oven. Then, dark-orange solid was taken. (1.17g, Yield 31.25%) ^{1}H NMR (300MH, $CDCl_3$, δ) 8.00 (d, J = 5.0 Hz, 2H), 6.77 (d, J = 5.0 Hz, 2H), 3.54 (d, J = 8.0 Hz, 4H), 1.80 – 1.68 (m, 2H), 1.45 – 1.20 (m, 18H), 1.00 – 0.83 (m, 10H).

(E)-4,4'-bis(2-ethylhexyl)-[6,6'-bithieno[3,2-b]pyrrolylidene]-5,5'-(4H,4'H)-dione (7, EH-TIID)

In a 100mL round bottom flask, compound (6) (1.0g, 3.77mmol) was dissolved in toluene 40mL. Lawesson's reagent (0.90g, 2.07mmol) was added to mixture and stirred. The reaction mixture was heated to 70℃ during 3hr. The solvent was evaporated and crude solid was purified with column chromatography. The magenta-purple solid was obtained. (1.0g, Yield 53.18%) ^{1}H NMR (300MH, $CDCl_3$, δ) 7.52 (d, J = 5.1 Hz, 2H), 6.78 (d, J = 5.1 Hz, 2H), 3.69 (d, J = 7.4 Hz, 4H), 1.94-1.85 (m, 2H), 1.80 – 1.68 (m, 2H), 1.45 – 1.20 (m, 18H), 1.00 – 0.83 (m, 10H).

(E)-2,2'-dibromo-4,4'-bis(2-ethylhexyl)-[6,6'-bithieno[3,2-b]pyrrolylidene]-5,5'(4H,4'H)-dione (8, EH-TIID-2Br)

In a 100mL round bottom flask, compound (12) (0.9g, 1.90mmol) was dissolved in THF 40mL. The reaction mixture was cooling down to 0℃. The tetrahydrofuran (THF) solution of N-bromosuccinimide (0.76g, 4.29mmol) was slowly added. Then, mixture was warmed to room temperature and stirred for 3hr. The solution was work-up with brine and extracted with dichloromethane. After flash alumina column, fresh purple colored solid was obtained. (0.6g, Yield 48%) ^{1}H NMR (300MH, $CDCl_3$, δ) 6.82 (s, 2H), 3.64 (d, J = 7.5 Hz, 4H), 1.85 – 1.72 (m, 2H), 1.42 – 1.20 (m, 18H), 0.97 – 0.82 (m, J = 8.1 Hz, 10H).

5-(tributylstannyl)thiophene-2-carbaldehyde (9)

5-bromothiophene-2-carbaldehyde (4.11g, 21.54mmol) and Tetrakis(triphenylphosphine) palladium(0) (0.058g, 0.05mmol) was dissolved 100mL of toluene to a 250mL round bottom flask. Hexa-n-buthylditin (25g, 43.09mmol) was added to mixture. The solution was refluxed during 4 days. After cooling to room temperature, solvent was evaporated. The yellow crude oil was purified with column chromatography (eluent as ethyl acetate and hexane). Obtained pale-yellow oil was dried through vacuum oven. (6.85g, Yield 79.23%) ^{1}H NMR (300MH, $CDCl_3$, δ) 9.93 (s, 1H) 7.84(d, *J* = 3.4 Hz, 1H) 7.25 (d, *J* = 3.4 Hz, 1H) 1.55-1.70 (m, 6H) 1.28-1.40 (m, 10H) 0.88-1.14 (m, 11H)

(E)-4,4'-(1,1'-bis(2-ethylhexyl)-2,2'-dioxo-[3,3'-biindolinylidene]-6,6'-diyl)dibenzaldehyde (10)

Ar bubbled compound (4) (0.36g, 0.56mmol) and (4-formylphenyl)boronic acid (0.29g, 1.96mmol) are dissolved anhydrous tetrahydrofuran (THF) 6mL was taken in the microwave reactor tube. Tetrakis(triphenyl-phosphine)palladium(0) (0.065g, 0.056mmol) was added to mixture and sealed tightly after degassing. Sodium bicarbonate (0.23g, 2.79mmol) was dissolved with H_2O and subsequently added through septum. The tube was subjected to the microwave reactor and stirred under conditions of 150 ℃ for 40 min. After cooling to room temperature, the mixture was extracted with dichloromethane and washed with brine. The organic phase was evaporated and brown crude solid was purified with column chromatography. The resulting brown colored powder was taken and dried overnight under vacuum. (0.22g, Yield 56.1%) ^{1}H NMR (300 MHz, $CDCl_3$) δ 10.09 (s, 2H), 9.30 (d, *J* = 8.4 Hz, 2H), 8.00 (d, *J* = 8.1 Hz, 4H), 7.80 (d, *J* = 8.1 Hz, 4H), 7.34 (dd, *J* = 8.4, 1.7 Hz, 2H), 7.03 (s, 2H), 3.89 – 3.67 (m, 4H), 2.02 – 1.84 (m, 2H), 1.33 (d, *J* = 44.9 Hz, 16H), 1.10 – 0.79 (m, 12H).

(E)-2,2'-(((1,1'-bis(2-ethylhexyl)-2,2'-dioxo-[3,3'-biindolinylidene]-6,6'-diyl)bis(4,1-phenylene))bis(methanylylidene))dimalononitrile (11, EH-IID-P-DCV)

Compound (10) (0.10g, 0.14mmol), malononitrile (0.03g, 0.43mmol) and aluminum oxide (0.10g, 0.98mmol) was dissolved in 30mL of dichloromethane to a 50mL round bottom flask. The mixture was stirring at room temperature overnight. The solution was passed through alumina packed short column, and

solvent evaporation was followed. The crude solid was reprecipitated on methanol. For further purification, recrystallization using ethyl acetate was followed. The highly pure dark brown powder was affordable. (0.06g, Yield 50%) ^{1}H NMR (300 MHz, $CDCl_3$) δ 9.31 (d, *J* = 8.4 Hz, 2H), 8.04 (d, *J* = 8.4 Hz, 4H), 7.82 (s, 2H), 7.81 (d, *J* = 6.2 Hz, 4H), 7.35 (dd, *J* = 8.5, 1.4 Hz, 2H), 7.03 (s, 2H), 3.84 – 3.69 (m, 4H), 2.00 – 1.86 (m, 2H), 1.49 – 1.24 (m, 16H), 0.97 (t, *J* = 7.4 Hz, 6H), 0.91 (d, *J* = 6.8 Hz, 6H)

(E)-5,5'-(1,1'-bis(2-ethylhexyl)-2,2'-dioxo-[3,3'-biindolinylidene]-6,6'-diyl)bis(thiophene-2-carbaldehyde) (12)

Compound (4) (0.30g, 0.45mmol) and compound (9) (0.45g, 11.28mmol) was dissolved to anhydrous tetrahydrofuran (THF) 10mL and degassing through Ar bubbling. The solution was injected to 50mL round bottom flask under Ar atmosphere. Tris(dibenzylideneacetone) dipalladium(0) (0.02g, 0.02mmol) and tri(o-tolyl)phosphine (0.03g, 0.09mmol) was also dissolved in anhydrous tetrahydrofuran (THF) 10mL and degassing. The solution was added to mixture of round bottom flask and refluxed 48hr. After cooling to room temperature, the mixture was extracted with dichloromethane and washed with brine. The organic phase was evaporated and residue crude was purified with column chromatography (eluent as dichloromethane, ethyl acetate and hexane). Obtained brown solid was dried overnight through vacuum oven. (0.15g, Yield 47.03%) ^{1}H NMR (300 MHz, $CDCl_3$) δ 9.93 (s, 2H), 9.24 (d, *J* = 8.4 Hz, 2H), 7.78 (d, *J* = 4.0 Hz, 2H), 7.50 (d, *J* = 4.0 Hz, 2H), 7.38 (dd, *J* = 8.4, 1.7 Hz, 2H), 7.04 (d, *J* = 1.4 Hz, 2H), 3.84 – 3.65 (m, 4H), 1.90 (s, 2H), 1.51 – 1.28 (m, 16H), 0.98 (t, *J* = 7.4 Hz, 6H), 0.91 (t, *J* = 6.8 Hz, 6H)

(E)-2,2'-(((1,1'-bis(2-ethylhexyl)-2,2'-dioxo-[3,3'-biindolinylidene]-6,6'-diyl)bis(thiophene-5,2-diyl))bis(methanylylidene))dimalononit-rile (13, EH-IID-T-DCV)

Compound (12) (0.15g, 0.21mmol), malononitrile (0.04g, 0.64mmol), and aluminum oxide (0.15g, 1.47mmol) was dissolved in 30mL of dichloromethane to a 50mL round bottom flask. The mixture was stirring at room temperature overnight. The solution was passed through alumina packed short column, and solvent evaporation was followed. The crude solid was reprecipitated on methanol. For further purification, recrystallization using ethyl acetate was followed several times. The highly pure dark brown powder was affordable. (0.14g, Yield 83%) ^{1}H NMR (300 MHz, $CDCl_3$) δ 9.26 (d, *J* = 8.4 Hz, 2H), 7.81 (s, 2H), 7.78 (d, *J* = 4.1 Hz, 2H), 7.53 (d, *J* = 4.1 Hz, 2H), 7.40 (dd, *J* = 8.4, 1.6 Hz, 2H), 7.04 (sd, *J* = 1.5 Hz, 2H), 3.83 – 3.68 (m, 4H), 1.94 – 1.80 (m, 2H), 1.51 – 1.28 (m, 16H), 0.98 (t, *J* = 7.4 Hz, 6H), 0.91 (t, *J* = 6.8 Hz, 6H)

(E)-4,4'-(4,4'-bis(2-ethylhexyl)-5,5'-dioxo-4,4',5,5'-tetrahydro-[6,6'-bithieno[3,2-b]pyrrolylidene]-2,2'-diyl)dibenzaldehyde (14)

Ar bubbled compound (8) (0.20g, 0.31mmol) and (4-formylphen-yl)boronic acid (0.16g, 1.07mmol) are dissolved toluene 20mL was taken in the 100mL round bottom flask under Ar atmosphere. Tetrakis(triphenyl-phosphine)palladium(0) (0.04g, 0.03mmol) was added to mixture. Sodium carbonate (0.19g, 1.83mmol) was dissolved with H_2O and subsequently added. The mixture was refluxed for 48hr. After cooling to room temperature, the mixture was extracted with dichloromethane and washed with brine. The organic phase was evaporated and crude solid was purified with column

chromatography. The resulting dark greenish cyan colored powder was taken and dried overnight under vacuum. (0.13g, Yield 60.37%) ^{1}H NMR (300MH, $CDCl_3$, δ) 10.03 (s, 2H), 7.95 – 7.86 (m, J = 5.9 Hz, 8H), 7.14 (s, 2H), 3.76 (d, J = 7.5 Hz, 4H), 2.00 – 1.81 (m, 2H), 1.48 – 1.18 (m, 18H), 1.05 – 0.79 (m, 10H).

(E)-2,2'-(((4,4'-bis(2-ethylhexyl)-5,5'-dioxo-4,4',5,5'-tetrahydro-[6,6'-bithieno[3,2-b]pyrrolylidene]-2,2'-diyl)bis(4,1-phenylene))-bis(methanyl-ylidene))dimalononitrile (15, EH-TIID-P-DCV)

Compound (14) (0.13g, 0.18mmol), malononitrile (0.04g, 0.64mmol), and aluminum oxide (0.13g, 1.26 mmol) was dissolved in 30mL of dichloromethane to a 50mL round bottom flask. The mixture was stirring at room temperature overnight. The solution was passed through alumina packed short column, and solvent evaporation was followed. The crude solid was reprecipitated on methanol. For further purification, recrystallization using dichloromethane was followed. The highly pure dark green powder was affordable. (0.10g, Yield 67.71%) ^{1}H NMR (300MH, $CDCl_3$, δ) 7.96 (d, J = 8.3 Hz, 4H), 7.87 (d, J = 8.7 Hz, 4H), 7.72 (s, 2H), 7.16 (s, 2H), 3.76 (d, J = 7.6 Hz, 4H), 1.98 – 1.83 (m, 2H), 1.47 – 1.21 (m, 18H), 1.02 – 0.80 (m, 10H).

(E)-5,5'-(4,4'-bis(2-ethylhexyl)-5,5'-dioxo-4,4',5,5'-tetrahydro-[6,6'-bithieno[3,2-b]pyrrolylidene]-2,2'-diyl)bis(thiophene-2-carbaldehyde) (16)

Compound (8) (0.30g, 0.46mmol) and compound (9) (0.64g, 1.60mmol) was dissolved to anhydrous toluene 10mL and degassing through Ar bubbling. The

solution was injected to flame dried 50mL round bottom flask under Ar atmosphere. Tris(dibenzylideneacetone)-dipalladium(0) (0.02g, 0.02mmol) and tri(o-tolyl)phosphine (0.03g, 0.09mmol) was also dissolved in anhydrous toluene 10mL and degassing. Then solution was added to mixture of round bottom flask and refluxed overnight. After cooling to room temperature, the mixture was extracted with dichloromethane and washed with brine. The organic phase was evaporated and residue crude was purified with column chromatography (eluent as dichloromethane, ethyl acetate and hexane). Obtained dark greenish solid was dried overnight through vacuum oven. (0.15g, Yield 45.35%) ^{1}H NMR (300 MHz, $CDCl_3$) δ 9.89 (s, 2H), 7.70 (d, J = 4.0 Hz, 2H), 7.45 (d, J = 4.0 Hz, 2H), 7.00 (s, 4H), 3.73 (d, J = 7.6 Hz, 4H), 1.96 – 1.80 (m, 2H), 1.49 – 1.14 (m, 18H), 1.05 – 0.74 (m, 10H).

(E)-2,2'-(((4,4'-bis(2-ethylhexyl)-5,5'-dioxo-4,4',5,5'-tetrahydro-[6,6'-bithieno[3,2-b]pyrrolylidene]-2,2'-diyl)bis(thiophene-5,2-diyl))bis-(methanylylidene))dimalononitrile (17, EH-TIID-T-DCV)

Compound (16) (0.15g, 0.21mmol), malononitrile (0.07g, 0.84mmol), and aluminum oxide (0.15g, 1.47mmol) was dissolved in 30mL of dichloromethane to a 50mL round bottom flask. The mixture was stirring at room temperature overnight. The solution was passed through alumina packed short column, and solvent evaporation was followed. The crude solid was reprecipitated on methanol. For further purification, recrystallization using dichloromethane was followed. The highly pure dark green powder was affordable. (0.10g, Yield 67.71%) ^{1}H NMR (300 MHz, $CDCl_3$) δ 7.77 (s, 2H), 7.64 (d, J = 4.1 Hz, 2H), 7.48 (d, J = 4.1 Hz, 2H), 7.05 (s, 2H), 3.74 (d, J = 7.3 Hz, 4H), 1.97 – 1.82 (m, 2H), 1.48 – 1.14 (m, 18H), 1.01 – 0.74 (m, 10H).

2.2.2 Instruments and measurements

All synthesized materials were identified with 1H NMR (Bruker, Avance-300) with deuterated solvent $CDCl_3$ and DMSO-d_6. Further, for target molecules, GC-Mass (JEOL, JMS-700) and elemental analysis (CE Instrument, EA1110) were also used. The melting temperature of the target molecules was determined using DSC (TA instruments, Q1000) under N_2 atmosphere. Decomposition temperature was determined using thermal gravimetric analyzer (TGA, TA instruments, Q-5000 IR) under N_2 atmosphere. FT-IR studies are done using FT-r spectrometer (Thermo Scientific, Nicolet 6700).

UV/VIS absorption spectra were detected by SHIMADZU UV-1650PC in both solution and film state. The frontier orbital energy levels, especially HOMOS, were recorded on cyclic voltammetry (CV, Princeton Applied Research, 273 A) for solution and solid state and ultraviolet photoelectron spectroscopy (UPS, Hitachi High Tech, AC-2) for film state. For CV detection, I used one-component electrolysis cell consisting of a platinum working electrode, a platinum wire counter-electrode, and a quati Ag^+/Ag electrode as a reference. The 0.1M of tetrabutylammonium tetrafluoroborate (TBATFB) in dichloromethane (DCM) was used for the solution state and 0.1M of tetrabutylammonium hexafluorophosphate (TBAHFP) in acetonitrile (ACN) was used for solid state as supporting electrolytes. The LUMO levels were calculated by the optical band-gaps that was recorded on UV/VIS spectroscopy and HOMO levels that were recorded on CV and UPS on film and solution both state. Furthermore, computational study was followed for comparison of IID-series and TIID-series. Theoretical molecular orbital calculation was carried out using density functional theory (DFT). Gaussian09 at B3LYP/6-31G* level was used to characterize optimized structure, electron density, and frontier

molecular orbital energy at ground state.

The morphology study was carried out thorough atomic force microscopy (AFM) which operating measurement was a Multimode with Nanoscope V controller, Bruker.

2.2.3 Fabrication and evaluation of organic thin-film transistors

Organic thin-film transistors (organic field-effect transistor, OFET) with a bottom-gate/top-contact configuration were fabricated on a SiO_2/Si (300nm thick SiO_2) substrate. Prior to device fabrication, SiO_2/Si was rinsed with acetone and isopropyl alcohol respectively for 10mins in ultrasonicator. Then, UV (360nm wavelength) ozone treatment was followed for 20mins. Before deposition of organic semiconductors, octadecyl-trichlorosilane (ODTS) was treated in a vacuum on substrates to form ODTS self-assembled monolayer. Substrates were brought into a nitrogen (N_2)-filled glove box. Next then, organic thin films were formed by vacuum deposition. Thermally deposition of gold (Au) electrodes (50nm thick) were followed up thorough a metal mask in a vacuum metal chamber. The I-V characteristics of individual devices were measured using Keithley 4200 connected to a probe station. The mobility values of OFETs in saturation region were calculated from $\partial I_{D,sat}^{1/2}/\partial V_G$, where,

$$I_{D,sat} = \frac{W}{2L} C_{ox} \mu_{sat} (V_G - V_T)^2$$

W, L values were estimated by optical microscope and V_D=100V.[4)]

2.3 Results and Discussion

2.3.1 Theoretical molecular orbital calculation used density functional theory (DFT)

Theoretical molecular orbital calculation was preceded for prediction of optoelectrical properties. Computational study based density functional theory (DFT) proceeded by using Gaussian09 and basis set was B3LYP/6-31G*.

To compare between IID and TIID core, geometry optimization was done. As shown at Figure 2.1, IID cores are more distorted due to steric hindrance between phenyl hydrogen and carbonyl oxygen. Dihedral angles on core at EHIID and EHIID2Br are 28.52° and 27.88° respectively. However, TIID core has very planar optimized structure as shown at Figure 2.1 (c) and (d). Torsion angles are almost zero so that expansion of π- conjugation is effective. It is because secondary S···O interaction between sulfur on thiophene and carbonyl oxygen. From these results, OFET targeting molecules are expected showing similar calculated optimized geometry.

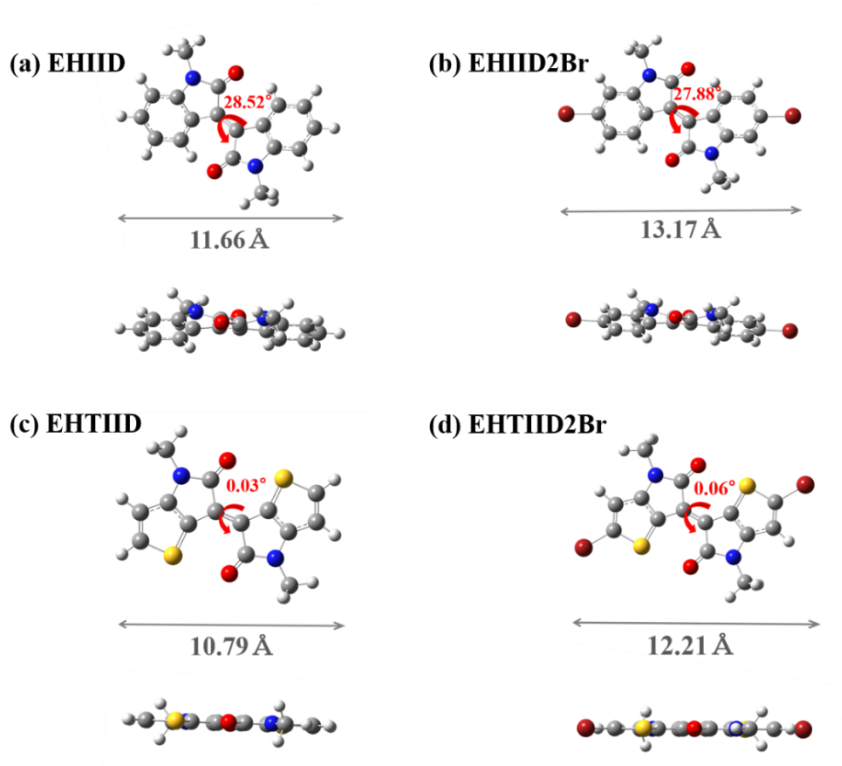

Figure 2. 1 The calculated geometry on ground state. Optimized geometries after calculation using basis set B3LYP/6-31G*. (Upper: top view, Lower: front view) (a) EHIID, (b) EHIID2Br, (c) EHTIID, and (d) EHTIID2Br (All alkyl chains were simplified from ethylhexyl to methyl for simple calculation)

In optimized ground state, as shown at Figure 2.2, TIID-based small molecules are less distorted than IID-based molecules. Dihedral angle show big difference each (a) and (c), and (b) and (d) in Figure 2.2. In case of P-DCV series, EHIIDPDCV has dihedral angles 10.89° at IID core's double bond and 34.06° between phenyl rings and EHTIIDPDCV has dihedral angles 0.08° in TIID core and 10.44° between core and phenyl ring. Similarly, in case of T-DCV series, EHIIDTDCV and EHTIIDTDCV have dihedral angles at each core position, 11.15° in IID and 0.03° in TIID. From these dihedral angles, IID-core has structural repulsion between hydrogen on phenyl rings and oxygen on carbonyl groups and IID-derivatives must have distorted structure. For TIID-derivatives, sulfur on thiophene and oxygen on carbonyl group have favorable dipole-dipole interaction so that TIID-derivatives have much planar structure than IID-derivatives. These facts are also shown from side view at Figure 2.2.

In addition, with the optimized geometry, frontier molecular orbital (FOM) energy levels were recorded. In that calculation, there was no other condition relevant real environment. As shown at Figure 2.3, they are not exactly matched with measured data from UV/VIS and CV. However, tendency of optoelectrical property was estimated with accuracy. IID core had deep HOMO than TIID core keeping similar stabilized LUMOs. And OFET targeting molecules were successfully tuned for stabilizing the LUMOs using DCV units. Calculated FOM energy levels are shown in Table 2.1.

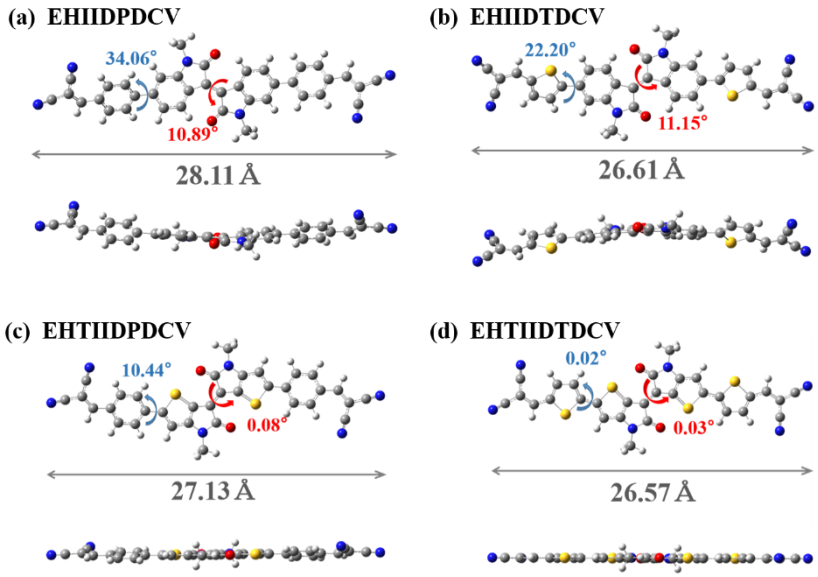

Figure 2. 2 The calculated geometry on ground state. Optimized geometries after calculation using basis set B3LYP/6-31G*. (Upper: top view, Lower: front view) (a) EHIIDPDCV, (b) EHIIDTDCV, (c) EHTIIDPDCV, and (d) EHTIIDTDCV (All alkyl chains were simplified from ethylhexyl to methyl for simple calculation)

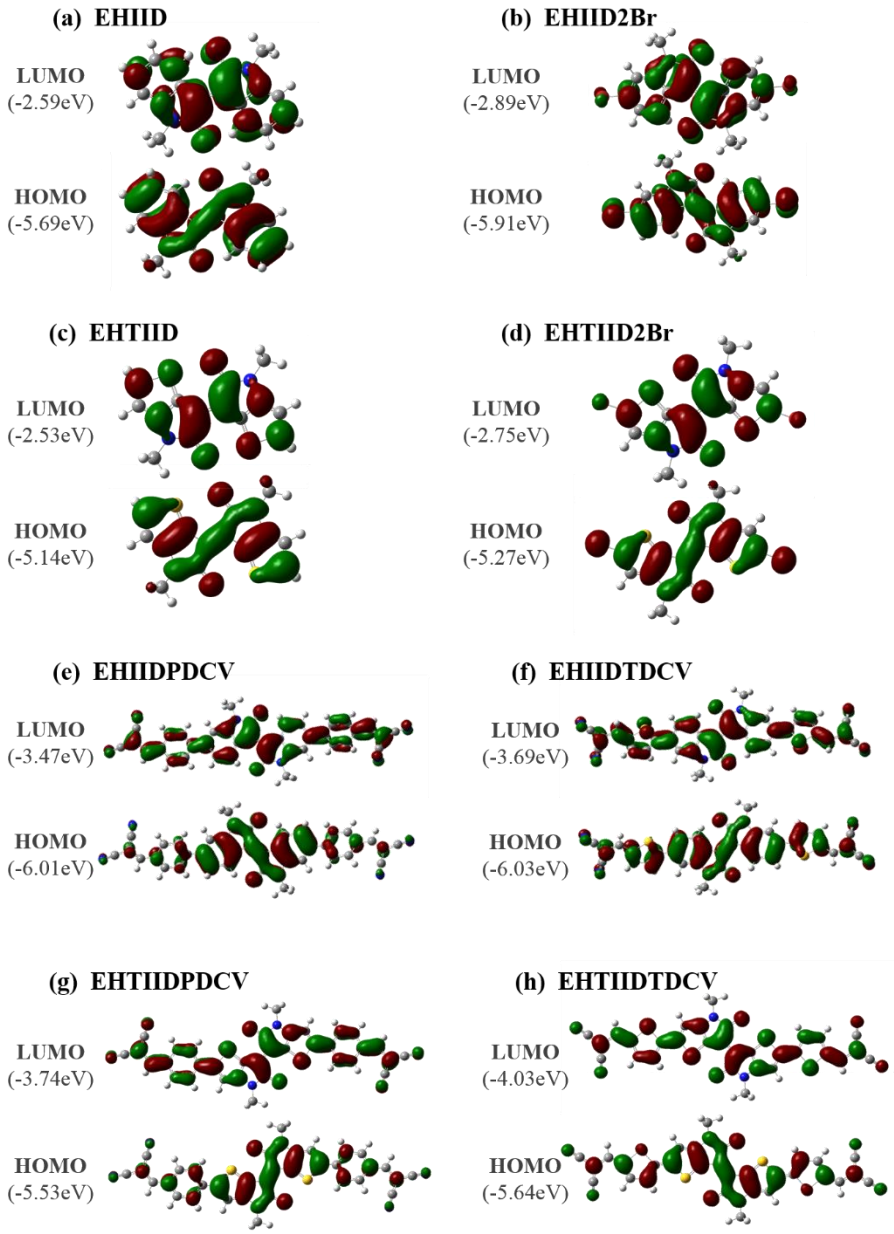

Figure 2. 3 Calculated frontier molecular orbital (FMO) energy levels and electron density maps of (a) EHIID, (b) EHIID2Br, (c) EHTIID, (d) EHTIID2Br, (e) EHIIDPDCV, (f) EHIIDTDCV, (g) EHTIIDPDCV, and (h) EHTIIDTDCV. Calculation method was DFT and basis set was B3LYP/6-31G*.

Table 2. 1 Theoretical molecular orbital [a)] of EHIIDPDCV, EHIIDTDCV, EHTIIDPDCV, and EHTIIDTDCV

Compound	E_{HOMO} (eV)	E_{LUMO} (eV)	λ_g (eV) [b)]
EHIID	-5.69	-2.59	3.10
EHIID2Br	-5.91	-2.89	3.02
EHTIID	-5.14	-2.53	2.61
EHTIID2Br	-5.27	-2.75	2.52
EHIIDPDCV	-6.01	-3.47	2.54
EHIIDTDCV	-6.03	-3.69	2.34
EHTIIDPDCV	-5.53	-3.74	1.79
EHTIIDPDCV	-5.64	-4.03	1.61

a) DFT calculation was carried out on molecular structures of four target molecules modified with methyl group at N-position in lactam, instead of 2-ethylhexyl group.
b) Calculated from the differences between theoretical HOMO and LUMO levels.

2.3.2 Optical and electrochemical properties of IID and TIID-based small molecules

Absorbance spectra of IID- and TIID- based small molecules in solution and film state, and molar absorption coefficients are shown in Figure 2.4, Figure 2.5, and Figure 2.6. And the electrochemical properties of IID- and TIID derivatives were measured by cyclic voltammetry (CV). The LUMO levels of them were calculated from optical band-gap from UV/VIS spectra. Onset point and peaks are summarized at Table 2.2. The HOMO levels as an aspect of electrochemical properties, that are also called oxidation potentials for each derivatives, were measured in relation to ferrocene (Fc/FC^{+}=4.8eV), which was typically used as a reference in solution and film state. Moreover, HOMO levels were recorded also by ultraviolet photoelectron spectroscopy (UPS) as an aspect of electrical energy levels. Energy levels of cores are shown at Figure 2.7 and those of OFET targeting molecules are shown at Figure 2.8 (UPS) and Figure 2.9 (CV). The HOMO, LUMO levels and optical band-gaps are shown in Table 2.3 and Table 2.4.

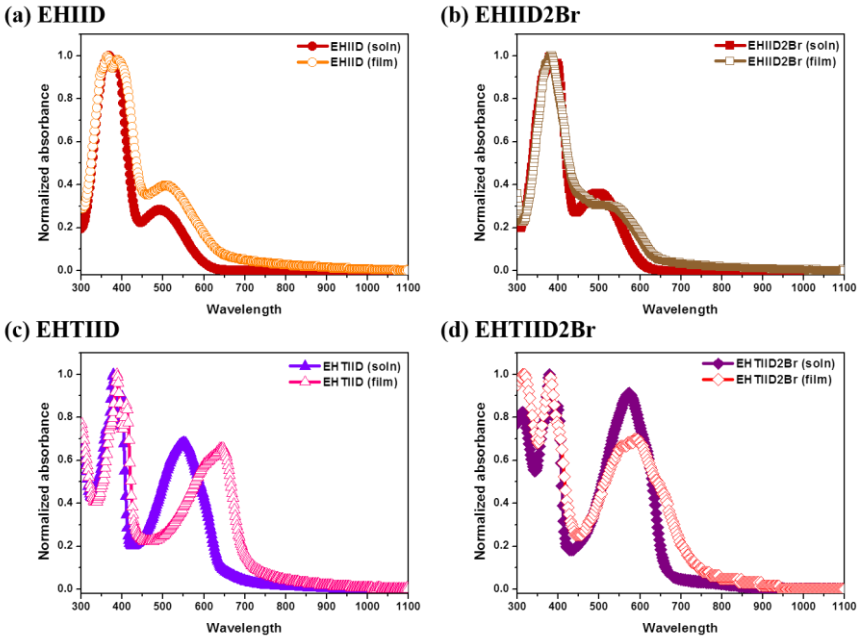

Figure 2. 4 UV/VIS absorption spectra (a) EHIID, (b) EHIID2Br, (c) EHTIID, and (d) EHTIID2Br at solution and film state.

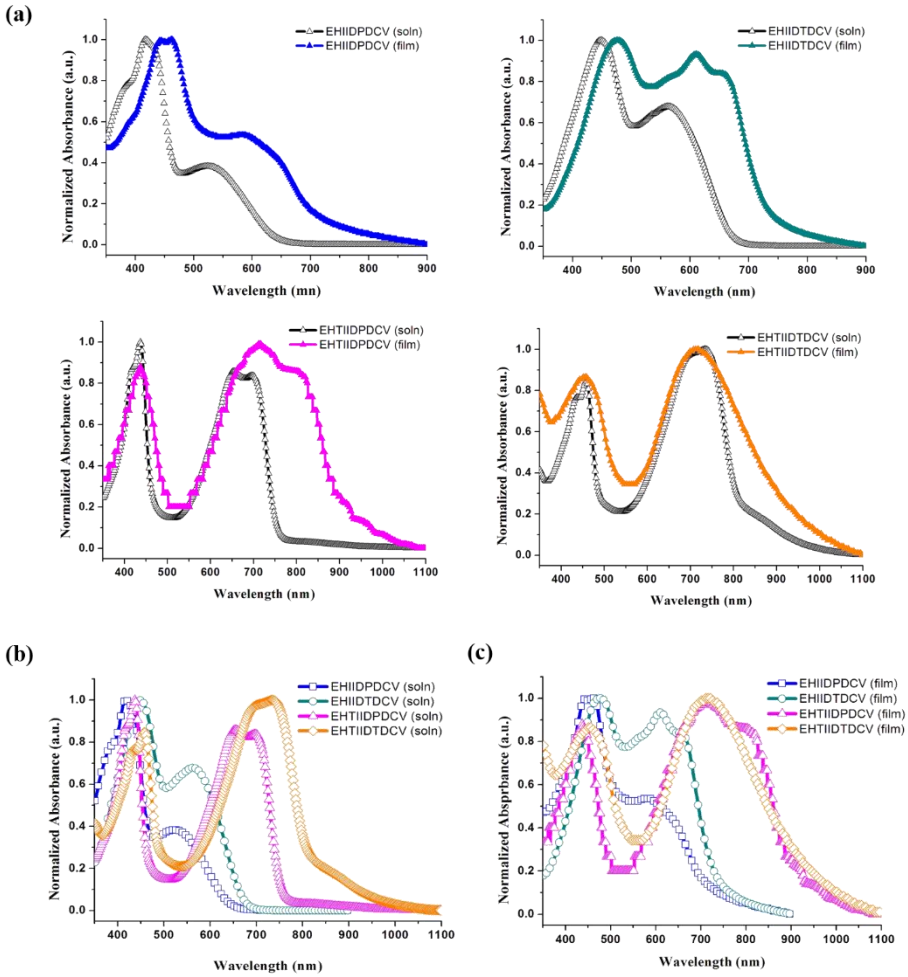

Figure 2. 5 UV/VIS absorption spectra (a) for each derivatives in solution and solid state. Absorption spectra of all derivatives (b) in solution state and (c) in film state

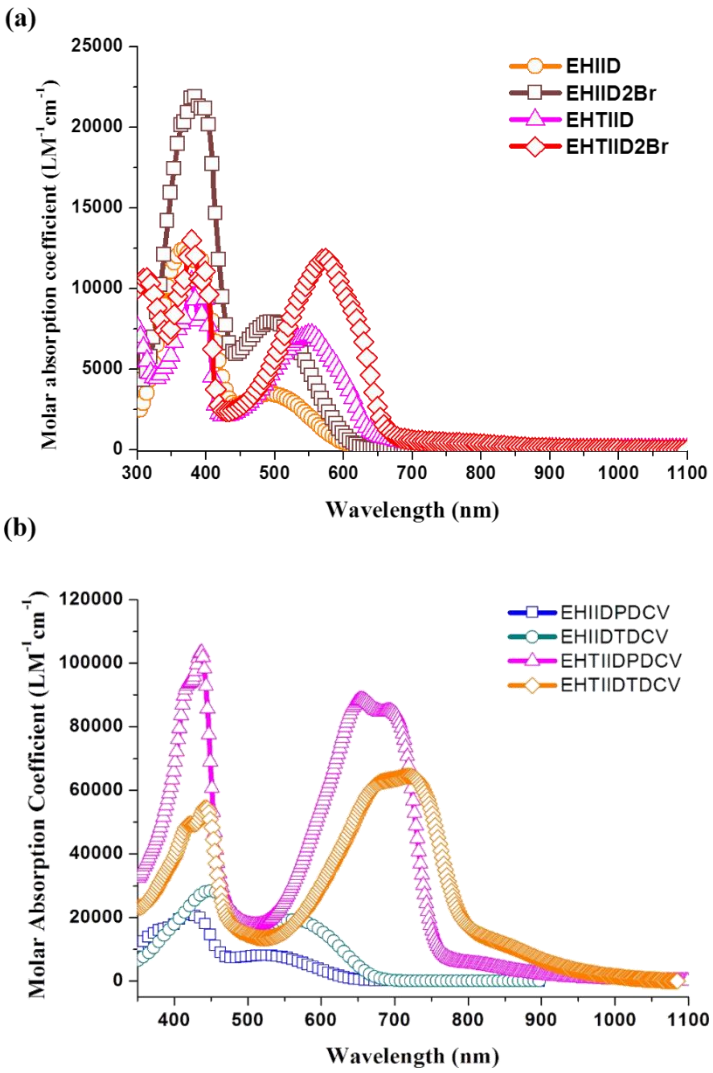

Figure 2. 6 Molar absorption coefficient for each materials. All data was calculated by solution absorbance spectra.

Table 2. 2 Optical properties of IID- and TIID-based small molecules in solution and solid state.

Compound	λ_{abs} (nm)	λ_{onset} (nm)	λ_g^{opt} (eV) [a)]
EHIID (soln) [b)]	368, 391, 492	604	2.05
EHIID (film) [d)]	364, 390, 509	644	1.93
EHIID2Br (soln) [b)]	381, 398, 496	610	2.03
EHIID2Br (film) [d)]	384, 530	640	1.94
EHTIID (soln) [c)]	378, 399, 551	639	1.94
EHTIID (film) [d)]	387, 411, 644	698	1.78
EHTIID2Br (soln) [c)]	379, 399, 573	663	1.87
EHTIID2Br (film) [d)]	380, 564 [e)], 590	721	1.72
EHIIDPDCV (soln) [b)]	417, 523	635	1.95
EHIIDPDCV (film) [d)]	446, 461, 587	715	1.73
EHIIDTDCV (soln) [b)]	448, 563	679	1.83
EHIIDTDCV (film) [d)]	478, 610, 653	737	1.68
EHTIIDPDCV (soln) [c)]	437, 656, 696	749	1.66
EHTIIDPDCV (film) [d)]	437, 715, 798	911	1.36
EHTIIDTDCV (soln) [c)]	458, 733, 874[e)]	818	1.52
EHTIIDTDCV (film) [d)]	434[e)], 450, 698[e)], 708	954	1.30

a) Optical band-gap energy was calculated from absorption edge (onset point).
Measured in THF solution of concentration of b) $5*10^{-5}$M and c) $1*10^{-5}$M.
d) Spin-coated with 10mg/ml concentration in THF solution with filter syringe.
e) It is not an apparent peak, just shoulder near absorption.

Figure 2.4 and Figure 2.5 show normalized UV/VIS absorption spectra of IID and TIID cores, and IID- and TIID-based small molecules in both solution and film state. As shown at Figure 2.4, IID and TIID cores are shown broad absorption spectra as expected and all cores are showed red-shifted spectra in film state compared to solution state. In particular, TIID cores have broader absorption range than IID cores and more red-shifted max peaks and onset points. It means that TIID is sufficiently expanded π-π conjugations because of its planarity. Compared with core and brominated core, absorption onset point and peaks are slightly red-shifted at brominated core. It means that Bromine withdraws electron density from core. In fact, IID and TIID cores are already electron-deficient due to lactam moiety so that significant change is not shown. However, degree of decreasement showed that IID own core had stronger withdrawing property than TIID own.

Furthermore, as shown at Figure 2.5, all of OFET target molecules show red-shifted spectra in film state compared to solution state which are similar to IID and TIID core characteristics. It meant all molecules were aggregated in J-aggregation form at film state and resulted in a smaller band-gap energy each. In case of IID-series, range of absorption spectra of EHIIDTDCV has larger absorption range than EHIIDPDCV. TIID-series, however, have broader absorption range than IID-series so that they have near-IR (NIR) absorption in solution and film both state. TIID-series have less absorption in yellow-green range (about 500-550nm) so that color of powder is dark green while IID-series show dark reddish colored powder.

In case of molar absorption coefficient, for cores, Maximum of molar absorption coefficient (ε_{max}) are followed: 12400 $LM^{-1}cm^{-1}$ at 369nm for EHIID, 21960 $LM^{-1}cm^{-1}$ at 382nm for EHIID2Br, 10420 $LM^{-1}cm^{-1}$ at 378nm for

EHTIID, and 13000 $LM^{-1}cm^{-1}$ at 379nm for EHTIID2Br. Cores are showed similar molar absorption coefficient through all absorption range. In contrast, for OFET targeting molecules, TIID-series has larger values than IID-series. Maxima of molar absorption coefficient (ε_{max}) are followed: 21100 $LM^{-1}cm^{-1}$ at 417nm for EHIIDPDCV, 28420 $LM^{-1}cm^{-1}$ at 448nm for EHIIDTDCV, 88500 $LM^{-1}cm^{-1}$ at 656nm for EHTIIDPDCV, and 64500 $LM^{-1}cm^{-1}$ at 733nm for EHTIIDTDCV. TIID-series are two times larger than IID-series. Such noticeable increases of ε_{max} are counted on improving charge carrier transport ability (Figure 2.6). The reason that TIID-series have larger onset point of absorption spectra might be come from their effective π-conjugation expansion by own structural planarity. More planar structure, more effective delocalization of π-electrons along the backbone. From this, TIID-series, EHTIIDPDCV and EHTIIDTDCV, have smaller bandgap energy (1.36eV and 1.30eV, respectively) than IID-series, EHIIDPDCV and EHIIDTDCV (1.73eV and 1.68eV, respectively) in film state. Although TIID- and IID-series have different bandgap, all the materials are suitable for n-type or ambipolar organic field-effect transistors because of their FMO levels.

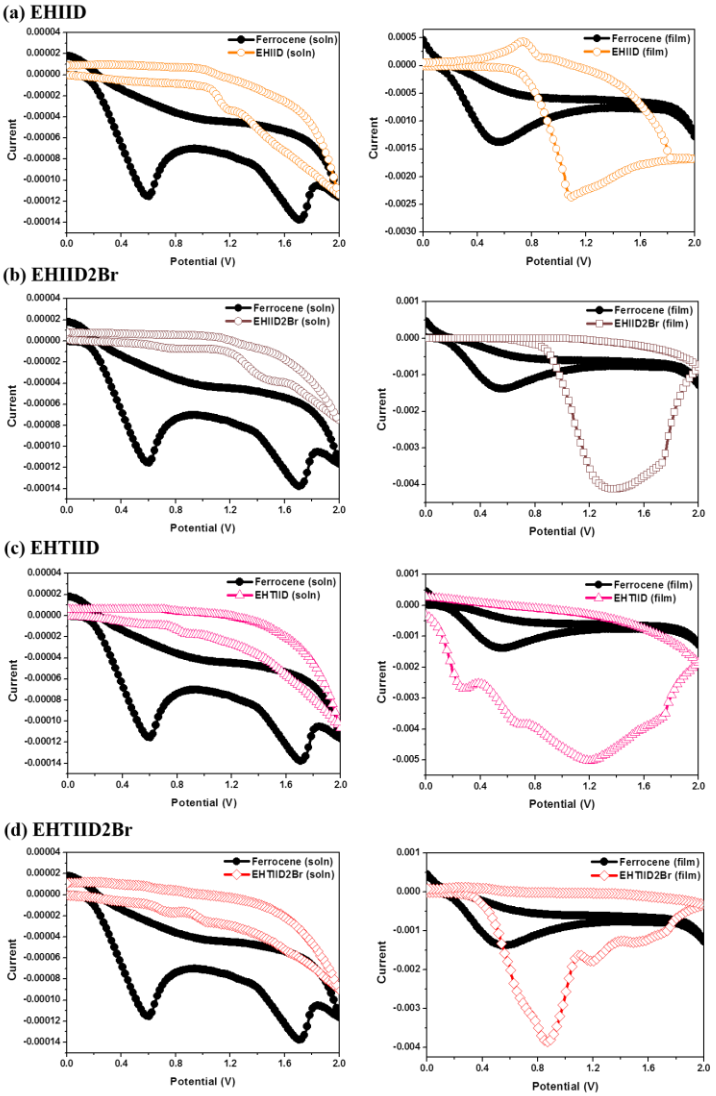

Figure 2. 7 Cyclic voltammetrams of IID and TIID cores (blanked) at solution (left) and film (right) state. (a) EHIID, (b) EHIID2Br, (c) EHTIID, and (d) EHTIID2Br. At solution state, supporting electrolyte was TBATFB in acetonitrile (DCM). Ferrocene (filled) with TBATFB in DCM solution as the reference. All were drop-casting for doping on ITO glass and supporting electrolyte was TBAHFB in acetonitrile (ACN). Ferrocene (filled) with TBAHFB in ACN solution as the reference.

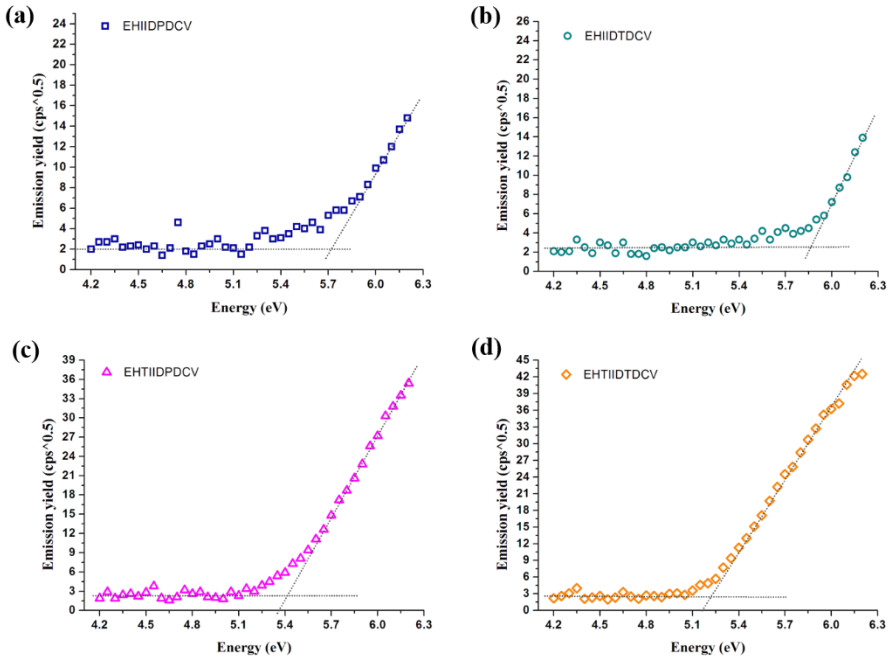

Figure 2. 8 Ultraviolet photoelectron microscopy data for HOMO as an aspect of electrical property, respectively (a) EHIIDPDCV, (b) EHIIDTDCV, (c) EHTIIDPDCV, and (d) EHTIIDTDCV

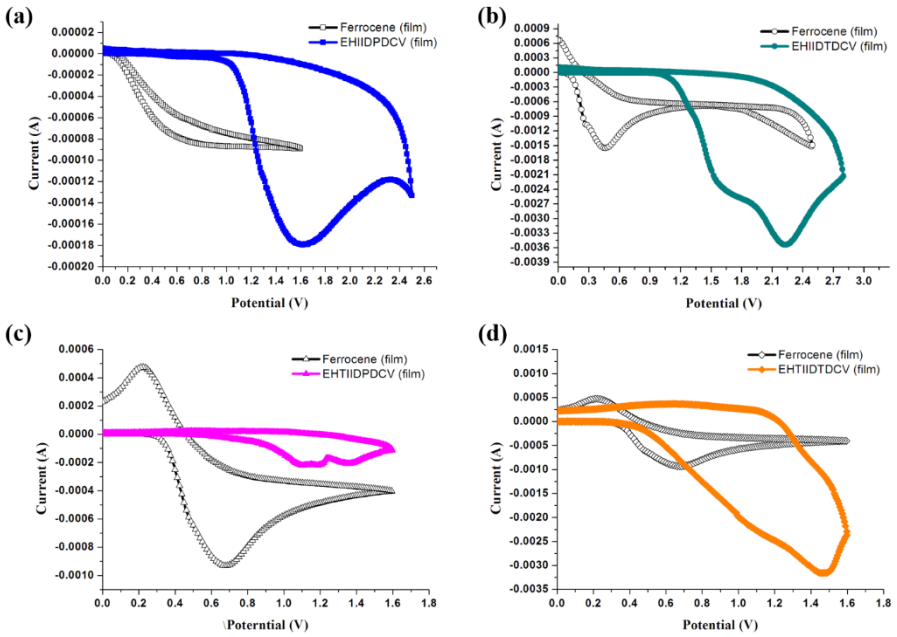

Figure 2. 9 Cyclic voltammetrams of IID- and TIID-based small molecules (filled) named (a) EHIIDPDCV, (b) EHIIDTDCV, (c) EHTIIDPDCV, and (d) EHTIIDTDCV. All small molecules were drop-casting for doping on ITO glass and supporting electrolyte was TBAHFB in acetonitrile (ACN). Ferrocene (blank) with TBAHFB in ACN solution as the reference.

Table 2. 3 Electrochemical properties and energy levels of IID and TIID cores in solution and film states.

Compound	E_{HOMO} (eV) [a)]	E_{LUMO} (eV) [b)]	λ_g^{opt} (eV) [c)]
EHIID (soln)	-5.72	-3.67	2.05
EHIID (film)	-5.35	-3.42	1.93
EHIID2Br (soln)	-5.82	-3.79	2.03
EHIID2Br (film)	-5.51	-3.57	1.94
EHTIID (soln)	-5.36	-3.42	1.94
EHTIID (film)	-4.66	-2.88	1.78
EHTIID2Br (soln)	-5.45	-3.58	1.87
EHTIID2Br (film)	-5.02	-3.30	1.72

a) Electrochemical HOMO level is recorded by cyclic voltammetry. It calculated from difference between ferrocene reference (-4.8eV) and each materials.
b) LUMO level is calculated with electrochemical HOMO and optical bandgap.
c) Optical bandgap was obtained by onset point of absorption.

Table 2. 4 Electrochemical properties and energy levels of IID- and TIID-based small molecules in solution and solid state.

Compound	E_{HOMO} (eV) [a]	E_{HOMO} (eV) [b]	E_{LUMO} (eV) [c]	E_{LUMO} (eV) [d]	λ_g^{opt} (eV) [e]
EHIIDPDCV (soln) [f]	-5.58	N.A [i]	-3.63	N.A.[j]	1.95
EHIIDPDCV (film) [g]	-5.79	-5.77	-4.06	-4.03	1.73
EHIIDTDCV (soln) [f]	-5.86	N.A [i]	-4.03	N.A.[j]	1.83
EHIIDTDCV (film) [g]	-5.81	-5.90	-4.13	-4.22	1.68
EHTIIDPDCV (soln) [f]	N.A. [h]	N.A [i]	N.A.[j]	N.A.[j]	1.66
EHTIIDPDCV (film) [g]	-5.30	-5.35	-3.94	-3.98	1.37
EHTIIDTDCV (soln) [f]	N.A [h]	N.A [i]	N.A.[j]	N.A.[j]	1.52
EHTIIDTDCV (film) [g]	-5.00	-5.20	-3.70	-3.90	1.30

a) Electrochemical HOMO level is recorded by cyclic voltammetry. It calculated from difference between ferrocene reference (-4.8eV) and each materials.
b) Electrical HOMO level is detected by ultraviolet photoelectron microscopy.
c) LUMO level is calculated with electrochemical HOMO (a) and optical bandgap.
d) LUMO level is calculated with electrical HOMO (b) and optical bandgap.
e) Optical bandgap was obtained by onset point of absorption.
f) Materials are dissolved in TBATFB/DCM electrolyte with concentration of 10^{-3}M.
g) Drop-casted on ITO glass twice and supporting electrolyte is TBAHFB/ACN.
h) Due to solubility problem, precipitation was in and not detected enough current.
i) UPS measurement was only for film state.
j) Not calculated because of solubility problems and UPS measurement states.

As summarized at Table 2.3, FMO levels of core molecules were detected. Compared to IID, TIID has higher about 0.4eV HOMO energy because of donating property of thiophene. Furthermore, brominated cores are slightly lowered HOMOs compared with each core about 0.1eV. It means that brominated cores are much electron deficient core so that lowered HOMOs are shown. LUMOs were calculated from optical band-gap and HOMOs. LUMOs are similar in IID and TIID. This result comes from lactam moiety of two cores so that LUMOs are stabilized. Optical bandgap is lowered for TIID compared to IID so that LUMOs are similar with difference about 0.2eV.

In OFET fields, the organic materials should have appropriate FMO levels considering work function of metals which were used for source and drain electrode. Already mentioned in previous chapter, for p-type transistors, HOMOs of organic materials are in range of -4.8eV to -5.5eV for matching work function of gold metal. In case of n-type transistor, LUMOs of organic materials are in range of -3.6eV to -4.5eV for effective electron injection.[5)]

Herein, I checked energy levels of OFET targeting molecules in solid state. The HOMO levels in film state were characterized by UPS measurement and CV method, and the LUMO level was calculated based on HOMO and optical bandgap. CV profiles are in Figure 2.6 and UPS profiles at the cutoff are in the Figure 2.5. From the data of all, molecular energy levels are indicated and summarized in the Table 2.3 and they correlate well with my initial research proposal.

As a result, IID-series show lower HOMOs than TIID-series. The reason that HOMO levels of IID-series (-5.77eV for EHIIDPDCV and -5.90eV for EHIIDTDCV) show very low values originates in isoindigo core. Isoindigo has very deep HOMO already and two DCV units slightly support lowering

HOMOs. TIID-series, however, have much higher HOMOs (-5.35eV for EHTIIDPDCV and -5.20eV for EHTIIDTDCV) because of donating property of thiophene in thienoisoindigo core even though DCV units slightly lower the energy levels. From this information, I expected that IID-series were proper for n-type OFET application and TIID-series are proper for ambipolar OFET application.

2.3.3 IR analysis of IID and TIID-core

For comparing between IID and TIID core, IR analysis was processed. IR affects vibrational motions of molecules and vibration peaks are identical for each molecules except fingerprint region. For analysis between IID and TIID core, I chose C=O stretch peak of two compounds. C=O stretch peak is strong and unique for each molecules and easy to define differences of molecules.[6)]

As shown in Figure 2.10 and Table 2.5, carbonyl stretch peak of EHTIID2Br is shifted to lower frequency compared with EHTPD instead that peak of EHIID2Br is not shifted compared with reference (Me-Indole). Due to structural hindrance between phenyl hydrogen and carbonyl oxygen, IID core did not show any secondary interaction. TIID core, however, showed secondary interaction. By shifting the carbonyl stretch peaks to lower frequency, It could be expected that carbonyl stretch strength were weaken thorough secondary interaction between sulfur of thiophene and carbonyl oxygen. This results support that S···O interaction of TIID core has been and TIID core has planar structure through it.

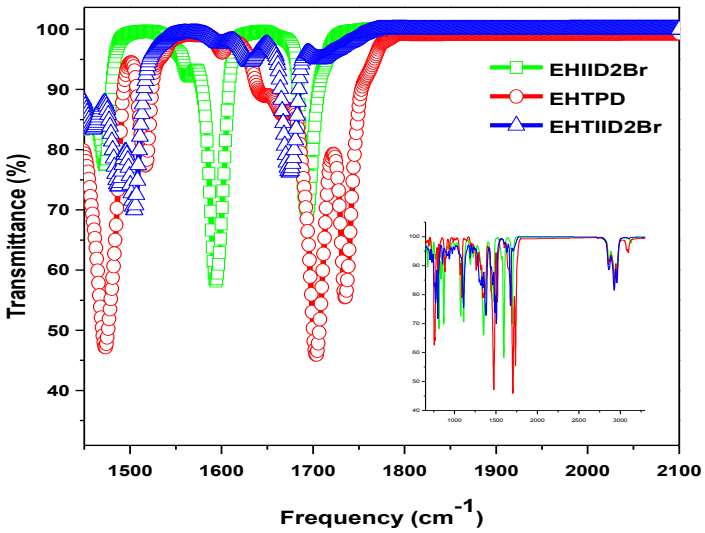

Figure 2. 10 FT-IR spectrum of core molecules named EHIID2Br and EHTIID2Br. EHTPD (synthetic route 6) is reference for comparing change of peak position.

Table 2. 5 Position of carbonyl stretch peak of cores and references.

Compound	υ_{max} (cm^{-1})
Me-Indole[a)]	1695
EHIID2Br	1693.53
EHTPD	1735.11,[b)] 1703.38
EHTIID2Br	1674.41

a) Reference at J. Org. Chem. 2006, 71, 6497.
b) Another stretch peak of the other carbonyl group which is not involved in lactam units..

2.3.4 Thermal stability of molecules

Thermal stability of four cores and four small molecules was checked using Thermogravimetry analysis at N_2 atmosphere. As shown at Figure 2.11, IID cores and IID derivatives are very stable until decomposition temperature with increasing temperature. Decomposition temperature of IID cores and IID derivatives are followed; EHIID is 282℃, EHIID2Br is 300℃, EHIIDPDCV is 396℃, and EHIIDTDCV is 385℃. However, TIID cores and TIID derivatives are quite instable during increase temperature. For EHTIID2Br and EHTIIDTDCV, thermal stability of two molecules was poor specifically. As shown at Figure 2.11, EHTIID and EHTIIDPDCV are quite stable to decomposition temperature but EHTIID2Br and EHTIIDTDCV are instable during increasing temperature with unknown gas. It means that EHTIID cores are quite instable at harsh experimental atmosphere so that fabrication of vacuum-deposited films would be difficult due to its instability. Decomposition temperature of those are followed; EHTIID is 192℃, EHTIIDPDCV is 402℃, and EHTIID2Br and EHTIIDTDCV are meaningless to define decomposition temperature because of cascade graph formations.

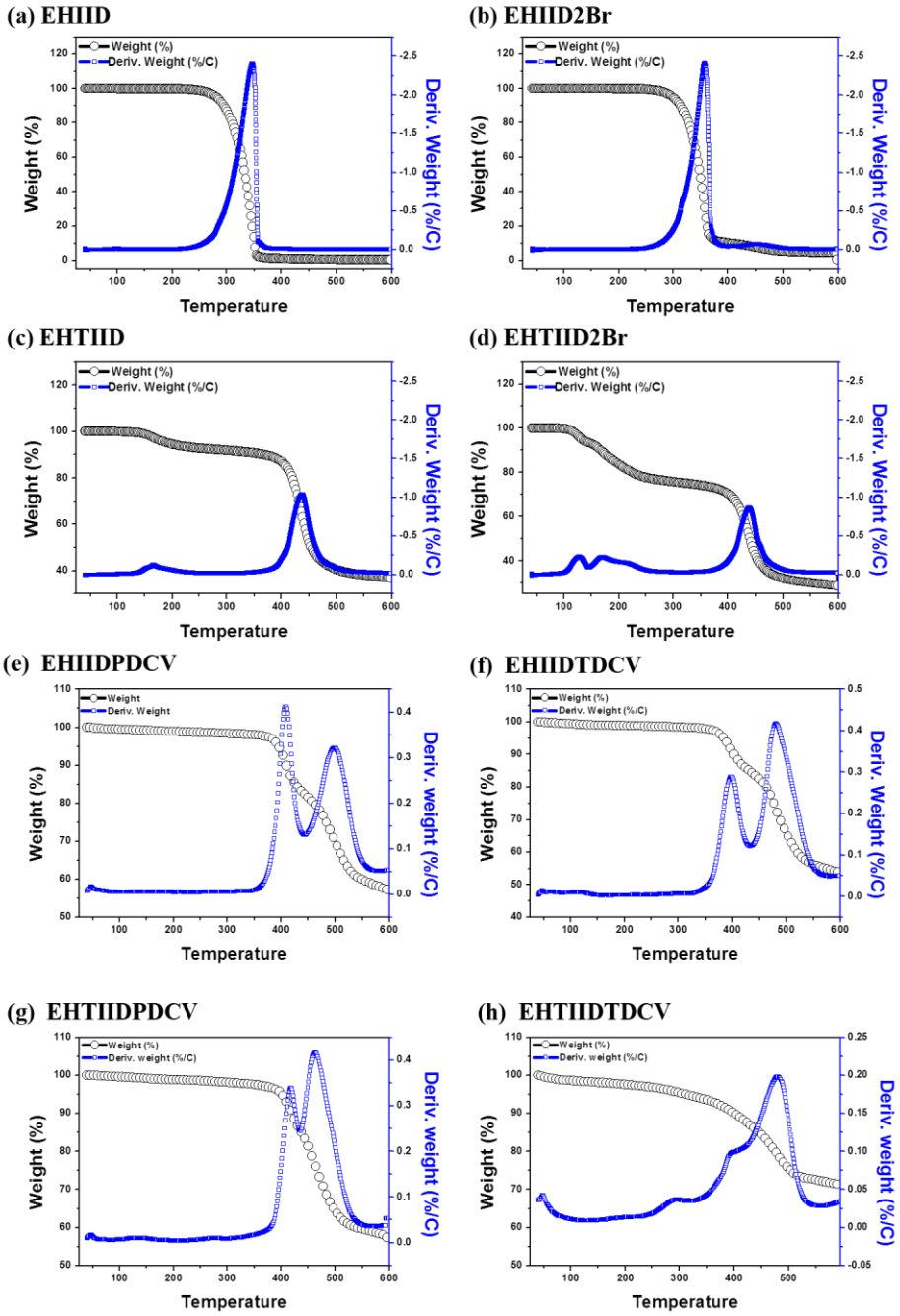

Figure 2. 11 TGA analysis of molecules for checking thermal stability. Increase of temperature is 10℃/min and range of temperature is 600℃.

2.3.5 OFETs performance

To throw light on structure-property relationships in IID-based molecules and TIID-based molecules, we fabricated bottom-gate/top-contact devices with gold electrodes. All the devices were generated n-octadecyltrimethoxysilane (ODTS) treated SiO_2/Si substrate. The highest performing devices were deposited on thermally annealed at 120℃ substrates in case of EHIIDTDCV whereas EHIIDPDCV showed similar performance among temperature ranges from room temperature to 110℃. All fabrication and device testing were performed under inert conditions. Transfer characteristics of each conditions are shown in Figure 2.12 as EHIIDPDCV and Figure 2.13 as EHIIDTDCV. Output characteristic is shown in Figure 2.14 with transfer curve of best performing devices that EHIIDTDCV was deposited in. All the average and maxima performances were summarized in Table 2.6 for EHIIDPDCV and Table 2.7 for EHIITDCV. Channel lengths were 30 and 40nm and width was 1mm. The field-effect mobility was extracted from the saturated region by fitting the slope of square root drain current vs. gate bias.

At electron-enhancement mode, n-type charge transport behavior was apparent at given 100V gate voltage due to sufficiently low-lying LUMOs for EHIIDPDCV. As you can show at Table 2.6, EHIIDPDV had similar performance for various temperature. Average value of electron mobility at 120℃ is 8.87×10^{-4} $cm^2V^{-1}s^{-1}$ and maxima is 1.70×10^{-3} $cm^2V^{-1}s^{-1}$. EHIIDTDCV, however, was shown better performance according to increasing temperature. As shown in Table 2.7, both average mobility and maxima mobility are increased with 10 times differences as temperature increases. As indicated better performance at annealed thin films at 130℃, average value of electron

mobility is 8.50×10^{-3} $cm^2V^{-1}s^{-1}$ and maxima is 1.83×10^{-2} $cm^2V^{-1}s^{-1}$. Compared between EHIIDPDCV and EHIIDTDCV, at same temperature 100℃, EHIIDTDCV had better performance at both average and maxima mobility. It is because EHIIDTDCV has lower lying LUMOs and has more planar backbone as optimized structure. EHTIIDTDCV has lower lying LUMOs so that electron injection was easier than EHIIDPDCV. EHIIDTDCV, also, has less torsion angles than EHIIDPDCV so that EHIIDTDCV was relevant for electron transport. To evaluate increase of device performance of EHIIDTDCV, atomic force microscopy (AFM) images were extracted. As shown at Figure 2.15, at 130℃, film morphology of EHIIDTDCV was very clean and crystalline thorough substrates. From this result, we could indicate that more crystalline at high temperature, better performance in OFET devices.

Unfortunately, EHTIIDTDCV and EHTIIDPDCV were not successful to vacuum deposit to substrate. It was because of its poor thermal stability. TGA data of four materials are shown in Figure 2.11. Thermally decomposition appeared at temperature that was begun annealing especially in case of EHTIIDTDCV. EHTIID-units, N-ethylhexylated thienoisoindigo with substituents might be thermally unstable at annealing. Because of poor thermostability and processability, devices of OFET targeted TIID series were not fabricated successfully.

Table 2. 6 Electrical performance of OFET devices based on EHIIDPDCV vacuum deposited thin films with Au electrodes

EHIIDPDCV (temperature)	$\mu_{e,avg}$ ($cm^2V^{-1}s^{-1}$)[a)]	$\mu_{e,max}$ ($cm^2V^{-1}s^{-1}$)	V_{th} (V)	**on/off ratio**
RT	3.21E-04	4.98E-04	68	10^3-10^4
70℃	8.29E-04	1.63E-03	67	10^3-10^4
100℃	9.11E-04	1.36E-03	40	10^3-10^4
120℃	8.87E-04	1.70E-03	46	10^3-10^4

a) The average mobility of all channel of the tested OFET devices

Table 2. 7 Electrical performance of OFET devices based on EHIIDTDCV vacuum deposited thin films with Au electrodes

EHIIDTDCV (temperature)	$\mu_{e,avg}$ ($cm^2V^{-1}s^{-1}$)[a)]	$\mu_{e,max}$ ($cm^2V^{-1}s^{-1}$)	V_{th} (V)	**on/off ratio**
RT	9.97E-06	1.14E-05	43	10^2-10^3
70℃	3.45E-04	8.87E-04	62	10^3-10^4
90℃	5.08E-04	1.73E-03	50	10^3-10^4
100℃	1.91E-03	3.56E-03	60	10^4-10^5
115℃	3.20E-03	7.07E-03	60	10^4-10^5
130℃	8.50E-03	1.83E-02	70	10^5
150℃	2.75E-03	4.39E-03	50	10^4-10^5

a) The average mobility of all channel of the tested OFET devices

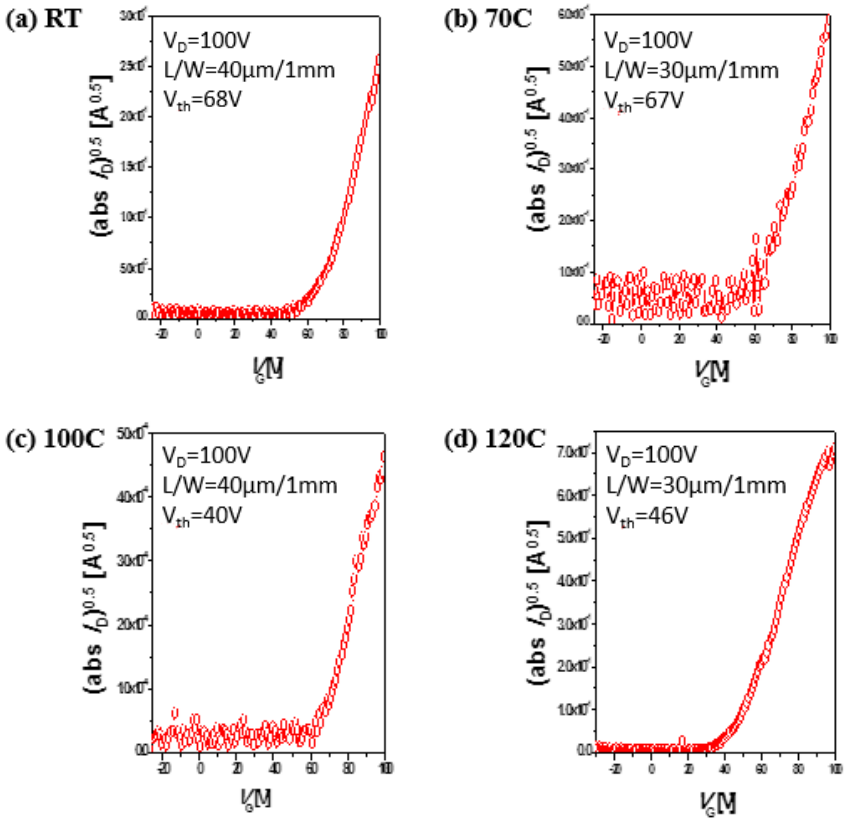

Figure 2. 12 Transfer I-V curve for EHIIDPDCV at each temperature. (a) room temperature, (b) 70℃, (c) 100℃ and (d) 120℃

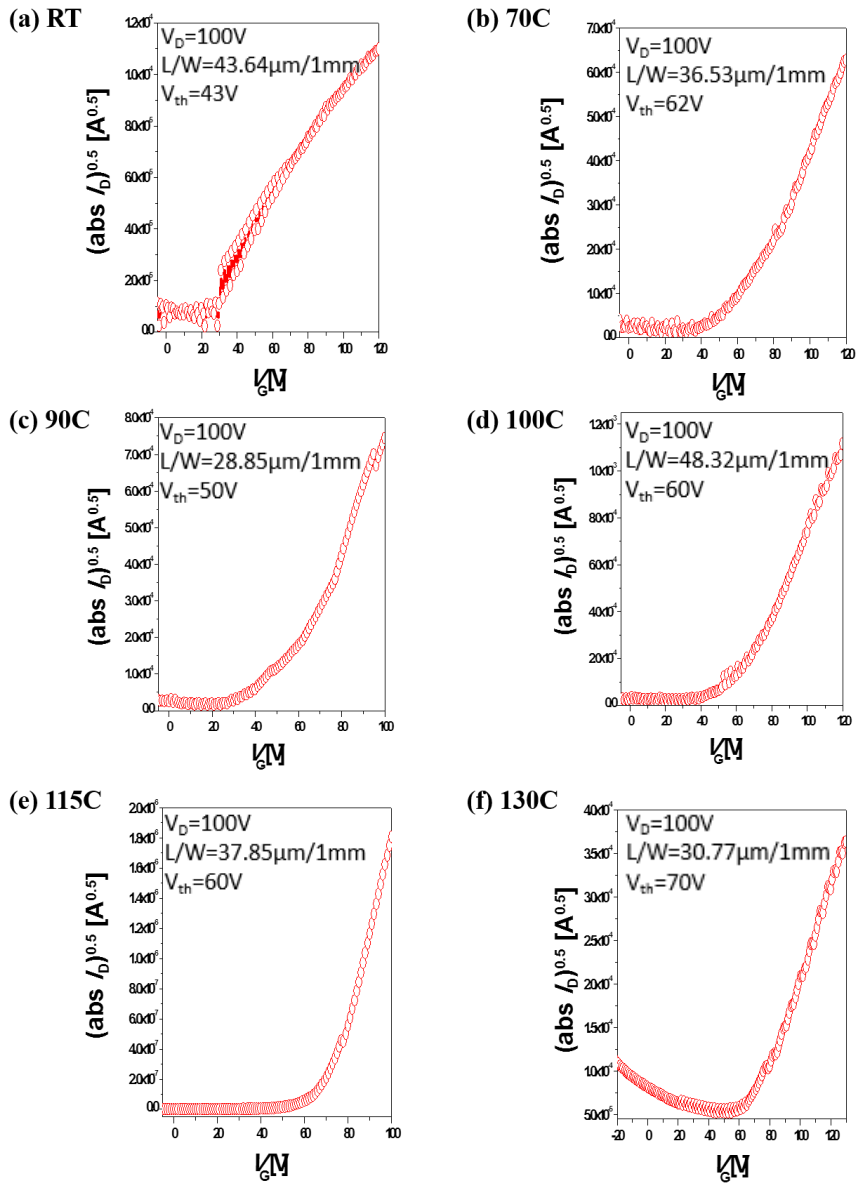

Figure 2. 13 Transfer I-V curve for EHIIDTDCV at each temperature. (a) Room temperature, (b) 70℃, (c) 90℃ (d) 110℃, (e) 115℃, and (f) 130℃

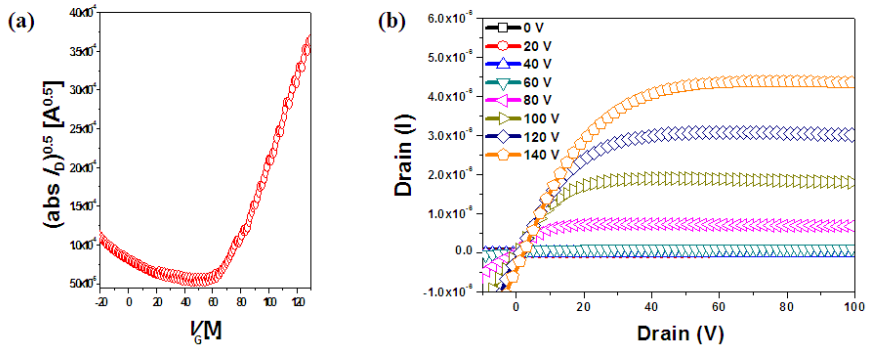

Figure 2. 14 Transfer and output curve of vacuum deposited device of EHIIDTDCV at optimized condition at 130℃.

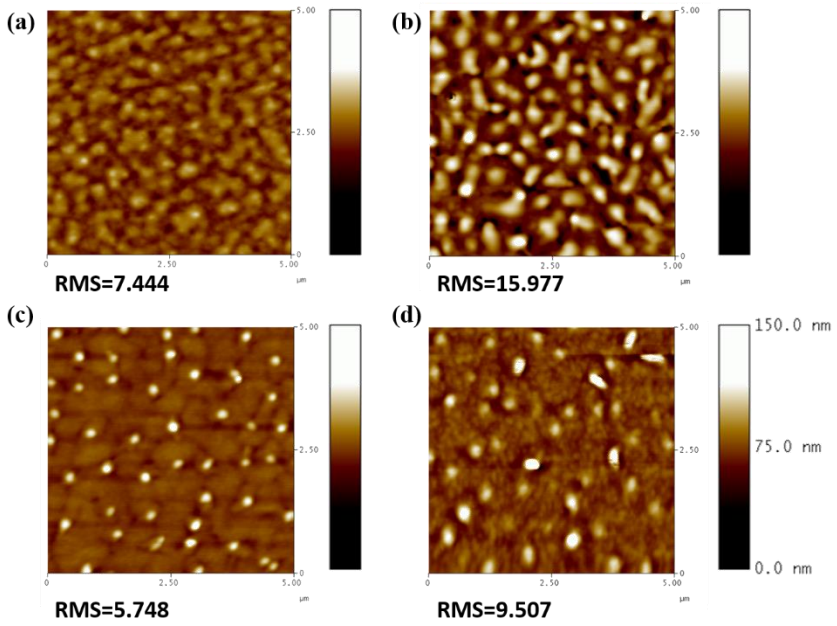

Figure 2. 15 AFM images of vacuum deposited devices at (a) 90℃, (b) 115℃, (c) 130℃ and (d) 150℃ of EHIIDTDCV.

2.4 Conclusion

In conclusion, I studied structure-property relationships between structural similar core IID and TIID. To explore difference of two cores, UV/VIS, CV, DFT, and IR studies were performed. Through those optical, electrochemical, and theoretical study, TIID has more planar structure than IID because of S···O secondary interaction although IID has structural hindrance between phenyl hydrogen and carbonyl oxygen. Furthermore, to compare field-effect transport ability of IID and TIID based on core study, OFET targeting 4 molecules were designed and successfully synthesized. Those molecules were characterized by UV/VIS, UPS, and DFT calculation. FMOs of IID series were shown suitable for n-type transistors and FMOs of TIID series were shown suitable for ambipolar transistors.

Vacuum deposited OFET devices of each molecules were fabricated. Unfortunately, TIID-series for OFET were failed fabrication of vacuum deposited devices due to its poor thermostability and processability. However, EHIIDPDCV and EHIIDTDCV exhibited n-type charge mobility expected with electron mobility 8.87×10^{-4} $cm^2V^{-1}s^{-1}$ (maximum is 1.70×10^{-3} $cm^2V^{-1}s^{-1}$) for EHIIDPDCV and 8.50×10^{-3} $cm^2V^{-1}s^{-1}$ (maximum is 1.83×10^{-3} $cm^2V^{-1}s^{-1}$) for EHIIDTDCV. EHIIDTDCV showed better performance than EHIIDPDCV because of its planarity thorough backbone.

2.5 Bibliography

1) E. Wang, W. Mammo, M.R. Andersson, *Adv. Mater.* **2014**, 26, 1801

2) W. Elsawy, C.L.Lee, S. Cho,S.H. Oh, S.H. Moon, A. Elbarbary, J.S. Lee, *Phys. Chem. Chem. Phys.* **2013**, 15, 15193

3) (a) W. Yue, T. He, M. Stolte, M. Gsanger, F. Wurthner, *Chem. Commun.*, **2014**, 50, 545 (b) R.R. Dasari, A. Dinder, C.K. Lo, C.Y. Wang, C. Quinton, S. Singh, S. Barlow, C.Fuentes-Hernandez, J.R. Reynolds, B. Kippelen, S.R. Marder, *Phys. Chem. Chem. Phys.* **2014**, 16, 19345 (c) T. Wu, C.Yu, Y. Guo, H. Liu, G. Yu, Y. Fang, Y. Liu, *J. Phys. Chem. C.* **2012**, 116, 22655 (d) Y. Chen, Z. Du, W. Chen, L. Han, Q. Liu, M. Sun, R. Yang, *Synthetic Metals*, **2014,** 187, 24

4) W. S. Yoon, S. K. Park, I. Cho, J.A. Oh, J. H. Kim, S. Y. Park, *Adv. Funct. Mater.*, **2013**, 23, 3519.

5) McCulloch, I.; Heeney, M.; Chabinyc, M. L.; DeLongchamp, D.; Kline, R. J.; Cölle, M.; Duffy, W.; Fischer, D.; Gundlach, D.; Hamadani, B.; Hamilton, R.; Richter, L.; Salleo, A.; Shkunov, M.; Sparrowe, D.; Tierney, S.; Zhang, W. *Adv. Mater.* **2009**, 21, 1091.

6) Donald Pavia, Gary Lampman, George Kriz, James Vyvyan, Introduction to Spectroscopy 4th ed. pp.15-104.

Chapter 3. Structure-Property Relationship of Isoindigo and Thienoisoindigo as Acceptor Units in D-A Polymers

3.1 Introduction

Combining electron-rich and electron-deficient units to form donor-acceptor (D-A) type of polymers is the most widely used strategy to develop low band-gap polymers. The advantages of this class of polymers are that they have broad absorption spectra and proper energy levels of polymers. Those can be easily tuned by combining different electron-rich and electron-deficient units as well as by substituting different side groups.[1)] D-A type polymers are good for high performance optoelectronic devices. The reasons of highly performing devices are followed. 1) Polymers are better for forming uniform film on substrates because of their viscosity. 2) Because of solubility issues, bulky alkyl chains are introduced so that polymer devices are able to solution-process with easiness. 3) Compared with small molecules, polymers are suitable for flexible devices considering mechanical properties and 4) D-A type polymers improve their intramolecular charge interaction and have low band-gap.[2)] In case of D-A type polymers, in particular lactam-containing acceptor units, frontier orbital energies are mostly dependent on own nature of donor and acceptor. That is, donor units mostly affect to HOMOs and acceptor units mostly affect to LUMOs. For application to OFET devices, planar structures through polymer backbone are essential. Donor units of D-A polymers are mostly used as heteroacenes because of their planarity and donating properties. For using acceptor units, imide-functionalized organic dyes are favorable. They have

already planar structure of lactam moiety and thienyl linkers are effectively planarized of D-A structures. Imide-functionalized organic dyes with thienyl group, specifically, have strong electron-withdrawing ability. Furthermore, with thienyl group, S···O conformational locking improves coplanarity of polymers.

In this chapter, new donor units were introduced for D-A type polymers. Indolo[3,2-b]indole has strong donating property and constructs rigid and planar backbone.[3] Fluorinated backbone is more rigid and induces planar backbone due to of secondary interaction by fluorine.[4] With fluorine, indoloindole backbone have more deep HOMOs by own property of fluorine. Also, fluorine on indoloindole interacts with neighbored counter units—with thiophene; S···F interaction, and with phenynl or thienyl hydrogen, F···H hydrogen bonding formatting interaction. This donor unit will be published soon.[5]

Herein, I designed two polymers named P(EHTIID2T-HDIDIDF) and P(EHIID2T-HDIDIDF) with above mentioned strategy. My design rules for these polymers are followed: 1) Combine strong electron-withdrawing unit and strong electron-donating unit for forming low bandgap D-A polymer to improve D-A intramolecular interaction. 2) Introduce thiophene in acceptor units for coplanarity conformation. 3) Use fluorinate indoloindole is used for S···F secondary interaction and lowering HOMOs of polymers. In this chapter, comparison of these polymers focused on acceptor units for indicating structure-property relationship as aspect of device performances that are shown at Scheme 3.1. Two polymers would be shown different photophysical properties and field-effect charge transport abilities. Two polymers were successfully synthesized and characterized. Characterization was performed by

UV/VIS spectroscopy, gel permeation chromatography (GPC) and cyclic voltammetry (CV). Frontier molecular orbital energy levels of film state polymers and their optoelectronic properties are extracted from these data. From frontier molecular orbitals (FMOs), two polymers were noticed proper to apply for organic layers in OFET devices. Bottom-gate top-contact OFET devices are fabricated and two polymer showed p-channel dominant ambipolar properties. As expected from design strategy, the case with two polymers, P(EHTIID2T-HDIDIDF) was more stable and higher n-channel performance than P(EHIID2T-HDIDIDF) and it showed more balanced ambipolarity at high temperature because of its well-ordered alignment of films.

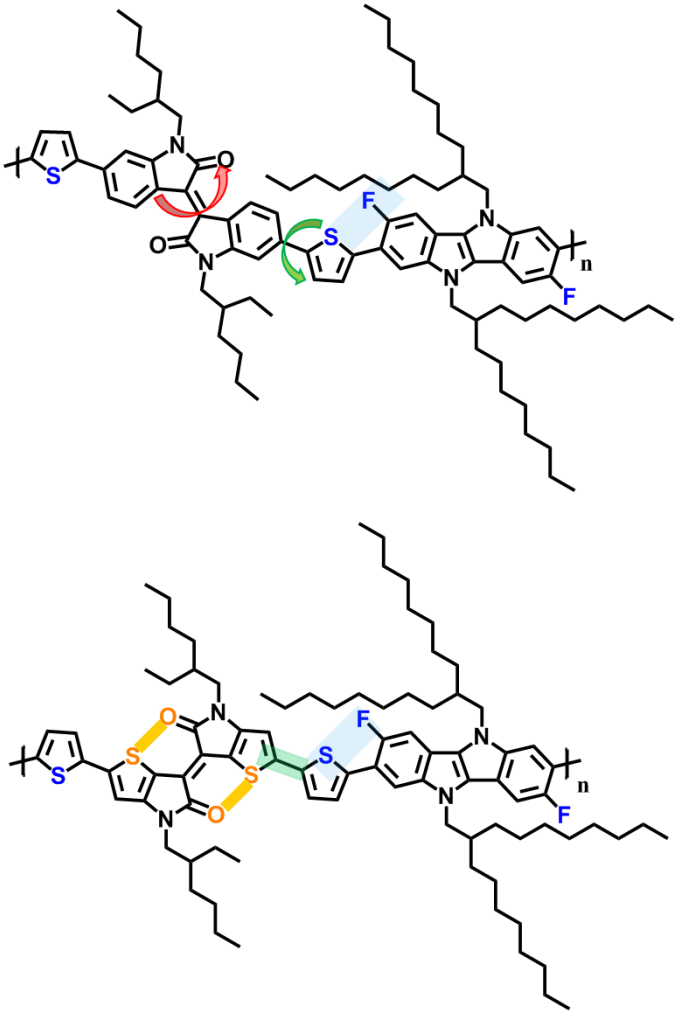

Scheme 3. 1 Schematic figure of design rules of two polymers. Upper : P(EHIID2T-HDIDIDF), Bottom : P(EHTIID2T-HDIDIDF)

3.2 Experimental

3.2.1 Synthesis

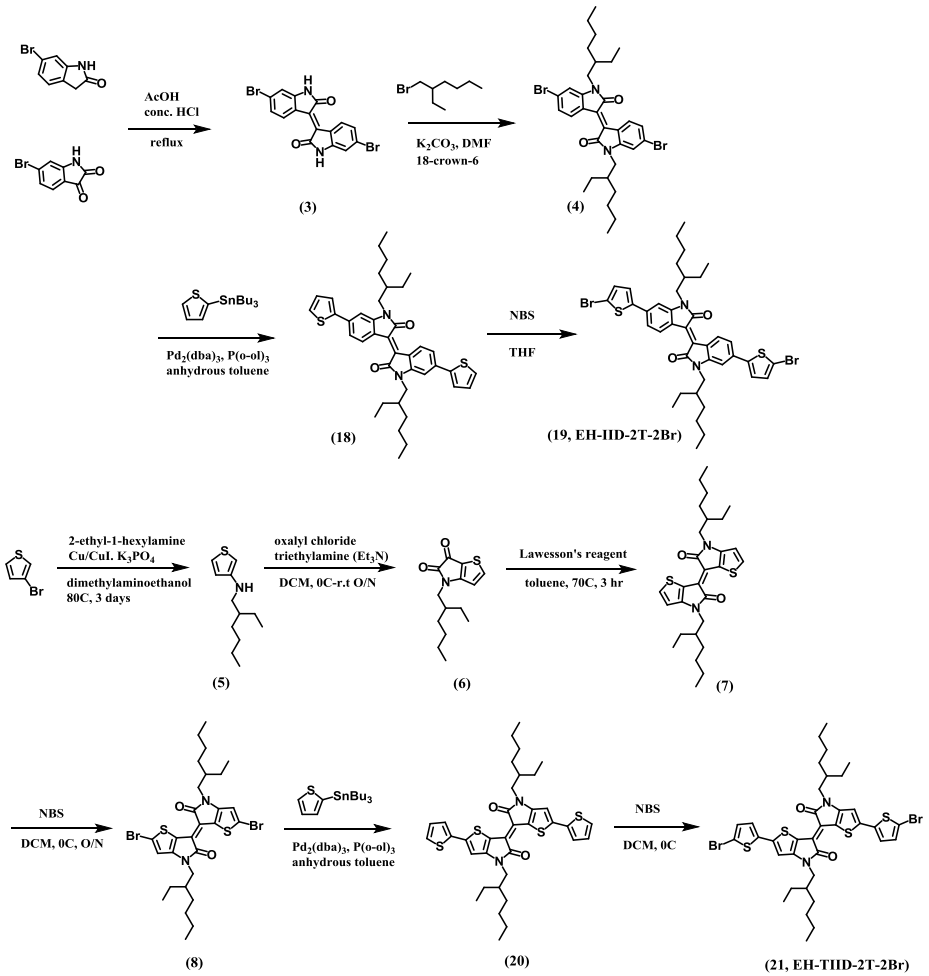

Scheme 3. 2 Synthetic route of monomers based on IID and TIID core for accepting unit

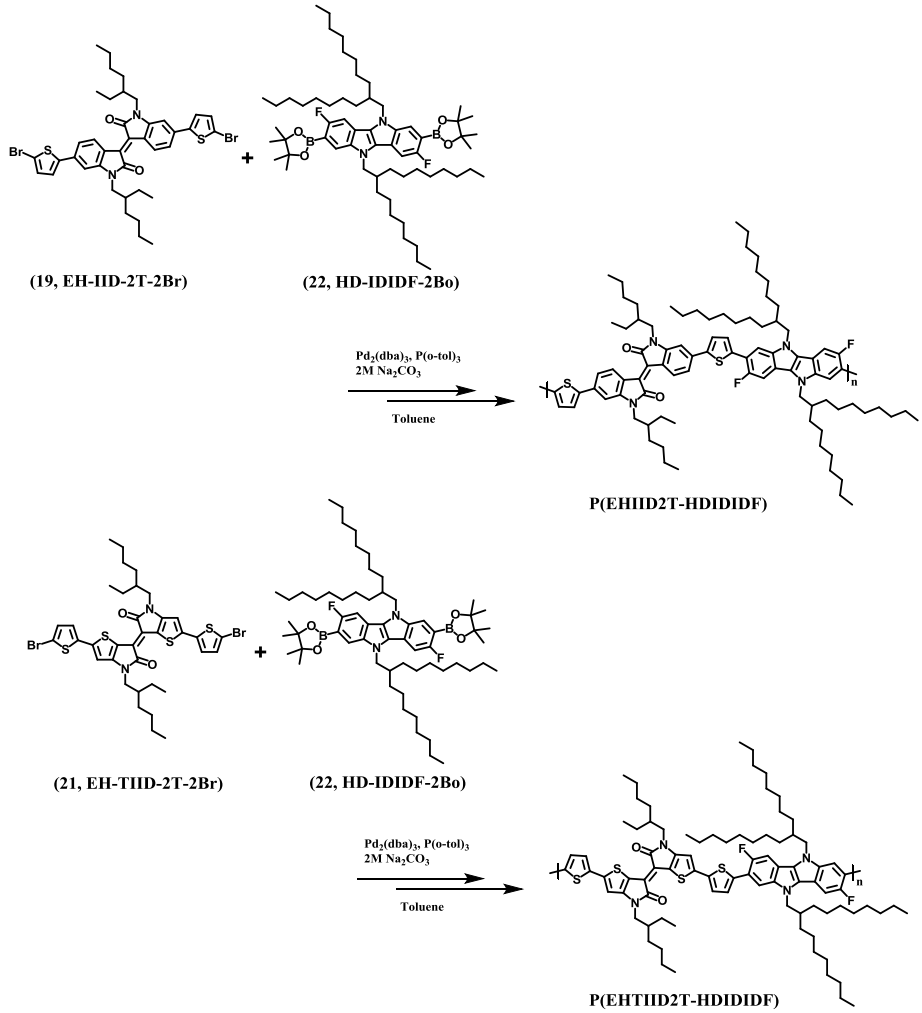

Scheme 3. 3 Suzuki polymerization schemes of two polymers P(EHIID2T-HDIDIDF) and P(EHTIID2T-HDIDIDF)

Target molecules are synthesized according to the procedure shown in Scheme 3.2 and 3.3. Unless stated otherwise, all reagents were purchased at Sigma Aldrich, TCI, Acros Organics, and Alfa Aesar.

(E)-6, 6'-dibromo-[3, 3'-biindolinylidene]-2, 2'-dione (3)

To a suspension of 6-bromoisatin (1) (1.066g, 4.72mmol) and 6-bromooxindole (2) (1.0g. 4.72mmol) in acetic acid (30mL), concentrated HCl (0.2mL) was injected to a 100mL round bottom flask. The mixture was refluxed at 120℃ for 24hr. After cooling to room temperature, the mixture was filtrated. The powder was washed with H_2O, ethanol, and ethyl acetate many times. The resulting maroon colored powder was taken and dried overnight under vacuum. (1.87g, 4.45mmol, Yield 94.4%) ^{1}H NMR (300 MHz, DMSO) δ 8.98 (d, *J* = 8.7 Hz, 2H), 7.17 (dd, *J* = 8.6, 1.9 Hz, 2H), 6.99 (sd, *J* = 1.9 Hz, 2H).

(E)-6, 6'-dibromo-1, 1'-bis (2-ethylhexyl)-[3, 3'-biindolinylidene]-2, 2'-dione (4)

Compound (3) (1.38g, 3.29mmol) and potassium carbonate (2.274g, 16.45mmol) were dissolved in dimethyl formaldehyde (DMF) (50mL) to a 100mL round bottom flask and stirring for 1hr under Argon at 100℃. 2-ethyl-1-hexyl bromide (1.29mL, 7.24mmol) and 18-crown-6 ether (0.2g) was added. The mixture was refluxed overnight. After cooling to room temperature, mixture was poured into water. The organic phase was extracted with diethyl ether, washed with brine, and dried over $MgSO_4$. The organic solvent was

evaporated and the deep red solids were purified by silica chromatography. The resulting dark red colored powder was taken and dried overnight under vacuum. (1.01g, Yield 47.9%) ^{1}H NMR (300 MHz, $CDCl_3$) δ 9.06 (d, *J* = 8.6 Hz, 2H), 7.17 (dd, *J* = 8.6, 1.8 Hz, 2H), 6.91 (sd, *J* = 1.8 Hz, 2H), 3.76 – 3.52 (m, 4H), 1.84 (s, 2H), 1.35 (dt, *J* = 13.2, 8.6 Hz, 16H), 1.05 – 0.78 (m, 12H).

(E)-1, 1'-bis(2-ethylhexyl)-6, 6'-di(thiophen-2-yl)-[3, 3'-biindolinylidene]-2, 2'-dione (18)

Compound (4) (0.5g, 0.78mmol) and tributyl(thiophen-2-yl)stannane (0.87g, 2.33mmol) was dissolved to anhydrous toluene 20mL and degassing through Ar bubbling. The solution was injected to flame dried 50mL round bottom flask under Ar atmosphere. Tris(dibenzylidene-acetone)-dipalladium(0) (0.036g, 0.04mmol) and tri(o-tolyl)phosphine (0.04g, 0.016mmol) was also dissolved in anhydrous toluene 10mL and degassing. Then solution was added to mixture of round bottom flask and refluxed overnight. After cooling to room temperature, the mixture was extracted with dichloromethane and washed with brine. The organic phase was evaporated and residue crude was purified with column chromatography (eluent as ethyl acetate and hexane). Obtained dark brown solid was dried overnight through vacuum oven. (0.46g, Yield 91.09) ^{1}H NMR (300 MHz, $CDCl_3$) δ 9.17 (d, *J* = 8.4 Hz, 2H), 7.42 (d, *J* = 3.6 Hz, 2H), 7.36 (d, *J* = 5.1 Hz, 2H), 7.31 (dd, *J* = 8.4, 1.6 Hz, 2H), 7.13 (td, *J* = 5.0, 3.7 Hz, 2H), 7.00 (sd, *J* = 1.5 Hz, 2H), 3.84 – 3.62 (m, 4H), 1.95 – 1.82 (m, 2H), 1.50 – 1.19 (m, 16H), 1.04 – 0.82 (m, 12H).

(E)-6, 6'-bis(5-bromothiophen-2-yl)-1, 1'-bis(2-ethylhexyl)-[3,3'-biindol-inylidene]-2,2'-dione (19, EH-IID-2T-2Br)

In a 100mL round bottom flask, compound (18) (0.2g, 0.31mmol) was dissolved in THF 40mL. The reaction mixture was cooling down to 0℃. The tetrahydrofuran (THF) solution of N-bromosuccinimide (0.11g, 0.62mmol) was slowly added. Then, mixture was warmed to room temperature and stirred for overnight. The solution was work-up with brine and extracted with dichloromethane. After column chromatography, as eluent as toluene and hexane, fresh dark brown colored solid was obtained. (0.19g, Yield 76.45%) ^{1}H NMR (300 MHz, $CDCl_3$) δ 9.16 (d, *J* = 8.4 Hz, 2H), 7.20 (dd, *J* = 8.4, 1.6 Hz, 2H), 7.16 (d, *J* = 3.9 Hz, 2H), 7.08 (d, *J* = 3.9 Hz, 2H), 6.89 (s, 2H), 3.71 (m, 4H), 1.95 – 1.80 (m, 2H), 1.47 – 1.22 (m, 16H), 1.05 – 0.82 (m, 12H).

N-(2-ethylhexyl)thiophen-3-amine (5)

Cupper powder (0.29g, 4.60mmol), Cupper Iodide (0.87g, 4.60mmol) and Potassium phosphate tribasic (39.06g, 184.01mmol) and dimethylaminoethanol 100mL was added to flame-dried 250mL round bottom flask. 3-bromothiophene (15.0g, 92.00mmol) was injected to mixture and vigorous stirred during 0.5hr. 2-ethyl-1-hexylamine (17.84g, 138.01mmol) was injected and refluxed 2days. After cooling to room temperature, the mixture was filtered with ethyl acetate. The filtrate was evaporated and crude oil was purified with column chromatography (eluent as ethyl acetate and hexane). The obtained yellowish brown oil was dried through vacuum oven. (Air-sensitive) (16g, Yield 82.28%) ^{1}H NMR (300 MHz, CDCl3) δ 7.14 (dd, J = 5.1, 3.0 Hz, 2H), 6.61 (dd, J = 5.1, 1.5 Hz, 2H), 5.92 (dd, J = 3.0, 1.5 Hz, 2H), 3.57 (s, 1H), 2.98

(d, J = 6.0 Hz, 2H), 1.67 – 1.48 (m, J = 11.9, 6.0 Hz, 2H), 1.48 – 1.33 (m, 6H), 1.00 – 0.75 (m, 10H).

4-(2-ethylhexyl)-4H-thieno[3,2-b]pyrrole-5,6-dione (6)

Compound (5) (3.0g, 14.19mmol) and dichloromethane 20mL was added to a flame-dried 100mL round bottom flask under Ar atmosphere and cooled down using ice-bath. The dichloromethane (10mL) solution of oxalyl chloride (2.70g, 21.29mmol) was drop-wise added. The mixture was stirring for 0.5hr at 0℃. The dichloromethane (10mL) solution of trimethylamine (7.18g, 70.96mmol) was drop-wise added carefully. Then ice-bath was removed and the reaction mixture was stirred at room temperature during overnight. The mixture was worked-up with H_2O and extracted with dichloromethane. The organic phase was washed with brine over 3 times. The solvent was evaporated and crude solid was purified with column chromatography. The dark-orange oil was obtained and dried overnight though vacuum oven. Then, dark-orange solid was taken. (1.17g, Yield 31.25%) ^{1}H NMR (300MH, $CDCl_3$, δ) 8.00 (d, J = 5.0 Hz, 2H), 6.77 (d, J = 5.0 Hz, 2H), 3.54 (d, J = 8.0 Hz, 4H), 1.80 – 1.68 (m, 2H), 1.45 – 1.20 (m, 18H), 1.00 – 0.83 (m, 10H).

(E)-4,4'-bis(2-ethylhexyl)-[6,6'-bithieno[3,2-b]pyrrolylidene]-5,5'(4H,4'H)-dione (7)

In a 100mL round bottom flask, compound (6) (1.0g, 3.77mmol) was dissolved in toluene 40mL. Lawesson's reagent (0.90g, 2.07mmol) was added to mixture and stirred. The reaction mixture was heated to 70℃ during 3hr.

The solvent was evaporated and crude solid was purified with column chromatography. The magenta-purple solid was obtained. (1.0g, Yield 53.18%) ^{1}H NMR (300MH, $CDCl_3$, δ) 7.52 (d, J = 5.1 Hz, 2H), 6.78 (d, J = 5.1 Hz, 2H), 3.69 (d, J = 7.4 Hz, 4H), 1.94-1.85 (m, 2H), 1.80 – 1.68 (m, 2H), 1.45 – 1.20 (m, 18H), 1.00 – 0.83 (m, 10H).

(E)-2,2'-dibromo-4,4'-bis(2-ethylhexyl)-[6,6'-bithieno[3,2-b]pyrrolylidene]-5,5'(4H,4'H)-dione (8)

In a 100mL round bottom flask, compound (7) (0.9g, 1.90mmol) was dissolved in THF 40mL. The reaction mixture was cooling down to 0℃. The tetrahydrofuran (THF) solution of N-bromosuccinimide (0.76g, 4.29mmol) was slowly added. Then, mixture was warmed to room temperature and stirred for 3hr. The solution was work-up with brine and extracted with dichloromethane. After flash alumina column, fresh purple colored solid was obtained. (0.6g, Yield 48%) ^{1}H NMR (300MH, $CDCl_3$, δ) 6.82 (s, 2H), 3.64 (d, J = 7.5 Hz, 4H), 1.85 – 1.72 (m, 2H), 1.42 – 1.20 (m, 18H), 0.97 – 0.82 (m, J = 8.1 Hz, 10H).

(E)-4,4'-bis(2-ethylhexyl)-2,2'-di(thiophen-2-yl)-[6,6'-bithieno[3,2-b]pyrrolylidene]-5,5'(4H,4'H)-dione (20)

Compound (8) (0.44g, 0.67mmol) and tributyl(thiophen-2-yl)stannane (1.25g, 3.35mmol) was dissolved to anhydrous toluene 20mL and degassing through Ar bubbling. The solution was injected to flame dried 50mL round bottom flask under Ar atmosphere. Tris(dibenzylidene-acetone)-dipalladium(0) (0.031g,

0.03mmol) and tri(o-tolyl)phosphine (0.035g, 0.013mmol) was also dissolved in anhydrous toluene 10mL and degassing. Then solution was added to mixture of round bottom flask and refluxed overnight. After cooling to room temperature, the mixture was extracted with dichloromethane and washed with brine. The organic phase was evaporated and residue crude was purified with column chromatography (eluent as ethyl acetate and hexane). Obtained dark blue solid was dried overnight through vacuum oven. (0.27g, Yield 60.78%) ^{1}H NMR (300 MHz, $CDCl_3$) δ 7.39 (d, *J* = 3.7 Hz, 2H), 7.31 (d, *J* = 5.1 Hz, 2H), 7.07 (td, *J* = 5.0, 3.7 Hz, 2H), 6.86 (s, 2H), 3.71 (d, *J* = 7.5 Hz, 4H), 1.93 – 1.83 (m, 2H), 1.47 – 1.22 (m, 18H), 1.00 – 0.82 (m, 10H)

(E)-2,2'-bis(5-bromothiophen-2-yl)-4,4'-bis(2-ethylhexyl)-[6,6'-bithieno[3,2-b]pyrrolylidene]-5,5'(4H,4'H)-dione (21, EH-TIID-2T-2Br)

In a 100mL round bottom flask, compound (20) (0.27g, 0.31mmol) was dissolved in dichloromethane (DCM) 40mL. The reaction mixture was cooling down to 0℃. The DCV solution of N-bromosuccinimide (0.145g, 0.81mmol) was slowly added. Then, mixture was stirred until reaction was finished through indicating thin-film chromatography. The solution was work-up with brine and extracted with dichloromethane. After column chromatography, as eluent as chloroform, ethyl acetate and hexane, fresh dark green colored solid was obtained. (0.25g, Yield 74.78%) ^{1}H NMR (300 MHz, $CDCl_3$) δ 7.12 (d, *J* = 3.7 Hz, 2H), 7.02 (d, *J* = 3.9 Hz, 2H), 6.77 (s, 2H), 3.69 (d, *J* = 7.2 Hz, 4H), 1.90 – 1.79 (m, 2H), 1.45 – 1.22 (m, 18H), 0.99 – 0.83 (m, 10H).

3,8-difluoro-5,10-bis(2-octyldecyl)-2,7-bis(4,4,5,5-tetramethyl-1,3,2-dioxaborolan-2-yl)-5,10-dihydroindolo[3,2-b]indole (22, HD-IDIDF-2Bo)

Procedures will be published.[5)] This material is provided by I. Cho.

P(EHIID2T-HDIDIDF)

In a 10mL round bottom flask, compound (19) (68.6mg, 0.08483mmol) and compound (22) (80.0mg, 0.08483mmol) were taken with exactly same equivalent. 2M of sodium bicarbonate solution 0.4ml was added. Degassed toluene 3ml was added slowly and step-wised. The reaction mixture was refluxed for 2days. The mixture was precipitated into cold methanol 300ml for solidification. The 73mg of crude polymers were taken and flash filtered in short silica and alumina column. Methanol, acetone, hexane and chloroform Soxhlet purification were followed. The dark brown colored polymer was collected. (55mg, Initial yield : 63.6%), GPC : M_n : 24000, M_w : 50000, PDI : 2.06

P(EHTIID2T-HDIDIDF)

In a 10mL round bottom flask, compound (21) (69.6mg, 0.08483mmol) and compound (22) (80.0mg, 0.08483mmol) were taken with exactly same equivalent. 2M of sodium bicarbonate solution 0.5ml was added. Degassed toluene 4.5ml was added slowly and step-wised. The color of mixture was changed immediately. The reaction mixture was refluxed for 36hrs. The mixture was precipitated into cold methanol 300ml for solidification. The 84mg of crude polymers were taken and flash filtered in short silica and alumina

column. Methanol, acetone, hexane and chloroform Soxhlet purification were followed. The dark green colored polymer was collected. (69mg, Initial yield : 77.6%), GPC : M_n : 16000, M_w : 39000, PDI : 2.48

3.2.2 Instruments and measurements

All synthesized materials were identified with ^{1}H NMR (Bruker, Avance-300) with deuterated solvent $CDCl_3$, THF-d_4, ACT-d_6, and DMSO-d_6. Further, for target molecules, GPC (Waters, refractive index detectors 2414, isocratic HPLC pump 1515) was also used for determine polydispersity index (PDI) and mass-average and number-average molecular weight of polymers with reference polymer in chloroform solution. The melting temperature of the target polymers was determined using differential scanning calorimeter (DSC, TA instruments, Q1000) under N_2 atmosphere. The thermostability of polymers was checked using thermal gravimetric analysis (TGA, TA instruments, Q-5000 IR) under N_2 atmosphere.

UV/VIS absorption spectra were detected by SHIMADZU UV-1650PC in both solution and film state for various temperatures. The frontier orbital energy levels, especially HOMOS, were recorded on cyclic voltammetry (CV, Princeton Applied Research, 273 A). For CV detection, one-component electrolysis cell was used consisting of a platinum working electrode, a platinum wire counter-electrode, and a quati Ag^{+}/Ag reference electrode. The 0.1M of tetrabutylammonium hexafluorophosphate (TBAHFP) in acetonitrile (ACN) was used for solid state as supporting electrolytes. The LUMO levels were calculated by the optical band-gaps that were recorded on UV/VIS spectroscopy and HOMO levels that were recorded on CV on film and solution state respectively. The morphology study was carried out thorough atomic force microscopy (AFM) which operating measurement was a Multimode with Nanoscope V controller, Bruker.

Also, computational study was followed for comparison of two polymers.

Theoretical molecular orbital calculation was carried out using density functional theory (DFT). Gaussian09 at B3LYP/6-31G* level was used to characterize optimized structure, electron density, and frontier molecular orbital energy at ground state.

3.2.3 Fabrication and evaluation of organic thin-film transistors

Organic thin-film transistors (organic field-effect transistor, OFET) with a bottom-gate/top-contact configuration were fabricated on a SiO_2/Si (300nm thick SiO_2) substrate. Prior to device fabrication, SiO_2/Si was rinsed with acetone and isopropyl alcohol respectively for 10mins in ultrasonicator. Then, UV (360nm wavelength) ozone treatment was followed for 20mins. Before deposition of organic semiconductors, octadecyltrichlorosilane (ODTS) was treated in a vacuum on substrates to form ODTS self-assembled monolayer. Substrates were brought into a nitrogen (N_2)-filled glove box. And organic thin films were formed by spin-coating process. And annealing steps were followed during 15mins. Each annealing temperatures were 100℃, 150℃, and 200℃ respectively. Thermally deposition of gold (Au) electrodes (50nm thick) were followed up thorough a metal mask in a vacuum metal chamber. The I-V characteristics of individual devices were measured using Keithley 4200 connected to a probe station. The mobility values of OFETs in saturation region were calculated from $\partial I_{D,sat}^{1/2}/\partial V_G$, where,

$$I_{D,sat} = \frac{W}{2L} C_{ox} \mu_{sat} (V_G - V_T)^2$$

W, L values were estimated by optical microscope and V_D=100V.[4)]

3.3 Results and Discussion

3.3.1 Theoretical molecular orbital calculation used density functional theory (DFT)

Theoretical molecular orbital calculation was preceded for prediction of optoelectrical properties. Computational study based density functional theory (DFT) was proceeded by using Gaussian09 and basis set was B3LYP/6-31G*.

As shown at Figure 3.1, polymers were simplified for easy and fast calculation. In optimized ground state, all of two polymers are shown slightly twisted. P(EHTIID2T-HDIDIDF), however, has more planar backbone thorough the polymer chains. Shown side-view of two polymers in Figure 3.1 and Figure 3.2 respectively, P(EHIID2T-HDIDIDF) has more distorted structure than P(EHTIID2T-HDIDIDF) as I expected. Isoindigo units of P(EHIID2T-HDIDIDF) has distorted structure with 24.67° even though thienoisoindigo units of P(EHTIID2T-HDIDIDF) has planar structure with nearly zero distortion angle(0.06°). From this, although HDIDIDF and thiophene linkers reduce distortion of backbone, P(EHIID2T-HDIDIDF) is more distorted than P(EHTIID2T-HDIDIDF). It is because S···O secondary interaction between carbonyl oxygen and sulfur on thiophene of thienoisoindigo core. As I mentioned in previous chapter, TIID core is proper for OFET applications due to its coplanarity.

With the optimized geometry in Figure 3.1 and Figure 3.2, frontier molecular orbital (FOM) energy levels were recorded. In that calculation, there were no other conditions, which were relevant real environment and polymers were simplified to D-A-D type small molecules. There were not exactly matched with measured data from UV/VIS and CV. However, tendency of optoelectrical

property was estimated with accuracy. Calculated FMO energy levels were shown in Table 3.1. P(EHTIID2T-HDIDIDF) had more high HOMO levels and more low band-gap energy. It originated in its planar structure and effective expansion of π-conjugation over maintaining similar LUMO levels.

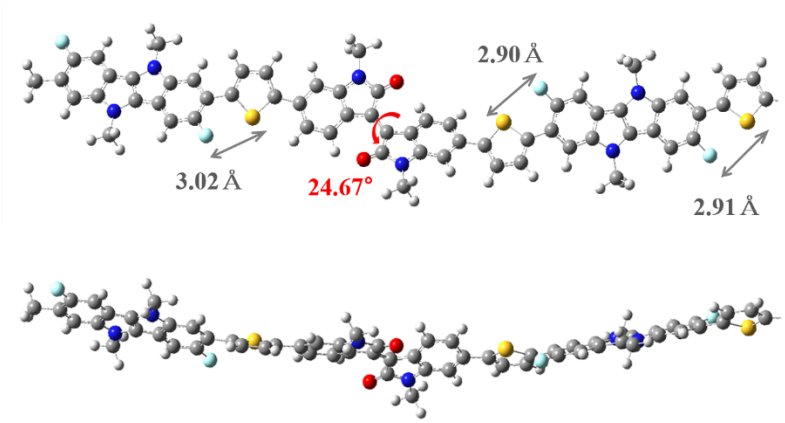

Figure 3. 1 Optimized structure of P(EHIID2T-HDIDIDF). Upper : top view, Bottom : side view.

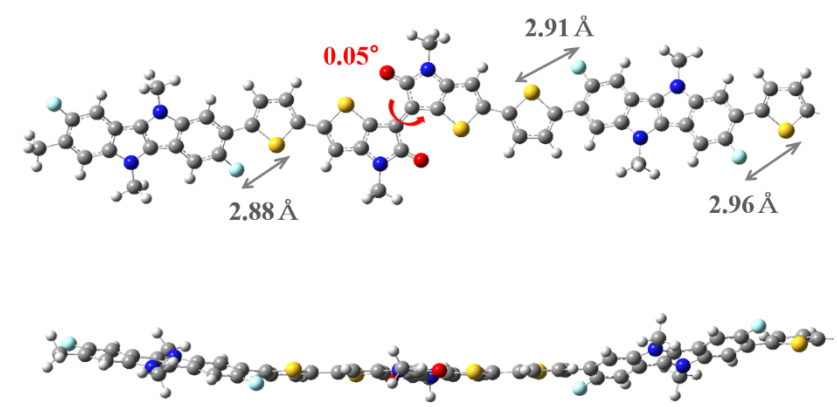

Figure 3. 2 Optimized structure of P(EHTIID2T-HDIDIDF). Upper : top view, Bottom : side view.

Table 3. 1 Theoretical molecular orbital [a] of two polymers, P(EHIID2T-HDIDIDF) and P(EHTIID2T-HDIDIDF)

Compound	E_{HOMO} (eV)	E_{LUMO} (eV)	λ_g (eV) [b]
P(EHIID2T-HDIDIDF)	-4.82	-2.88	1.94
P(EHTIID2T-HDIDIDF)	-4.43	-2.72	1.71

a) DFT calculation was carried out on molecular structures of four target molecules modified with methyl group at N-position in lactam, instead of 2-ethylhexyl group and polymers were simplified to small molecules for easy and fast calculations.
b) Calculated from the differences between theoretical HOMO and LUMO levels.

3.3.2 Optical and electrochemical properties of polymers

Absorbance spectra of IID- and TIID- based polymers in solution and film state are shown in Figure 3.3. And the electrochemical properties of polymers were measured by cyclic voltammetry (CV). The LUMO levels of them were calculated from optical band-gap from UV/VIS and HOMOs extracted from CV data. The HOMO levels as an aspect of electrochemical properties, that was also called oxidation potentials for each derivatives, were measured in relation to ferrocene (Fc/FC^{+}=4.8eV), which was typically used as a reference in solution and film state. UV/VIS absorption spectra are shown at Figure 3.3. Further, UV/VIS and CV data of films are shown at Figure 3.4. Optical properties of polymers are shown at Table 3.2. The HOMO and LUMO levels and optical band-gaps are in Table 3.3.

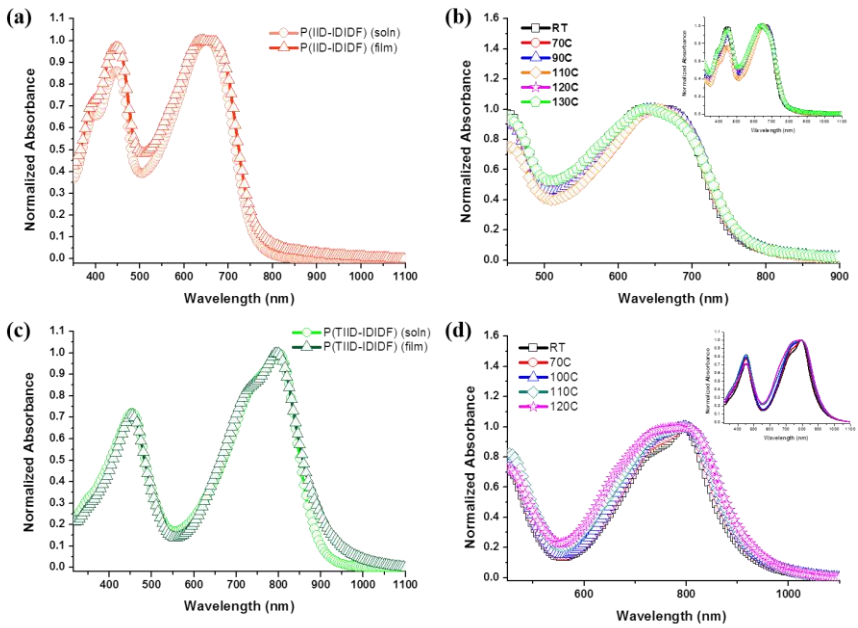

Figure 3. 3 UV/VIS absorption spectra of polymers in solution and film state. Solution and film state UV/VIS absorption spectra of (a)P(EHIID2T-HDIDIDF) and (c)P(EHTIID2T-HDIDIDF). Film state absorption spectra via annealing substrates with increasing temperatures (b) P(EHIID2T-HDIDIDF) and (d)P(EHTIID2T-HDIDIDF)

Table 3. 2 Optical properties of two polymers in solution and film state.

Compound	λ_{abs} (nm)	λ_{onset} (nm)	λ_g^{opt} (eV) [a]
P(EHIID2T-HDIDIDF) (soln) [b]	398 [d], 450, 652	756	1.64
P(EHIID2T-HDIDIDF) (film) [c]	397 [d], 448, 642	772	1.61
P(EHTIID2T-HDIDIDF) (soln) [b]	454, 739 [d], 800	892	1.40
P(EHTIID2T-HDIDIDF) (film) [c]	452, 793[d], 796	910	1.36

a) Optical band-gap energy was calculated from absorption edge (onset point).
Measured in $CHCl_3$ solution of b) concentration of 0.02075mg/ml.
c) Spin-coated with 8mg/ml concentration in $CHCl_3$ solution with filter syringe.
d) It is not an apparent peak, just shoulder near absorption.

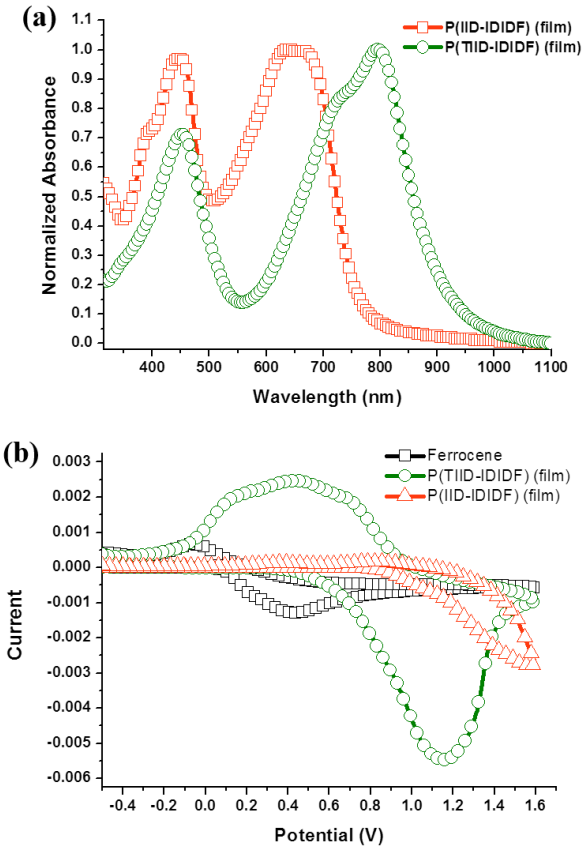

Figure 3. 4 (a) UV/VIS spectra and (b) CV graph of each polymers in film state. Polymers were spin-coated on glass for UV/VIS absorption spectra. Polymers were drop-casting for doping on ITO glass and supporting electrolyte was TBAHFB in acetonitrile (ACN) for CV detection. Ferrocene (blank) with TBAHFB in ACN solution as the reference.

Table 3. 3 Electrochemical properties and energy levels of each polymers on solution and solid state.

Compound	E_{HOMO} (eV) [a]	E_{LUMO} (eV) [b]	λ_g^{opt} (eV) [c]
P(EHIID2T-HDIDIDF) (soln)	N.A [d]	N.A [d]	1.64
P(EHIID2T-HDIDIDF) (film)	-5.56	-3.95	1.61
P(EHTIID2T-HDIDIDF) (soln)	N.A [d]	N.A [d]	1.40
P(EHTIID2T-HDIDIDF) (film)	-5.25	-3.89	1.36

a) Electrochemical HOMO level is recorded by cyclic voltammetry. It calculated from difference between ferrocene reference (-4.8eV) and each materials.
b) LUMO level is calculated with electrochemical HOMO and optical bandgap.
c) Optical bandgap was obtained by onset point of absorption.
d) Solution CV data was not detected because it was useless data for OFET.

Figure 3.3 shows normalized UV/VIS absorption spectra of each polymers in both solution and film state. Both of two polymers showed very slightly blue-shifted spectra in film state, actually almost same position on peaks, however, onset points are red-shifted. It meant solution and film state were similar state. On film state, as you can show at Figure 3.3 (b) and (d), shoulder peak of 600-800nm ranges was enhanced for P(EHTIID2T-HDIDIDF) and was blue-shifted for P(EHIID2T-HDIDIDF) when substrates were annealed increasing temperature step-wise. It meant that both of polymers are aggregated as form H-aggregate state. In case of P(EHIID2T-HDIDIDF), absorption was panchromatic and its color was dark brown. P(EHTIID2T-HDIDIDF), however, was green powder like suede because its absorption range was panchromatic also and to NIR region but less absorption on green region (500-600nm).

The reason that TIID-based polymer had larger onset point of absorption spectra might be come from its effective π-conjugation expansion by TIID's own structural planarity. More planar structure, more effective delocalization of π-electrons along the backbone. From this, TIID-based polymer, P(EHTIID2T-HDIDIDF), has smaller bandgap energy (1.36eV at film state and 1.40eV at solution state) than IID-based polymer, P(EHIID2T-HDIDIDF) (1.61eV at film state and 1.64eV at solution state). Although TIID- and IID-based polymers have different bandgap, all the materials are suitable for ambipolar organic field-effect transistors because of their FMO levels.

Mentioned in previous chapter, the organic materials should have appropriate FMO levels considering work-function of metals which were used for source and drain electrode. I checked energy levels of target molecules in solid state using CV method. UV/VIS spectra are shown in Figure 3.4(a) and CV profiles are in Figure 3.4(b) in film state. From the data of all, molecular energy levels

are indicated and summarized in Table 3.3 and they correlate well with initial research proposal. Comparing two polymers, P(EHIID2T-HDIDIDF) has more deep HOMO level (-5.56eV) than HOMO level (-5.25eV) of P(EHTIID2T-HDIDIDF) because of total donating strength of polymers. P(EHTIID2T-HDIDIDF) has stronger donating strength due to thiophenes of thienoisoindigo cores. So, they are high-lying HOMOs of polymers compared with P(EHIID2T-HDIDIDF). From those all information, I expect that two polymers are both proper for ambipolar OFET applications.

3.3.3 Thermal properties of polymers

The thermal properties of both polymers were investigated by differential scanning calorimetry (DSC) and thermogravimetric analysis (TGA) under N_2 atmosphere. Glass temperature (Tg) and decomposition temperature (Td) were checked. Melting point (Tm) was not detected. Thermal properties are summarized in Table 3.4 and shown in Figure 3.5.

Table 3. 4 Thermal properties of polymers [a)]

Polymers	T_g(℃)	T_d(℃)[b)]
P(EHIID2T-HDIDIDF)	100.06	378
P(EHTIID2T-HDIDIDF)	98.85	290

a) Increase rate of temperature is 5℃/min.
b) Decomposition temperature was checked when 5wt% weight loss occurred.

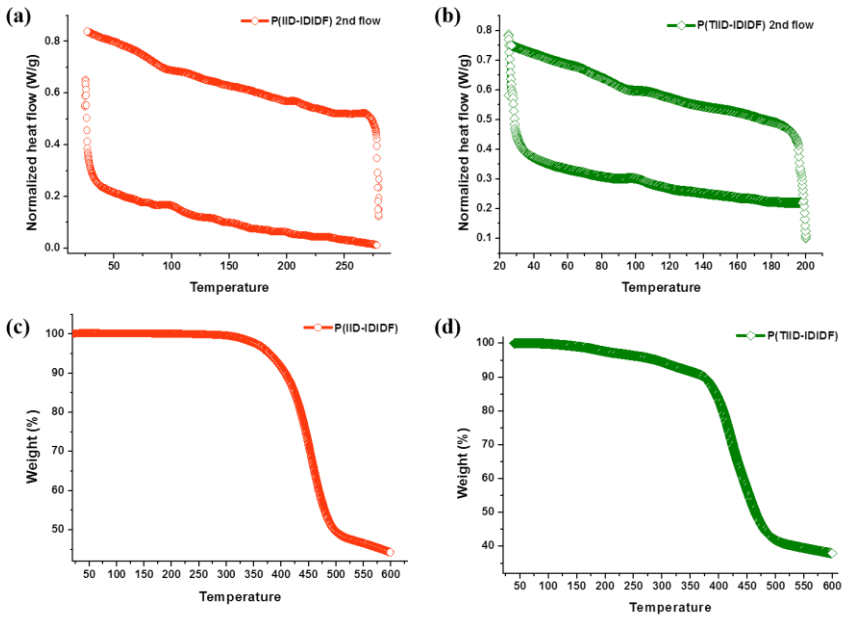

Figure 3. 5 DSC results of (a) P(EHIID2T-HDIDIDF) and (b) P(EHTIID2T-HDIDIDF), and TGA traces of (c) P(EHIID2T-HDIDIDF) and (d) P(EHTIID2T-HDIDIDF).

3.3.4 GI-XRD analysis

To throw light on structure-property relationships in two polymers, grazing incidence X-ray diffraction (GI-XRD) ise progressed. For determining packing nature differences between two polymers named P(EHIID2T-HDIDIDF) and P(EHTIID2T-HDIDIDF), GI-XRD patterns are supported.

GI-XRD patterns were carried out to investigating molecular stacking of each polymers at pristine films and optimized condition films. Each films were fabricated with 0.3wt% chloroform solution using spin-coating on ODTS treated Si/SiO^2 substrates. Pristine films were fabricated just spin-coating. Annealing temperature and times are same with optimized device conditions (150℃ for 15mins for P(EHIID2T-HDIDIDF) and 200℃ for 15mins for P(EHTIID2T-HDIDIDF)). Figure 3.6 (a) shows GI mode X-ray crystallography of P(EHIID2T-HDIDIDF) and Figure 3.6 (b) shows that of P(EHTIID2T-HDIDIDF). Theoretical calculations of lamellar stacking distance and π-π distance were based on Bragg's law, as follows,

$$n\lambda = 2d\sin\theta$$

where λ=1.54Å Cu Kα radiation and n=1.

In the P(EHIID2T-HDIDIDF) films, both of pristine and annealed films showed face-on stacking on substrates. Diffraction angle of (010) peak meant face-on π-π distance is 21.5°, representing 4.135Å. At annealed films, diffraction peak of (100), 5.38°, appeared representing lamellar stacking distance 16.433Å. In the P(EHTIID2T-HDIDIDF) films, both of pristine and annealed films show face-on stacking on substrates similarly with P(EHIID2T-HDIDIDF). Diffraction angle of (010) peak meant face-on π-π distance is 21.1°,

representing 4.212 Å. At annealed films, diffraction peak of (100), which is 5.26°, appeared representing lamellar stacking distance 16.808 Å. Furthermore, P(EHTIID2T-HDIDIDF) showed also diffraction peak of (200), which is 10.7°, appearing lamellar stacking. It means that alignment at each annealed films is better in case of P(EHTIID2T-HDIDIDF). Well-alignment of P(EHTIID2T-HDIDIDF) polymer films annealing at optimized condition showed better n-channel performance than P(EHIID2T-HDIDIDF) keeping similar high p-channel mobility. This results support that P(EHTIID2T-HDIDIDF) has more planar structure than P(EHIID2T-HDIDIDF) because of planarity of thienoisoindigo cores.

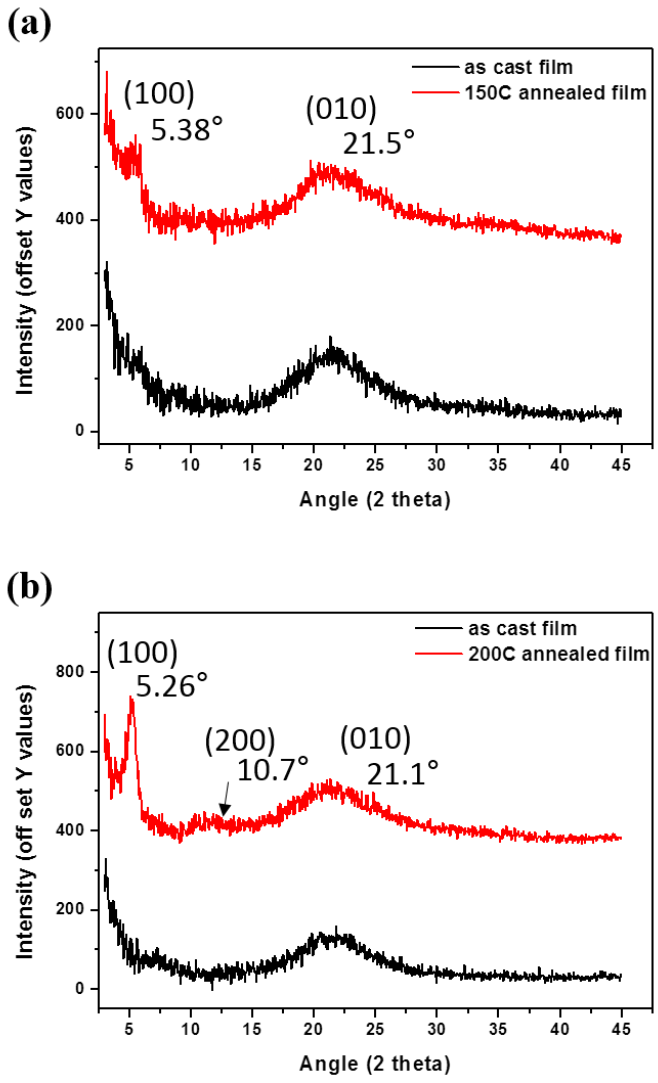

Figure 3. 6 XRD diffraction data of (a) P(EHIID2T-HDIDIDF) with 3000rpm and (b) P(EHTIID2T-HDIDIDF) with 2000rpm, using 0.3wt% chloroform solution at each optimized conditions and pristine films in GI-mode.

3.3.5 OFETs performance

To throw light on structure-property relationships in IID-based polymer and TIID-based polymer, we fabricated bottom-gate/top-contact OFET devices with gold electrodes. All the devices were generated n-octadecyltrimethoxy-silane (ODTS) treated SiO_2/Si substrate. Organic layers were spin-coated with spin-rate 2000rpm for P(EHTIID2T-HDIDIDF) and 3000rpm for P(EHIID2T-HDIDIDF) using 0.3wt% chloroform solutions. Channel lengths were 30 and 40nm and width is 1mm. The field-effect mobility was extracted from the saturated region by fitting the slope of square root drain current vs. gate bias. All fabrication and device testing was performed under inert conditions. Two polymers showed that p-channel dominant ambipolar properties because of their own FMO levels.

In P(EHIID2T-HDIDIDF), the highest performing devices were 150℃ annealed film. Max mobilities were $\mu_e = 3.09\times10^{-4} cm^{-1}V^{-1}s^{-1}$ and $\mu_h = 3.04\times10^{-2} cm^{-1}V^{-1}s^{-1}$. It showed p-channel dominant ambipolar transistor property. As I mentioned above, because of limit of isoindigo unit, p-channel dominant ambipolarity shown at devices is poor transport ability. Charge transport ability was enhanced according to increasing spin rates and temperature. As increased spin rate, organic layers were uniforms on substrates so that mobility was increased. As temperature was increased, organic layers were well ordered so that n-channel mobility was increased dramatically.

However, in P(EHTIID2T-HDIDIDF) devices, the highest performing devices were 200℃ annealed film. Unlike P(EHIID2T-HDIDIDF), P(EHTIID2T-HDIDIDF) showed more balanced ambipolarity keeping high p-channel mobility. Charge transport ability was enhanced according to increasing spin

rates and temperature. As temperature was increased, organic layers were well-ordered so that n-channel mobility was increased dramatically and all tested channel showed mobility. From those results, P(EHTIID2T-HDIDIDF) showed better n-channel charge transport ability because of its coplanarity I expected from DFT calculation and UV/VIS spectra. Max mobilities were $\mu_e = 4.44\times10^{-3} cm^{-1}V^{-1}s^{-1}$ and $\mu_h = 1.14\times10^{-2} cm^{-1}V^{-1}s^{-1}$. So, P(EHTIID2T-HDIDIDF) had less torsion angles so that it is relevant for OFET application.

Better mobilities of each polymers were caused by well-ordered films from film XRD studies which I discussed at prvious section. Transfer curves and output curves of P(EHIID2T-HDIDIDF) and P(EHTIID2T-HDIDIDF) in best performed devices are shown at Figure 3.7 and Figure 3.8 respectively. Figure 3.8 (a) and (b) show clear ambipolar curve because of balancing of transport. However, transfer curves not showed typical ambipolar curve but currents are flown when voltage value is 0V. Through these, ambipolarity was checked.At Table 3.5, average and max mobilities of P(EHIID2T-HDIDIDF) on various conditions are summarized. P(EHTIID2T-HDIDIDF) mobilities on various conditions are also summarized at Table 3.6.

Table 3. 5 Electrical performance of OFET devices based on polymer P(EHIID2T-HDIDIDF) solution-processed thin films with Au electrodes [a)]

Temp. (℃) [b)]	n/p	1000rpm		2000rpm		3000rpm	
		Aver. (n)	Max.	Aver. (n)	Max.	Aver. (n)	Max.
RT	n	2.51E-06 (10)	6.78E-06	1.31E-06 (11)	5.19E-06	1.69E-06 (12)	4.45E-06
	p	2.93E-03 (21)	5.15E-03	1.46E-03 (11)	2.44E-03	1.64E-03 (12)	2.97E-03
100	n	2.00E-05 (15)	8.81E-05	N.A.[c)]		1.34E-05 (8)	8.35E-05
	p	4.62E-03 (16)	8.94E-03	N.A.[c)]		5.44E-03 (9)	9.24E-03
150	n	1.40E-05 (18)	5.25E-05	9.62E-05 (9)	5.73E-04	1.21E-04 (11)	3.09E-04
	p	5.06E-03 (18)	7.96E-03	1.41E-02 (10)	2.12E-02	1.90E-02 (11)	3.04E-02
200	n	N.A.[c)]		N.A.[c)]		6.14E-05 (12)	2.02E-04
	p	N.A.[c)]		N.A.[c)]		1.39E-03 (11)	1.97E-02

a) Unit of mobility is $cm^2V^{-1}s^{-1}$.
b) Annealing substrates after spin-coating during 15mins.
c) Not tested condition.

Table 3. 6 Electrical performance of OFET devices based on polymer P(EHTIID2T-HDIDIDF) solution-processed thin films with Au electrodes [a)]

Temp. (℃) [b)]	n/p	1000rpm		2000rpm		3000rpm	
		Aver. (n)	Max.	Aver. (n)	Max.	Aver. (n)	Max.
RT	n	3.30E-07 (1)	3.30E-07	2.45E-06 (8)	9.37E-06	1.68E-06 (10)	5.79E-06
	p	9.42E-04 (19)	2.66E-03	9.43E-04 (9)	1.25E-03	1.23E-03 (12)	2.20E-03
100	n	9.57E-07 (4)	1.65E-06	3.07E-05 (11)	8.45E-05	N.A.[c)]	
	p	3.32E-03 (17)	7.60E-03	2.63E-03 (12)	5.37E-03	N.A.[c)]	
150	n	3.74E-05 (12)	1.28E-04	2.33E-04 (12)	1.15E-03	1.16E-05 (12)	2.25E-05
	p	7.17E-03 (21)	1.75E-02	5.43E-03 (13)	9.84E-03	4.27E-03 (12)	5.36E-03
200	n	N.A.[c)]		1.19E-03 (13)	4.44E-03	N.A.[c)]	
	p	N.A.[c)]		6.33E-03 (16)	1.14E-02	N.A.[c)]	

a) Unit of mobility is $cm^2V^{-1}s^{-1}$.
b) Annealing substrates after spin-coating during 15mins.
c) Not tested condition.

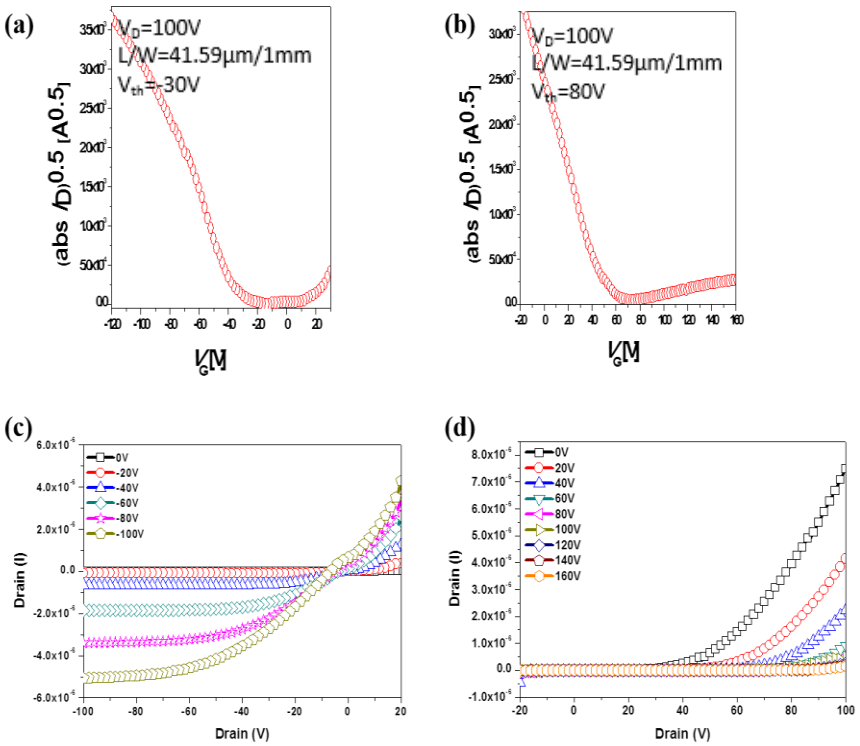

Figure 3. 7 Transfer curves of (a) p-channel operation and (b) n-channel operation. Output curves of (c) p-channel operation and (d) n-channel operation. These characteristics of P(EHIID2T-HDIDIDF) were detected at best conditions

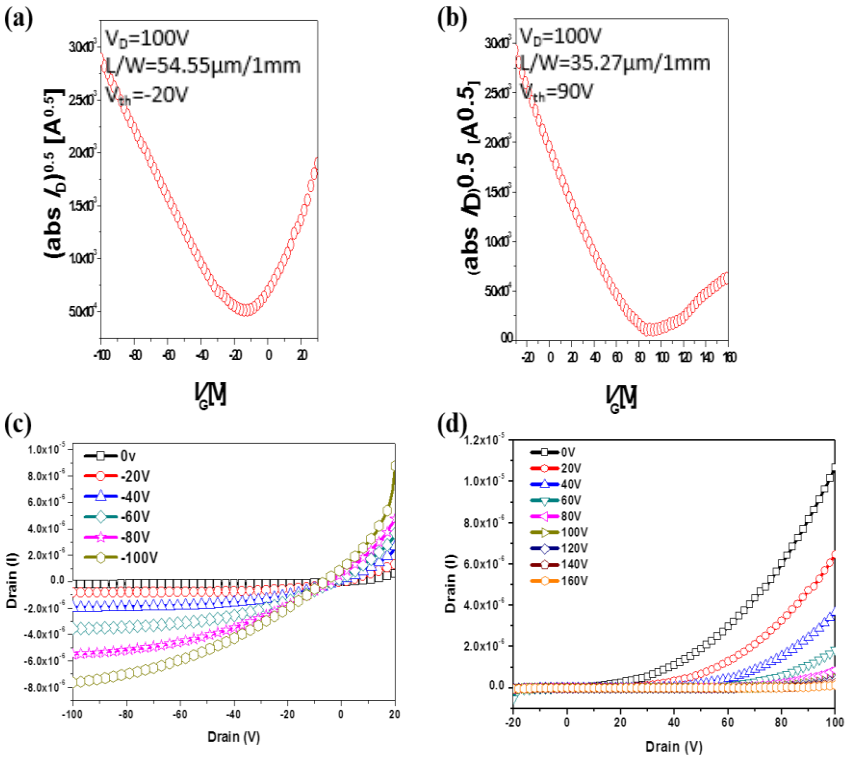

Figure 3. 8 Transfer curves of (a) p-channel operation and (b) n-channel operation. Output curves of (c) p-channel operation and (d) n-channel operation. These characteristics of P(EHTIID2T-HDIDIDF) were detected at best conditions

3.3.6 Morphology studies of polymer OFET devices

To throw light on structure-property relationships in two polymers, atomic force microscopy (AFM) is progressed. For determining increase of mobility at higher temperature, AFM images are supported.

Tapping mode AFM topographies are shown in Figure 3.9 and Figure 3.10 for P(EHIID2T-HDIDIDF), and Figure 3.11 and Figure 3.12 for P(EHTIID2T-HDIDIDF). Figure 3.9 and Figure 3.11 show topology of each organic layers according to spin-rate of P(EHIID2T-HDIDIDF) and P(EHTIID2T-HDIDIDF) respectively. Their topological images according to temperatures are shown at Figure 3.10 and Figure 3.12 each. More rapid spin rate and higher temperature, less values of root-mean square (RMS) roughness. It means that smooth and uniform films are formed at optimized conditions.

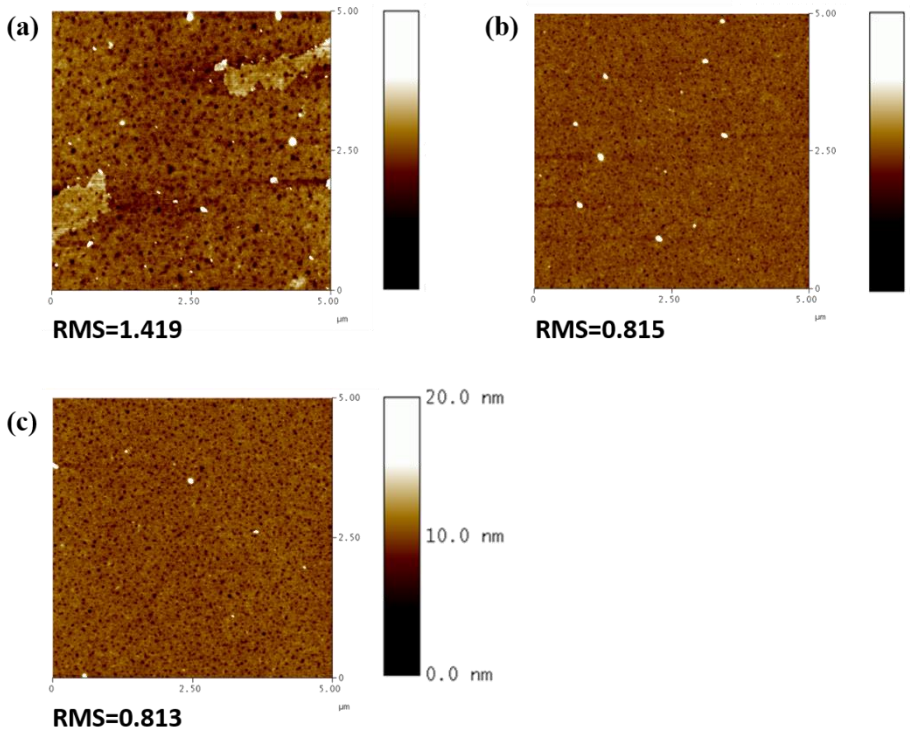

Figure 3. 9 Tapping mode AFM topology of P(EHIID2T-HDIDIDF) devices fabricated using 0.3wt% chloroform solution with spin rate (a) 1000rpm, (b) 2000rpm and (c) 3000rpm.

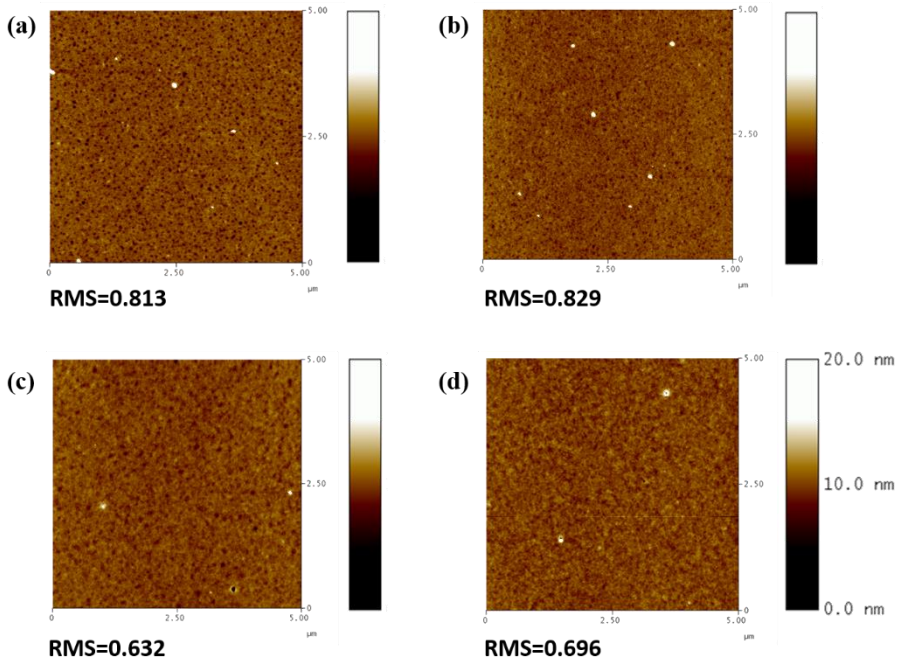

Figure 3. 10 Tapping mode AFM topology of P(EHIID2T-HDIDIDF) devices fabricated using 0.3wt% chloroform solution with spin rate 3000rpm at (a) RT, (b) 100℃, (c) 150℃and (d) 200℃

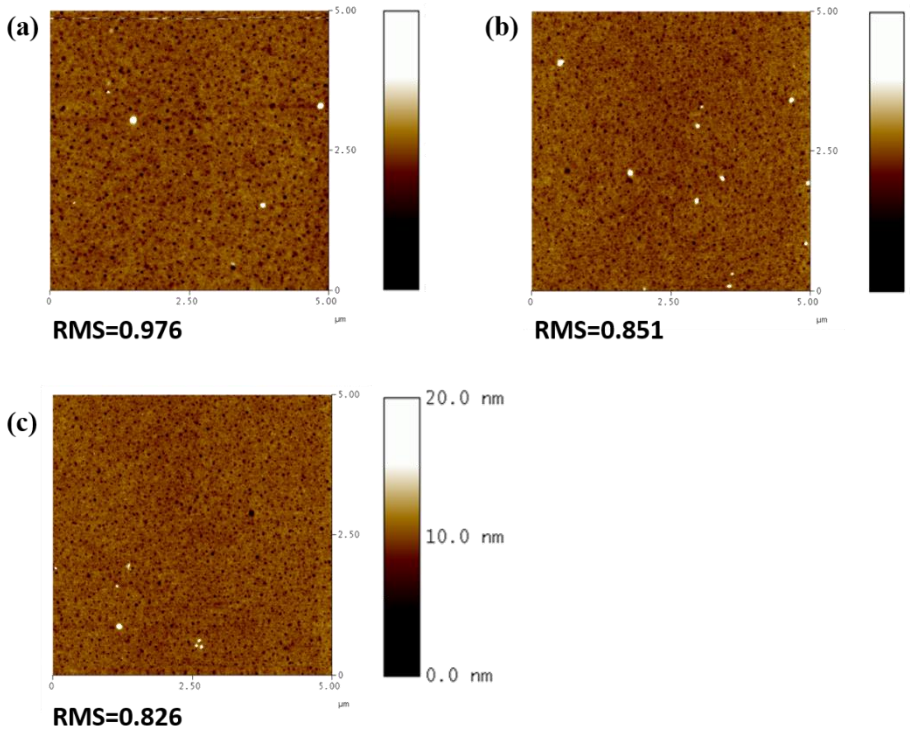

Figure 3. 11 Tapping mode AFM topology of P(EHTIID2T-HDIDIDF) devices fabricated using 0.3wt% chloroform solution with spin rate (a) 1000rpm, (b) 2000rpm and (c) 3000rpm.

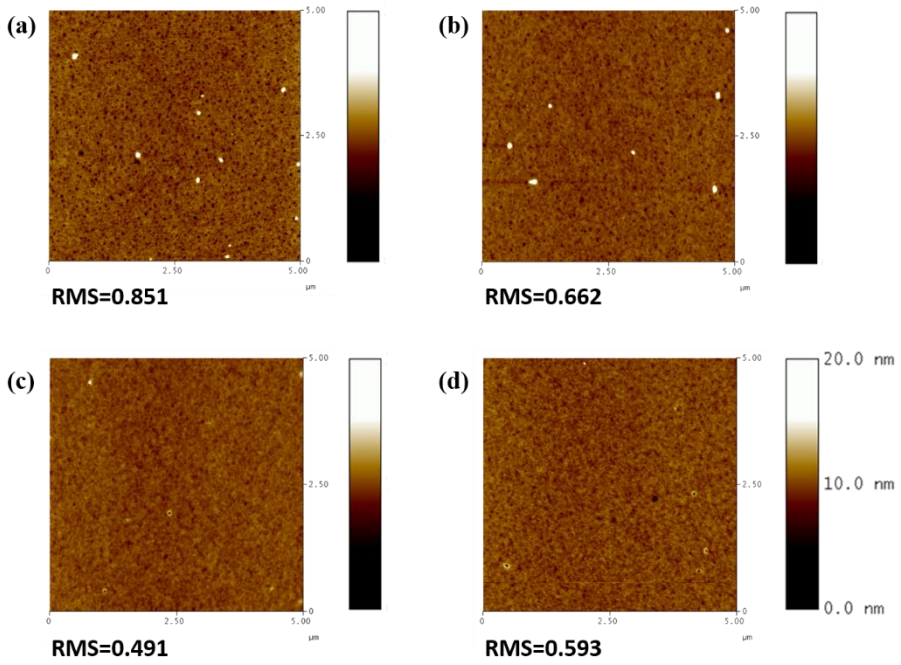

Figure 3. 12 Tapping mode AFM topology of P(EHTIID2T-HDIDIDF) devices fabricated using 0.3wt% chloroform solution with spin rate 2000rpm at (a) RT, (b) 100℃, (c) 150℃and (d) 200℃

3. 4 Conclusions

To throw light on structure-property relationships in isoindigo (IID) and thienoisoindigo (TIID), IID- and TIID-based D-A polymer named P(EHIID2T-HDIDIDF) and P(EHTIID2T-HDIDIDF) were designed and successfully synthesized using fluorinated indoloindole (IDIDF) for donor units. Their ground state optimized geometries were expected through DFT calculation. Optimized geometry of each polymer showed structural difference between IID and TIID core so that TIID-based polymer, P(EHTIID2T-HDIDIDF), had more planar backbone and was expected well-aligned lamellar structure. Optical, electrochemical, and field-effect properties were measured.

Due to effective D-A intramolecular charge-transfer transition, both polymers showed broad light absorption property with very low band-gap. More effective expanded conjugation due to planar structure, more broad absorption range and lower band-gap energy shown for P(EHTIID2T-HDIDIDF). In order to thiophenes of TIID, HOMOs of P(EHTIID2T-HDIDIDF) were high-lying compared with that of P(EHIID2T-HDIDIDF). These results came from TIID and IID own properties. Energy levels were suitable for testing ambipolar field-effect properties.

Based on these basic characteristics, solution-processed OFET performances were checked. Both polymers showed p-channel dominant ambipolar charge transport ability. Especially, P(EHTIID2T-HDIDIDF) showed balanced ambipolarity compared to P(EHIID2T-HDIDIDF). Max mobility of each polymers was followed. Max mobilities of P(EHIID2T-HDIDIDF) were $\mu_e = 3.09 \times 10^{-4} cm^{-1}V^{-1}s^{-1}$ and $\mu_h = 3.04 \times 10^{-2} cm^{-1}V^{-1}s^{-1}$. In case of P(EHTIID2T-HDIDIDF), max mobilities were $\mu_e = 4.44 \times 10^{-3} cm^{-1}V^{-1}s^{-1}$ and μ_h

$= 1.14 \times 10^{-2} cm^{-1}V^{-1}s^{-1}$. From those results, although two polymers showed ambipolarity, P(EHTIID2T-HDIDIDF) was more suitable because of its planar structure and charge transport ability. P(EHIID2T-HDIDIDF) also showed good performance at p-channel but poor electron transport ability was limit of this polymer. The device performances were associated with the flat structure of TIID unit, which minimized the steric hindrance to facilitate the stacking nature. Those were supported by GI-XRD patterns at annealed films.

Through this work, comparison of TIID and IID was clearly demonstrated with optical and electrochemical property and field-effect transistor performances. As a results, P(EHTIID2T-HDIDIDF) was preferred for balanced ambipolar OFET because of their proper energy level and co-planarity through polymer backbone.

3.5 Bibliography

1) E. Wang, W. Mammo, M.R. Andersson, *Adv. Mater.* **2014**, 26, 180

2) X. Guo, A. Facchetti, T. J. Marks., *Chem. Rev.* **2014**, 114, 8943

3) Y. Lai, J. Yeh, C. Tsai,Y. Cheng, Eur. *J. Org. Chem.*, **2013**, 23, 5076

4) T. Lei, J. Dou, Z. Ma, C. Yao, C. Liu, J. Wang, J. Pei, *J. Am. Chem. Soc.*, **2012**, 134, 20025 ; Y. Deng, J. Liu, J. Wang, L. Liu, W. Li, H. Tian, X. Zhang, Z. Xie, Y. Geng, F. Wang, *Adv. Mater.* **2014**, 26, 471

5) Will be published in I. Cho's Ph.D. thesis.

Abstract in Korean

초 록

아이소인디고와 싸이에노아이소인디고의 구조특성 상관관계: 합성, 특성분석, 그리고 유기전계효과 트랜지스터로의 응용에 대한 연구

박 영 주
공과대학 재료공학부 WCU 하이브리드
서울대학교 대학원

락탐 작용기를 포함하는 유기 물질들의 유기 반도체 소자로의 응용에 대한 연구가 활발하게 진행되어 왔다. 락탐 작용기를 포함하는 유기 물질들은 락탐 작용기의 고유한 특성에 의해 LUMO 레벨이 안정화되어 있으며 넓은 빛 흡수 영역을 가지기 때문에 밴드갭 에너지가 작다. 이러한 락탐 작용기를 가지는 물질들 중에서 아이소인디고 (IID)와 싸이에노아이소인디고 (TIID) 유도체들은 유기 태양전지와 유기전계효과 트랜지스터로서의 적용에 있어 뛰어난 효율을

보이고 있다. 하지만, 아이소인디고와 싸이에노아이소인디고의 구조적 유사성에도 불구하고 구조특성 상관관계에 대한 연구가 드물게 진행되었다. 아이소인디고는 카보닐 그룹의 산소 원자와 인접한 벤젠고리의 수소 원자의 전자밀도에 의해 구조체의 뒤틀림이 일어나고, 이로 인해 분자 간의 효과적인 $\pi-\pi$ 상호작용이 어렵다. 이러한 한계점을 해결하기 위해 아이소인디고의 벤젠고리가 싸이오펜으로 치환된 싸이에노아이소인디고가 보고되었고, 싸이오펜의 황 원자와 카보닐 그룹의 산소 원자 사이의 이차적 상호작용에 의하여 구조체의 동일평면성이 크게 증가한다.

본 연구에서는 아이소인디고와 싸이에노아이소인디고 사이의 구조특성 상관관계를 연구하기 위해 단분자와 전자주개형 물질과 전자받개형 물질이 교차된 구조의 폴리머(D-A 유형의 폴리머)를 설계, 합성하였다.

우선적으로 아이소인디고와 싸이에노아이소인디고의 기본 특성 비교를 위하여 흡광도와 전기화학적 특성, IR 분석이 진행되었다. 광학적, 전기화학적 특성을 통해 싸이에노아이소인디고가 아이소인디고보다 더 평면성이 좋고 밴드갭이 작다는 것을 알 수 있다. 이를 토대로 유기전계효과 트랜지스터로 응용하기 위한 아이소인디고와 싸이에노아이소인디고의 유도체들을 설계, 합성하여 광학적, 전기화학적 특성을 확인하였다. 본 유도체들을 유기전계효과 트렌지스터에 적용해본 결과, 아이소인디고 유도체들은 n형 단독 광소자의 특성을, EHIIDPDCV 와 EHIIDTDCV 각각, 전자이동도 1.70×10^{-3} $cm^2V^{-1}s^{-1}$ 와 1.83×10^{-3} $cm^2V^{-1}s^{-1}$ 를 보여주었다.

앞서 확인하지 못한 소자특성과 물질특성의 상관관계를 명확히 알아보고자, 아이소인디고와 싸이에노아이소인디고의 강한 전자받개 특성을 이용하여 전자주개형 물질과 함께 D-A형 폴리머를 합성하였다. 강한 폴리머 사슬 내의 전하이동 상호작용으로 인하여 낮은 밴드갭을 가지는 것을 알 수 있었고, 이를 토대로 양극성 전하이동도를 가지는 트랜지스터를 구현하였다. 싸이에노아이소인디고를 기반으로 하는 폴리머가 동일평면성이 더 우수하기 때문에 높은 정공이동도를 유지하면서도 전자 이동도는 10배 증가한 전하 이동도를 보였다. 두 폴리머의 양극성 트랜지스터 특성은, P(EHIID2T-HDIDIDF)의 경우 전자이동도 $3.09\times10^{-4}cm^{-1}V^{-1}s^{-1}$, 전공이동도 $3.04\times10^{-2}cm^{-1}V^{-1}s^{-1}$를 보이고, P(EHTIID2T-HDIDIDF)의 경우 전자이동도 $4.44\times10^{-3}cm^{-1}V^{-1}s^{-1}$, 정공이동도 $1.14\times10^{-2}cm^{-1}V^{-1}s^{-1}$를 보였다. 두 폴리머의 박막의 구조를 GI-XRD를 통해 분석해 본 결과, P(EHTIID2T-HDIDIDF) 필름이 더 잘 배열된 형태를 하고 있는 것을 확인하였다. 이를 통해 싸이에노아이소인디고의 우수한 평면성에 의해 폴리머의 동일평면성이 우수해져 트랜지스터 효과 또한 증진됨을 확인하였다.

주요어 : 아이소인디고, 싸이에노아이소인디고, 단분자, D-A형 폴리머, 구조특성 상관관계, 유기전계효과 트랜지스터

학번 : 2013-22475

List of Presentation

Youngjoo Park, Won Sik Yoon, Sang-yoon Oh, Soo Young Park, ″Synthesis and Characterization of Isoindigo and Thienoisoindigo Derivatives for Organic Field Effect Transistor Application″, **KJF-ICOMEP 2014,** September 21-24, 2014, Tsukuba, Japan. (**Poster Award**)